# STUDY OF THE EFFECT OF ELASTIC FOUNDATION ON THE ACCELERATED DURABILITY TESTING OF GROUND VEHICLES

By

**Ebadur Rahman**

A Thesis Submitted to the Faculty of Graduate Studies of the

University of Manitoba

In Partial Fulfilment of the Requirements of the Degree of

## Master of Science

Department of Mechanical Engineering

University of Manitoba

Winnipeg, Manitoba

# Abstract

Accelerated durability testing of automotive components has become a major interest as it may predict the life characteristics of the vehicle by testing fatigue failure at higher stress level within a shorter period of time. In this work, a specially designed sub-scaled experimental testing bed with the rigid and elastic supports of a simply supported beam was designed and built to compare the effects of the elastic foundation on the change of modal parameters of the tested structure which was later used to tune the FE model. Afterwards, the accelerated loading profiles of both sine sweep and random vibration were applied on the FE model to compare the deviation of the cumulative fatigue damage between the elastic and rigid supports. This work reveals a significant amount of inaccuracy in the current laboratory testing system where the dynamic properties of the tested structure are not maintained close to the real situation.

# Acknowledgements

Firstly, I would like to show my deepest gratitude to my thesis supervisor Dr. Christine Wu and Dr. Nan Wu for whom I have got the chance to fulfill my dream of pursuing higher studies here in Canada. I am really grateful to them for showing their interest in taking me as a graduate research assistant and introducing me to the exciting fields of vehicle structure dynamics and vibration analysis. Their valuable time, guidance, ideas, encouragement and financial support have been influential in the successful completion of this thesis. I would also like to thank Dr. Yunhua Luo and Dr. Young-Jin Cha for serving my committee.

It was a great pleasure to be a part of the Nonlinear Systems Research Laboratory of the University of Manitoba. Here I have met with some excellent personalities as my colleagues. Their valuable suggestion and ideas were really helpful when I was stuck in some complex problems. I would like to give my special thanks to Mr. Sushil Doranga, Md. Nuruzzaman, Tamrin Tanha, Rony Chandra Shaha, Alix Bartel for their mental support during the course of this work. I would also like to express my sincere appreciation to Mr. Thomas Irvine from NASA who extended his helping hand when I was in trouble with MATLAB Coding.

I would like to give special thanks to Md. Iqbal Mahmud Chowdhury, Md. Ahmeduzzaman, Zahid Rahman, Rabiul Islam Khan, Silvia Sekandar, Ummy Habiba Tithi, Sheikh Mohammed Rifat, Md. Anis Rahman and many more for always being good friend and source of encouragement during my stay here in Canada. You guys never let me feel that I am staying seven thousand miles away from my family.

At last but not the least I am forever indebted to my parents, sister, brother- in- law and friends back in my country for their countless support and inspiration.

# Dedication

This piece of work is dedicated to my respectful parents whose love, affection, prayers, encouragements and sacrifices make me able to achieve success and honor in both personal and academic career. Thanks for your great support, teachings and continuous care throughout my entire life which cannot be described in words.

# Table of Contents

# List of Figures

**List of Figures from Appendices**

# List of Tables

# Nomenclature

| | | |
|---|---|---|
| AD | : | Accelerated Durability |
| FRF | : | Frequency Response Function |
| FFT | : | Fast Fourier Transform |
| IFFT | : | Inverse Fourier Transformation |
| CAD | : | Computer Aided Design |
| FEM | : | Finite Element Method |
| FDS | : | Fatigue Damage Spectrum |
| ERS | : | Extreme Response Spectrum |
| SRS | : | Shock Response Spectrum |
| S-N | : | Stress-Number of Cycle |
| UTS | : | Ultimate Tensile Strength |
| PSD | : | Power Spectral Density |
| SDOF | : | Single Degree of Freedom |
| MDOF | : | Multi Degree of Freedom |
| SAST | : | Single Axis Simulation Table |
| RMS | : | Root Mean Square |
| RPC | : | Remote Parameter Control |
| PDF | : | Probability Density Function |

CHAPTER 1

# 1 INTRODUCTION

## 1.1 Background

Safety and reliability have become one of the most vital features for automobile industries which need to be improved continuously without compromising the quality of the products. Ground vehicles are always susceptible to fatigue failure due to the random behavior caused by the road surface and customer usage. To meet client satisfaction and create a solid leader image in this competitive world market, vehicle companies are showing their high interest in the studies for improving productivity, durability, strength and longevity. Hence, the need for accurate and effective laboratory testing technique comes into play to improve the quality and consistency of the service components.

### 1.1.1 Metal Fatigue

During the $19^{th}$ century, engineers discovered one of the major and crucial damage mechanisms for structural components which consisted of the process of inaugurating material cracks due to repeated fluctuating loads[1]. This type of failure is known as fatigue because the load might not be large enough to go beyond the ultimate tensile strength but due to its certain number of repetitions the accumulated damage may cross a critical level which causes the component to fail abruptly[2].

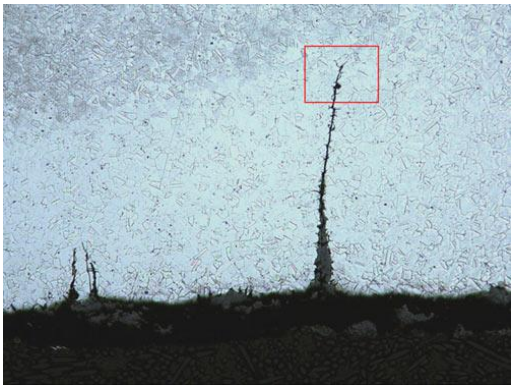

**Figure 1: Fatigue fracture surface of a steel beam[3]**

### 1.1.2 Fatigue Properties of Materials

Fatigue is the common type of failure mechanism that occurs in almost every metal structure which is subjected to cyclic loading such as suspended bridges, rails, or airplane wings. The type of loading can take a variety of forms such as bending, axial, rotation or torsion. The loading may be completely reversed or between equal or unequal positive and negative values.

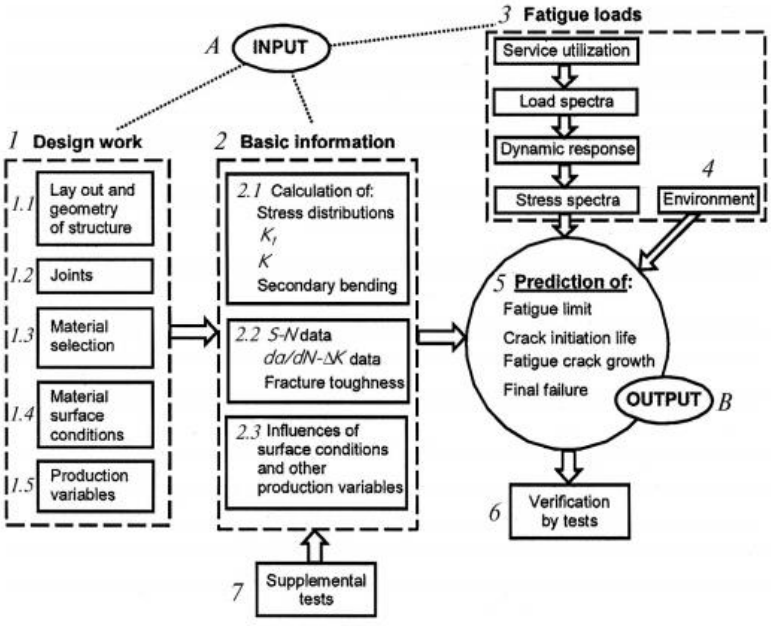


**Figure 2: Steps involved in fatigue testing[4]**

Figure 2 describes the general steps required for estimating fatigue load and damage of a component. In fatigue testing, a number of specimens are subjected to different stress levels and the corresponding number of cycles to failure is recorded. The plot of these two terms is called stress-cycle diagram or S-N diagram which will be used to determine fatigue life of the material subjected to repeated loading.

Mainly three steps are involved in the fatigue failure mechanism. Due to irreversible dislocation movements of the atoms, slip bands are nucleated that form micro cracks inside the metal's grain. The stress concentration factor ($K_t$) plays a vital role during the **Crack Initiation** stage[3]. When the dislocation density increases the slip bands merge together and form a short crack which is termed as the **Grain Growth** stage[5]. The stress intensity factor (K) is used to predict the stress severity around the crack. After the crack length reaches to a critical value the material's capacity to sustain the applied load fails and ultimate failure occurs. This **Rapid Fracture** stage occurs abruptly which is why in fatigue life calculation there is no mathematical term associated with it.

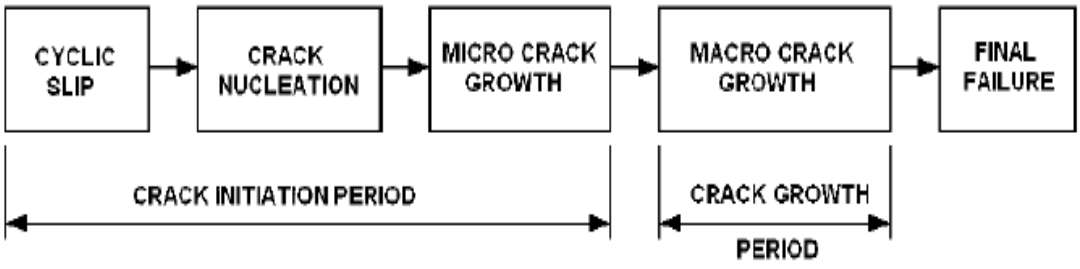


**Figure 3: Different stages of the fatigue life[4].**

## 1.2 Vehicle Durability Tests

Road tests are used to assess the safety, durability, comfort and reliability of a particular vehicle. Due to the rapid development of automobile industries, shortening of the product development time and cost reduction have become the crucial part of manufacturing ground vehicles. Automobiles are driven continuously on proving grounds of different surfaces up to hundreds of hours to simulate the real world failure mechanism. To certify the marketability of the vehicles, they should withstand the random road loading without introducing any failure that includes crack initiation in the critical points of the structure[6]. Sometimes this method may become risky if any of the components suddenly fails which is undesired and will cost an enormous amount of time and money. In Figure 4, a real world proving ground testing facility is shown which is located at *Pennsylvania Transportation Institute*[7].

In durability testing, any types of extreme crash loading or acoustic loads are ignored as these are not considered as part of the metal fatigue damage mechanism. The general methods to perform a durability test include:

- Proving ground test or off road tests
- Laboratory test rig to simulate real world behavior
- Computer aided engineering (CAE)

General road tests require a huge investment of time, money and labour that can be minimized by introducing lab tests through accelerating the loading profile. The procedure to simulate the infield driving condition in a small time period is known as the Accelerated Durability (AD) test. The most straightforward approach is to accelerate the accumulated damage by introducing the rise in extreme loading events.

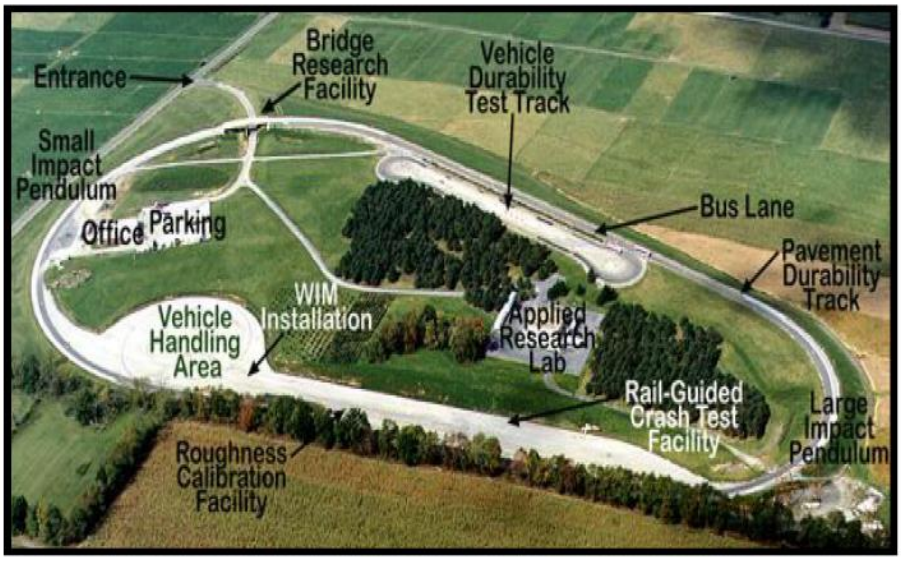


**Figure 4: A typical testing facility for automotive vehicles[7].**

Conducting an AD test is an effective way to deal with the post-sale warranty time period of the vehicle components, henceforth increasing the reliability and marketability of the product. AD loading profiles can be reproduced and observed in each case of the testing period and individual components can be tested instead of running a full vehicle for a longer period of time. These properties make the AD tests more reliable, unique and beneficial comparing with the conventional field tests. An effective AD test should meet the following two criteria to obtain reliable results[6]:

- The failure mechanism in the laboratory test and the infield test should be similar which means the fatigue law must be followed.
- The accelerated test loading should not contain any event that creates an unrealistic situation i.e. failure due to an abrupt high load is prohibited in the AD testing mechanism.

The reproduction of the responses such as displacement, acceleration and strain of the structure generated in the actual field environment is obtained in the laboratory by the combination of the servo hydraulic testing system and the remote parameter controller[8]–[10]. The AD test loadings in the laboratory are acquired either by employing the MAST or SAST. These are contrived to apply a variety of excitation techniques to reproduce a wide range of vibration phenomena or real world service situations with high conformity[11]. Figure 5 shows the prototype of MAST/SAST that is broadly used in the testing industries.

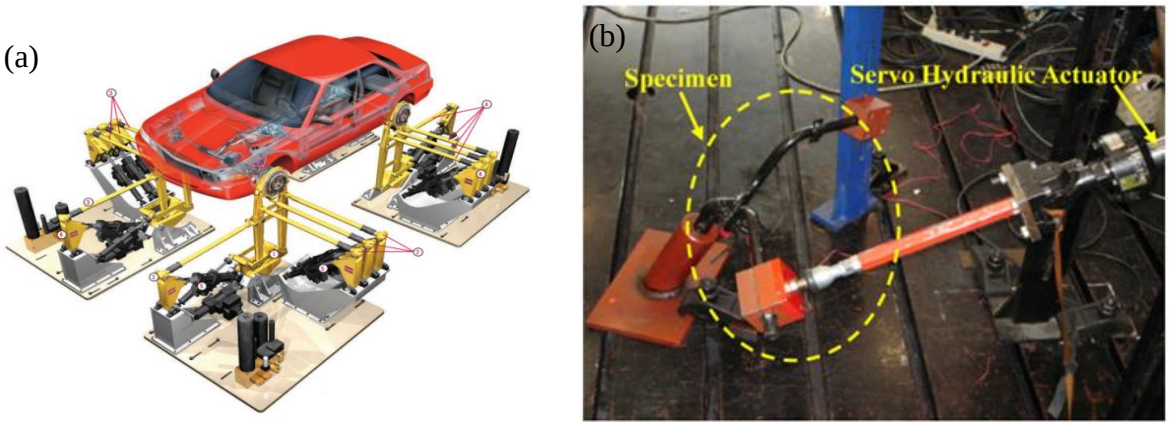


**Figure 5: Setup condition of AD test and target specimen (a) MAST[12], (b) SAST[13]**

Firstly, the loading profile is compressed by accelerating time, cycle or the amplitude to generate a fast-tracked time series input or PSD from the proving ground test data. RPC is used to drive the shaker machine by a number of iterations based on the tolerable deviation of the input and the reaction of the sample. The input loading is, therefore, maintained at shorter frequency history to minimize testing time and cost. Generally the loadings are generated for 60 seconds and repeated uninterruptedly to obtain the preferred FDS of the component.

## 1.3 Objectives of the Thesis

The key purpose of this work is to ensure the real world dynamic properties in the laboratory durability assessments. In previous work, 'modified test tailoring approach'[14] was used to derive accelerated loading profiles from field test data and later were experimentally validated for a cantilever beam[15]. That work lacks the knowledge of applying appropriate boundary conditions and damping effect in the lab testing facility.

In reality, a vehicle consists of a number of components which are subjected to different types of support and joints for their proper functioning. Figure 6 shows a simplified model of an automobile where the tire and suspension system are examined as single stiffness and the body is considered as a beam.

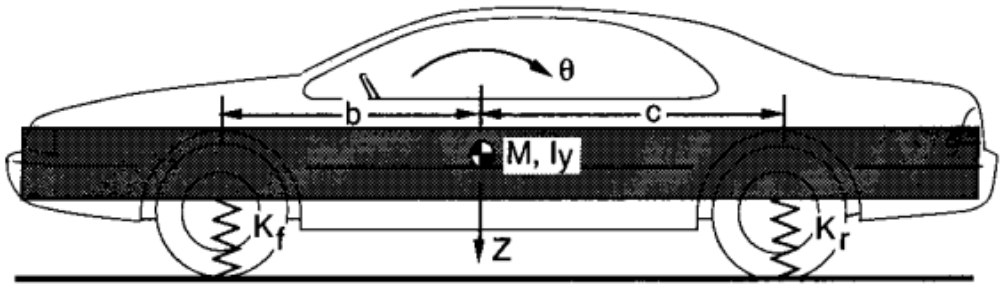


**Figure 6: Typical simplified model of tire and suspension in a vehicle[16].**

While placing the 'in service' components in a laboratory it is not always possible to provide the exact boundary conditions of a real test. During durability testing, vehicle components are directly mounted on the shaker table. As the vehicle body is supported by the tires and suspension system, current tradition of AD test neglects the effect of unsprung stiffness and damping effect. We know from the knowledge of structural dynamics that stiffness has a large impact on natural frequencies and damping controls the amplitude of the response during

resonance. In other words, we are altering the dynamic properties of the vehicle to a large extent. As a result we would not get the proper vibrational characteristics of that structure. The purpose has therefore been to investigate how well a new type of fixture can be designed to behave closer to the real world situation and show the differences in cumulative fatigue damage between the existing and the modified test rig fixture.

### 1.4 Delimitations

In this thesis, a simple beam model with some holes was expected to behave like a real world vehicle component. The reason of adding the holes was to increase the stress concentration and locate the most severe position without any trouble. To replicate the real world dynamic properties a uniaxial spring, a friction shaft and an end mass were attached at both ends to tune the natural frequencies and equivalent damping. Whereas, a rigid pin joint was used at two extreme points to consider the current lab testing fixture. Two assumptions were made for this thesis based on the design of the physical experiment:

a) Beam supported by a semi rigid or elastic fixture would act like a real world vehicle component as if it was held by the tires and the suspension systems.
b) Beam supported by a pin or rigid fixture would replicate the current trend of AD testing in the laboratory.

Generally, shaker tables are used to simulate any kind of vibration fatigue problem as it can perform the base excitation directly. Due to the unavailability of a vertical shaker table, we used a small modal shaker to experimentally validate the global dynamic properties e.g. natural frequencies and modal damping ratios. That modal shaker[17] can provide up to 7 pounds pk

sine force during testing which is more than enough to excite such small structure in our experiment.

Experimental modal testing was carried out to tune the FEM model. This includes the use of commercial software package ANSYS Workbench 2015 academic licensed version. After tuning the FEM with the physical setup, the model was further forwarded to analyse forced vibration responses using harmonic analysis and modal transient analysis.

The thesis work was limited to include only two types of vibration loading profiles e.g. constant amplitude sine sweep and random vibration excitation. Furthermore, stress histories for 60 second loading of both fixtures were then sent to MATLAB for advanced fatigue damage calculation. The purpose of using 60 second loading was to minimize the simulation time and associated hardware cost and avoid anomalies induced by the long random testing profile. Our purpose was well served as our aim was to show the differences in fatigue damage between the beam supported by the rigid and elastic foundation. The validation of the loading profiles was skipped to simplify the whole work.

### 1.5 Outline of the Thesis

The beginning of this thesis work involves a general background on the road induced fatigue failure and AD testing which is used to shorten the developing time and increase the reliability and safety of the newly built vehicles.

In **Chapter 2**, a pre study of current AD tests and its applications are discussed. This chapter enlighten us with the knowledge of the generation of loading profiles and the types of fixtures used in the laboratories. Current literatures based on the effect of spring, damper and elastic foundation and tuning those properties are studied extensively. This section also present the

commonly used modal parameter extraction techniques and vibration fatigue damage calculation methods to use further in this thesis.

Theoretical, FEM and experimental methodologies used in the thesis are described in **Chapter 3**. Theoretical background of the mathematical modeling of lateral vibration of a beam is studied with the effect of different boundary conditions. Modeling the shaker table characteristics using large mass method (LMM) in FEM is discussed. Theoretical background related to the fatigue damage identification using the S-N curve and rainflow matrix calculation is presented. Moreover, different types of frequency domain algorithms are discussed to compare the results with the time domain analysis and proof the consistency.

**Chapter 4** is dedicated to the findings obtained from chapter three. The effect of spring and mass on the natural frequencies of the beam is analysed and compared with the results found from a rigid support. Experimental modal analysis results using curve fitting techniques are also shown. Responses due to the application of the sine sweep and random vibration loading are investigated. The differences in fatigue life using different stiffness and damping ratios are presented in this chapter.

Lastly, **chapter 5** recaps the works done in this thesis, highlighting the novel contributions and major findings. This chapter provides an inclusive conclusion and recommend areas for future research. References and appendices used in this thesis are given at the end.

CHAPTER 2

# 2 LITERATURE REVIEW

In this chapter, published literatures regarding the development of durability testing, application of jigs and fixtures, effect of spring and damper and vibration fatigue analysis are reviewed.

## 2.1 Vehicle Durability Engineering

The main goal to design a vehicle is to meet some certain physical properties or design targets that can provide customer satisfaction, product safety, less maintenance and warranty costs and recalls[18]. A number of studies have been carried out to explain the necessity of consistency and robustness in the field of vehicle structure dynamics which are essential for the development of a reliable vehicle[19],[20],[21],[22],[23].

Typical design constraint of a vehicle includes high stiffness, smooth ride and handling, good fuel efficiency which must be accomplished along with adequate durability and improved reliability within the warranty timeframe[24]. Vehicle safety and attainment of expected service life are realized by the mean of vehicle durability tests which deals with metal fatigue.

Durability testing of an automobile component mainly depends on the imposed boundary conditions, geometry and type of loading[25]. Road roughness or irregularity[26] is one of the most important parameters that affects the warranty life of a vehicle. Due to exposure to random high loads under normal driving conditions it is sometimes difficult to predict the loading situations which may trigger undesirable variation. Hence, the need of precise statistical

overview of loading conditions has become one of the key aspects of vehicle service life[20],[27],[28]. Durability testing at this point serves as the basic requirement to improve weak vehicle designs and fulfil customer demands by reducing unexpected failure rate of its components[29].

## 2.2 Development of Accelerated Durability Testing

Due to the time and cost constraints, proving ground situations are replicated in the automobile test laboratories so that the road load parameters can be extracted by the mean of hydraulic actuators[30],[10]. In an AD test the cumulative damage of a test structure is accelerated by increasing the severity of road load profiles beyond what is expected in the normal driving condition[18]. The most beneficial part of an AD test is its capability to test individual vehicle components in the laboratory which saves money as well as time required for a full vehicle test.

In 1945, Miner[31] proposed cumulative fatigue damage theory, later which becomes the theoretical base of Accelerated durability tests along with the equivalent stress technique[32]. The trend of accelerated durability test began many years ago, more specifically during early 90's with the development of required mathematical modeling and equipment. The analytical models presented by Caruso *et al.*[33], Nelson[34] and Meeker *et al.*[35] are considered as the pioneer research in the area of AD testing. Different testing parameters (road surface, loading, condition, customer usage) were taken into consideration while developing the theory of AD tests. The effect of vehicle speed and roughness of the test field was analysed by Ashmore *et al.*[36] to validate the acceleration factor (AF) to generate the loading profiles. Jeong *et al.*[37] used multiaxial simulation table to simulate real world vibration fatigue environment in the laboratory and was successful to reduce the required test time to one fourth of its original duration. On the other hand, Su *et al.*[38] and Dowling[39] presented an accelerated component

test approach using equivalent damage technique based on CAE and data correlation. Panse *et al.*[40] and Haq *et al.*[41] had applied the accelerated durability test profile to the complete vehicles and also to the components based on the equivalent damage technique and customer usage correlation. In 2013 Prakash[42] developed a hybrid method of accelerating durability test by pseudo damage editing technique using stochastic event analysis.

### 2.2.1 Loadings Used for AD testing

Determination of the exact loading condition has become one of the biggest challenges in AD testing process. In general, two types of loading conditions are used extensively in the area of durability testing: sine-sweep loading and random vibration loading which are totally different based on their characteristic governing equations[36]. The PDF of the sinusoidal loading follows the shape of the bathtub curves[43], whereas the probability density function of a random vibration loading looks like a bell shape curve[44].

Constant amplitude loading is the most common form of durability test where a sinusoidal input load is applied to the test structure usually near the resonance frequency to monitor its effect on the designed test piece[45]. The loading can be applied by sweeping the frequency to a finite range and also can be done with variable amplitude loading depending on the customer preference. The speed of the sweep expressed as 'octaves per minute' can be monitored to control the time spent at the frequency of interest[46]. Sunil *et al.*[47] suggested an approach for accelerated fatigue testing of resonating structure where a sweep endurance test was carried out to find the stress and acceleration response from the structure. In this research, contribution of each frequency band towards the damage was monitored and an optimized proving ground load profile was generated while retaining the failure modes. Heydinger et al.[48] conducted sinusoidal sweep steering test at 20 mph speed along a straight path to generate the roll angle,

lateral acceleration, yaw rate and roll rate frequency responses to steering inputs to inspect any issue that might arise from the resonant frequency.

Another type of loading used in the durability tests is the random vibration profiles which are accepted as the best testing method by the engineers. As a vehicle experiences dynamic loads while running on the road that are non-deterministic and non-periodic, it is better to use statistical approach to generate random loading profiles. These are produced by driving a vehicle on proving ground for a specific amount of time and then constructing a test rig driving profile by considering only the severely damaging contents[49]. Gopalkrishnan and Agarwal[50] introduced an example of generation of input loading profile by taking random measurement of triaxial wheel forces using a specially developed load cell by placing it inside the wheel hub. Berger *et al.*[51] provided load sequences by using the measured data from the German Automotive Industry for vertical, longitudinal and lateral directions.

The most effective approach of generating vibration loading profiles for accelerated durability test was first recommended by Halfpenny[45] in 2006 based on the French Military Standard[52] and the NATO Draft Standard[53]. The general procedure of this 'test tailoring approach' consists of two steps: mission profiling and test synthesis. In mission profiling stage, at first the FDS[54] and SRS[55],[56] are calculated applying SDOF transfer function to input field test data. These steps are carried out for the first couple of vibration modes to find out the maximum response. Once the FDS and SRS are calculated the ERS[57] is calculated by multiplying the input with few AFs which can be controlled up to a certain theoretical limit. Due to avoid unrealistic loading the ERS is kept lower than the SRS and the FDS of field test and the laboratory test is kept as close as possible to the real field to maintain the same failure mechanism[58].

Loading profiles generated from mission profiling and test synthesis are sent to MAST to implement AD testing in the test rig using RPCS format data. Application of this full test period loadings are very time consuming and expensive as the controller has to read each cycle and send it to the actuator. Therefore, the loadings are compressed to 60 sec partial profile keeping all the major dynamic features and information of the full test period which are repeated couple of times to create desired amount of FDS[59].

The partial test data from the full period loading is separated using the Custom Fourier Transformation under GlyphWorks software package developed by HBM nCode. The biggest challenge of generating partial loading profiles using GlyphWorks is to identify the major damaging events from the full period loading. Usually the test track of Pennsylvania Transportation Institute[7] constitutes of seven different damaging events with three clockwise and three counter clockwise orientation. Initially two types of event identification methods were used: visual identification and the curve fitting method[59],[60]. Both of the methods were based on many approximations and assumptions which led to inaccurate and limited event identification. Later, Xu *et al.*[6] proposed a method of event identification using wavelet analysis, clustering and Fourier analysis to generate a partial PSD testing profile with more dynamic features and precision. In 2008 Halfpenny[61] used the test tailoring approach to generate loading profiles and validated it in the test rig with the use of GlyphWorks software. Aviation industries[62] also embedded this approach to evaluate durability of the components in uni-axial[63] and tri-axial[64] directions by accelerating a 12000 hour field test to a 4 hour lab test which could not validate the exactness of the AF used in their analysis.

### 2.2.2 Durability Testing Using FEM

The loading profiles generated by the test tailoring approach are broadly used in FEM nowadays with the advancement of CAE. Wannenburg and Heyns[65] gave an overview of numerical methods used for durability assessments in their publication. Virtual AD testing is done mainly in three steps where the load history input are generated by the methods discussed in the previous section, following by the accurate calculation of the local stress and strains and at the later stage fatigue life assessments are carried out using the time and frequency domain methods.

In 2000, Bishop and Sherratt[66] described a basic method to perform stress analysis using quasi-static FEA where the output stress response was calculated based on the quasi-static transfer matrix [K]. This transfer matrix calculation does not include the computational complexity related with solving the mass and damping equilibrium matrices. Co-variance method was established by Dietz *et al.*[67] for the purpose of stress analysis where a load matrix [B] was calculated only in the region of interest. The simplest method to achieve fatigue assessments is to superimpose equivalent static load gathered from dynamic load histories[68]. Due to the inaccuracy of local vibrations and dynamics effects the use of equivalent static load has become obsolete[69],[70]. Liao[71] discussed about the static analysis technique with inertia relief where the external forces are balanced by the inertial accelerations at the reference points yielding a static equilibrium condition. The most efficient method was presented by Bathe[72] where the eigenvalue finite element method was employed to solve for the natural frequencies, mode shapes and damping. Apart from these robust methods, transient dynamic direct integration method[66] and modal superposition method[73] are widely used in FEM to perform durability analysis.

Multi-body Dynamics plays a vital role where the input loads at the interfaces of the component are unknown or exists only as the wheel spindle load. Conle and Mousseau[74] used rigid multi body simulation technique to predict the loading at the control arm of a suspension system and later used that loading to assess stress, strain and fatigue life separately. Adams commercial software introduced flexible multi body dynamics to deal with computational complexity and accurate load predictions by using Craig-Bampton sub structuring technique[75]. However, Ottarsson[76], in 1998 made some modifications over the previously described technique to overcome the problem related with constraining rigid body modes.

Durability testing using CAE can be again divided into two sections: semi virtual and fully virtual. In semi virtual testing the acceleration spindle loads measured from the field test data are transferred to the FEM model to find out the responses. Tebbe *et al.*[77] and Liu *et al.*[78] applied the displacement collected from the field test directly to the unconstrained component model in FEM which introduced large error due to the computation error of extraction of displacements from the accelerometer data. The unconstrained model can also introduce roll over or drift in the space domain due to the variations of physical loading and MBS model. This problem could be solved using fully virtual durability analysis. In this kind of analysis a vehicle with tire model is driven over a range of virtual proving grounds of different road profiles. Zhang and Tang[79] performed nonlinear dynamic analysis using LS-DYNA solver where they combined the vehicle FEM model and tire model to collect loading at the different components of the vehicle. Later Zhang *et al.*[80] extended this field of research to perform safety and crashworthiness analysis. However, the results obtained from this kind of virtual analysis are not considered realistic as these lacks the information about random customer usage and accurate tire modeling which might introduce inaccuracy in shifting load input from wheel to the components.

### 2.2.3 Durability Simulation Test Rigs

To perform a successful accelerated durability test in the laboratory, the test must have to be the representative of infield road loading environment. Servo hydraulic test rigs are used to replicate the road loading in the laboratory based on the mathematical principle called Iterative Learning Control (ILC)[81],[82]. Yudong *et al.*[83] described the reproduction techniques of road loads in the test rig using different software programs e.g. TWR, MIMIC, ITFC, RPC. These software programs are used to reproduce the proving ground loading with higher accuracy and minimal human involvement in the laboratories.

According to Ledesma[84], there are two types of test rigs used in durability testing engineering: inertia reacted and fixture reacted. The testing should include either the whole body or the subsystem wherein the loads are applied directly to the wheel hub or the spindle. In inertia reacted test rigs the whole vehicle remains unconstrained and the sprung masses are free to move in the direction of loading. On the other hand, in spindle coupled or fixture reacted assembly the sprung mass is grounded. Although the excitation of inertia reacted rigs behaves similar to the real road excitations, fixture reacted rigs are more popular to the durability engineer because of its better control and reproducibility. Wu *et al.*[85] presented the theoretical and experimental analysis of the effect of spindle acceleration on a fixture reacted test rig. It was found that the accuracy of this kind of rigs may be improved by replicating the spindle accelerations in the upper frequency range.

It is always recommended to use full vehicle body for durability tests as the boundary conditions are better replicated than the subassembly or component testing. But sometimes it is not feasible to test the whole vehicle at the early stage due to cost constraints. In this case, performing a critical component rig test will be much for faster and cost efficient as it will provide a guideline

to the designers about individual component before building the whole model[86]. In 2007, Dressler *et al.*[87] introduced the concept of virtual durability test rig for vehicles using MBS model. In their work, they used tire coupled full vehicle rig and spindle coupled suspension rig to illustrate the complex servo hydraulic test system. Optimization of test rigs was carried out using numerical simulations prior to the physical test which might save both time and money.

### 2.3 Effect of Elastic Boundary Condition and Tuning Structural Dynamic Properties

During analysing a component from a full structure in most of the cases it is assumed that the connections are either fixed or hinged[88]. In real condition, typical behavior of a joint or a connection is more close to a semi rigid or elastic manner. From the theory of elasticity it has been proved that slight change in boundary conditions may drastically affect the structural dynamic properties such as natural frequency, damping ratio and mode shapes.

The ride comfort and handling properties of a vehicle largely depend on the characteristics of suspension system and tires. They are designed such a way so that the input forces and disturbances from road rough surfaces and irregularities are managed easily. Cole[89] reviewed the major objectives and fundamental design issues of a heavy vehicle suspension system in his research article. The crucial part of vehicle structure dynamics is to design a test that can obtain accurate tire-ground interaction model. Related theoretical background and requirements of tire modeling can be found at[90]. The movement and characteristics of tires and suspension systems are modeled by the mechanical systems that consist of springs, dampers and other linkages[91]. As a result the combination of tire and suspension system is treated as the primary source of damped elastic foundation for an automobile component. Therefore, direct mounting vehicle components with rigid support on a shaker table may alter the infield properties to a great extent. Tuning of these properties must be done in order to get satisfactory test results. In the following

section published literature based on the effect of elastic foundation and tuning processes of the dynamic properties will be discussed.

Based on the information regarding the modification of natural frequencies available on the literature the approaches may be divided into three major groups: changing structural geometry, active control by piezoelectric actuation and adding elastic support by the mean of spring and dampers. Changing structural geometry by adding notch and dimples[92] and piezoelectric actuation[93] is not recommended in durability testing as it will alter the internal stiffness of the component. The most effective way is to select a fixture with appropriate combination of spring and damper of different stiffness to tune the dynamic properties close to the real situation.

Timoshenko[94] and Blevins[95] have made a huge contribution in the field of free vibration analysis of beam like structures. They have presented detail information about the effect of material properties and boundary conditions on the dynamic properties. Based on the characteristic equation of free vibration many researchers published articles by changing the related parameters. Rao has derived an exact solution of a clamped-clamped beam with internal elastic support[96]. Szelag and Mroz[97] did same type of research and varied the position and stiffness of the internal support to record the change in fundamental and other natural frequencies of the beam. Forbes studied the influence of axial boundary condition on the pipelines where interaction with the soil at the span shoulders created much more complex elastic foundation with a drastic change in the natural frequencies. Smith and Shust[98] analysed the effect of various parameters (material, cross section, boundary conditions) to bind the natural frequency of a structure. They found the variation of the first natural frequency by a factor up to 6.4 by varying the boundary conditions. Wu and Chou[99] established an equation to find out the natural frequencies and mode shapes of by adding a number of sprung mass, spring and damper

elements along the beam. Lower natural frequencies were tuned to desired value by varying the number of point masses, boundary condition and spring ratio. Wu and Lin[100] studied the effect of adding concentrated masses to a cantilever beam using Numerical Assembly Method (NAM) and found increased fundamental frequency of the beam while moving the single mass from free end to fixed end. They also derived the frequency response equation of both free and forced vibration with different boundary conditions of a multiple span beam. Cha[101] proposed a numerical method to determine the dynamic properties of a beam with arbitrary supports and lumped attachments (linear spring, torsional spring, dampers etc.) using generalized eigenvalue determinant formulation.

Naguleswaran[102] developed a frequency response equation while examining the Euler-beam carrying several particles by using a recurrence relationship. Jia-Jang[103] determined the mode shapes and natural frequencies of beams carrying two degrees of freedom spring damper system using an equivalent damper method. He found a negligible change in natural frequencies with different amount of damping coefficient. However, higher values of damping coefficient were responsible for changing the decay rate which influenced the amplitude of the force vibration to a great extent.

Banerjee[104] formulated an eigenvalue solution method by assembling the dynamic stiffness matrices of the beam to determine the mode shapes and natural frequencies of a beam based on Wittrick-Williams algorithm[105]. He extended the research up to several complex structures by investigating the effect of varying the stiffness and mass properties on the natural frequencies and mode shapes.

## 2.4 Modal Parameter Extraction Techniques

Modal parameter extraction is a principle tool to analyse any kind of vibration related problem that occurs in bridge, machineries or any other engineering structures. The accuracy and exactness of accelerated durability testing i.e. loading profile generation, numerical testing is mostly dependent on modal parameters. As the natural frequencies are used to characterize the resonance behavior and damping ratio controls the amplitude of the resonance, both of these properties must be defined accurately[106]. A modal model of a structure fundamentally contains all the required in formation of an original structure. The main idea to accelerate the AD testing is concentrating the input energy around the natural frequency so that the failure takes place earlier. A lot of work has been published describing the improvement and development of different experimental modal parameter extraction techniques which will be summarized in the following section.

Most of the modal parameter extraction techniques can be divided into two groups: time domain and frequency domain method. Frequency domain method can be again divided into Single degree of freedom and multi degrees of freedom methods. In case of SDOF methods, it is assumed that limited number of modes and a small frequency broadband is involved in the calculation. The most popular method is the Peak-pick method[107] that consists of selecting the peak amplitude from a frequency response function which is called the pole of the function. The position corresponding to the location of the amplitude denotes the natural frequency of that mode and damping can be found by observing the sharpness of the curve. The mode shapes can be calculated based on the imaginary FRF amplitude of different locations on the structure. This method is only suitable for lightly coupled modes where the modes are separated by specific amount of space. For the heavily coupled modes determining damping from SDOF peak-pick

method has become a great challenge for the engineers. At this stage, circle fitting[108] or quadrature response techniques[109] can show satisfactory results to determine the modal parameters. The basic idea of circle fit analysis is based on the circular shape of the Nyquist plot in the imaginary plane of a FRF function[110]. The general procedure involves selecting a point and then a circle is fitted to the real and imaginary part of the FRF. Quality of the fit can be determined by minimizing the error between the fitted curve and the experimental data. Some basic adjustment term can also be added in this method to consider out of band effects and achieve good coherent results, but it becomes difficult when the number of data points around the resonant frequency is limited and the modes are too close to each other. On the other hand, SDOF quadrature response technique involves fitting the amplitude of the real part of FRF using least square method in the vicinity of resonance where the FRF is dominated by that particular mode[111].

In order to extract the parameters of several modes simultaneously MDOF curve fitting[112] technique is used widely in the field of structural dynamics. This method is highly suitable to find out the parameters of closely spaced modes when the effect of multiple modes is taken care at the same time. Among different MDOF curve fitting algorithms, RFP is considered as the most acceptable method to deal with noisy measurements. In this method the least squared error sense algorithm is used to fit a FRF by identifying the appropriate coefficient of the denominator and numerator[113]. Although the frequency domain parameter extraction techniques are quite simple, still it contains some uncertainties and limitations. The effect of input influence, leakage or frequency resolution of frequency response function may lead to inaccurate identification. There might be difficulties to obtain auto power correlation spectral and decay function for each individual mode which might result in poor damping estimation[114].

To deal with the shortcomings of frequency domain modal parameter extraction techniques, time domain methods are used which can provide more accurate and reliable results. The most popular and simplest method used in time domain analysis is “Time Domain Complex Exponential” curve fitting method[115]. The free vibration response is nothing but the sum of couple of damped sinusoidal exponentially decaying signals. By guessing the coefficient of logarithmic decrement equation, one can fit the experimental data close to the theoretical equation using least squared method. In the early days, Ibrahim Time Domain (ITD)[116] method was used extensively specially for the Multi input Multi Output (MIMO) system which was theoretically based on the Modal Confidence Factor (MCF)[117]. The main problem associated with ITD is the complex mathematical calculations that includes large eigenvalue modal model. Utilizing sparse matrix[118] it was conceivable to build the computational effectiveness but still it was extremely slow compared with the current time domain analysis techniques.

Eigensystem Realization Algorithm (ERA)[119],[120] is another well-established method used in time domain analysis. Despite the fact that this calculation has been effectively connected in numerous modular investigation applications, the difficulties related with the singular value decomposition of Hankel matrix made it a complex computational algorithm. Apart from this, many other algorithms such as Canonical Variation Algorithm (CVA), Multivariable Output-Error State sPace(MOESP), Balanced Realization (BR)[121] are used with great convergence result among the identification techniques.

Both frequency and time domain methods can be used depending on the situation and amount of damping present in the structure. Usually it is acceptable to use time domain techniques for low damped structures and frequency domain techniques for highly damped structures. The most

advantageous role of frequency domain techniques is its ability to predict the structural damping for each and every mode separately whereas time domain techniques are suitable to determine the properties of first couple of modes.

## 2.5 Vibration Fatigue Analysis

Engineering structures are often subjected to different types of cyclic loadings which are sinusoidal or random in nature. Vibration fatigue is the term used to analyse the metal fatigue induced by these oscillating loads. Fatigue life estimation of parts experiencing periodic vibration is fairly a straightforward procedure where the life can be predicted using S-N curve. The damage content can be found by multiplying the amplitude of each stress cycle with the number of cycle that the part is undergoing. On the other hand, random vibration is the combination of number of sinusoidal curves of different oscillation frequency at the same time[122]. Hence, prediction of random vibration requires complex statistical terms as the amplitude of different points largely varies with time but their average tends to remain almost similar. Methods of vibration fatigue calculation can be broadly divided into two parts i.e. time domain and frequency domain fatigue analysis which will be described in the following sections.

### 2.5.1 Time Domain Fatigue Analysis

Time domain fatigue analysis is the most conventional term used in fatigue damage estimation of any kind of vibrating structure. The core idea of this type analysis involves generating a large stress-strain or displacement time history from a specific location using different types of sensors (accelerometer, strain-gauge, LVDT etc.) and then passing it to different cycle counting algorithm[123]. Once the cycle counting is done, S-N curve is used to find out the damage generated by each cycle individually. According to Miner[31], the total damage of that location

will equal to the sum of individual damages created from each cycle. The reliability of time domain based techniques depends on the accuracy of the cycle counting algorithms. Those algorithms are based on trigonometric series method[124], parameter model method[125], short inverse Fourier transformation method[126] and so on.

Dowling[127] proposed several methods to accomplish cycle counting that include: (1)Level crossing count, (2) Fatigue meter count, (3) Range count, (4) Peak between mean crossing count , (5) Range mean count and (6) Peak count. Due to the lack of certain fatigue properties some of the methods became out-dated. The most widely used time domain techniques can be briefly classified into two subgroups: (1) Range pair method and (2) Rainflow cycle count algorithm. In case of Range pair method, a full cycle is counted in the event if it can be combined with a consequent straining of equivalent size the other way.

The Rain Flow Cycle Counting Method[123] is more broadly utilized than all other techniques used in fatigue analysis. The lines associating strain crests are envisioned to be a progression of Pagoda rooftops. Principles are forced on rain falling from these rooftops so that cycles and half cycles are characterized. Rainflow starts progressively at within every strain crest and is permitted to drop down and proceed aside from that, in the event that it starts at the very least, it must stop when it comes inverse a base more negative than the base from which it started.

Apart from these, subsequence researches have been published where these techniques have been modified to conduct a successful AD test. Canfield and Villaire[128] suggested a strategy for AD testing, which included the withdrawal of cycle locales that did not bring about critical segment damage. Conle and Topper[129] used a procedure including the altering of local strain history to discard strain cycles underneath specific levels and to take into account the most destructive

strain history. Sharp *et al.*[130] connected the accumulated damage theory to decrease the multiaxial road load information of the original testing, which was altered to lessen the test time while keeping up the most damaging portion untouched. The displacement or acceleration of the shaker table can be correlated with the altered signal to perform the test in the research facility[131]. Additionally, accelerated durability testing can also be performed using 'racetrack editing technique'[132] or 'strain-range editing technique'[133] by modifying the service strain histories which are generally labelled as 'Fatigue Damage Editing Techniques' .

### 2.5.2 Frequency Domain Fatigue Analysis

The time domain investigation requires the information of time histories of the full local stress and strain to cycle counting, which is computationally complex and costly. Again this method does not perceive the effect of frequency; it is just the quantity of cycles that matters[134]. If the response of the structure is dynamically magnified around the resonance zone, it would be difficult to deal with a complex structure with the knowledge of time domain techniques. Hence, overlooking dynamic amplification factor might affect the design and test stage of a component. To overcome these kinds of problems, frequency domain fatigue analysis techniques are widely used among the researchers as it successfully deals with the limitations of time based techniques.

In actuality, structures, for example, an automobile on a rough road surface or a wind turbine are presented to arbitrary loads. Such arbitrary random loads can be seen as the acknowledgment of an irregular Gaussian process that can be explained in the frequency domain by a power spectral density function[135]. Working with a power spectral density demonstrates particularly beneficial when dealing with complex FEM where the computation of the frequency response is much speedier than a transient analysis in the time domain[136]. Some of the notable researches will be discussed in the succeeding section where input and output PSD is used to estimate the

fatigue life in frequency domain. The most acceptable approach of determining fatigue life in frequency domain is to obtain a cycle distribution that follows the basic feature of rainflow method which is treated as the most accurate tool for fatigue calculation.

Rice[137] developed the first genuine effort at utilizing power spectral density to estimate the fatigue damage. Spectral moments of the PSD signal were used to build a relationship among fatigue damage, upward mean crossing and peak obtaining rate. Bendat[138] exhibited the hypothetical statement for the Narrow Band random processes. According to the theory, the spectral moments value can be raised to fourth order to estimate the expected damage of the component. Many authors have proposed the extension of narrow band solution theory to solve broad band problems. These methods include the production of sample time histories from the PSD signal using inverse Fourier Transformation technique and then estimating the PDF of the stress ranges[139],[140],[141],[142].

In 1973, Steinberg[143] published a book where he proposed three band technique to determine fatigue life of electric components. Although, the book focuses on the electric equipment, the theory can be roughly used for many engineering structures including beam, plate and so on. He suggested a mathematical model, where the calculation can be done without large computational effort. According to the proposed method, large amount of random vibration test data can be rearranged to find out the distribution of stress ranges in the frequency domain approach with sensible precision. Dirlik[144] proposed a mathematical equation utilizing Monte Carlo Technique to find out the probability density function of a broad band excitation directly from the power spectral density signal. It calculates the empirical closed form PDF of the stress rainflow ranges as a function of spectral moments.

Wu et al.[145] used a number of aluminum composites to inspect the relevance of different random vibration fatigue life analysis. The outcome showed that application of Morrow's plastic work damage rule can improve the accuracy of estimating fatigue damage using Miner's theory. Moreover, using random vibration theory Rayleigh distribution can be used to determine the PDF of the stress amplitudes. On the other hand, Bishop et al.[66] compared time domain and frequency domain fatigue results for a fixed bracket with a hole inside it. They proposed a fatigue tool to extract rainflow stress ranges from stress PSD which showed a good agreement with the time domain analysis result.

Petrucci[135] utilized a closed form expression to predict life of components under random vibration loading using an irregularity factor instead of using four parameters of PSD calculated from spectral moments. For a narrowband random process the proposed methodology gives solid assessments of the fatigue cycle distribution, with the utilization of the range-mean counting algorithm. Later, he improved his old theory to extend its applicability in high cycle fatigue life prediction of structures experiencing broad band random loading[146]. Fatigue life can be determined from any shape of uniaxial stress PSD. He suggested a relationship between the spectral moments of a PSD and irregularity factor to predict accurate fatigue damage and compared with some other methods to validate its reliability.

Many other frequency domain techniques were introduced during last three decades. Lagoda et al.[147] studied the fatigue damage of multiaxial random loading which showed good agreement with Wirsching-Light method[148]. Percentage Error Index (IEP) was proposed by Braccesi et al.[149] and validated its effectiveness with Dirlik[144], Zhao-Baker[150], Fu-Cebon[151] bi-modal triangular spectra. Tovo[152] suggested a new method to predict fatigue life under broad band loading by establishing relationship between analytical solutions and cycle counting of

expected fatigue damage. Comparing with all other frequency domain fatigue damage calculation techniques, Dirlik's method was suggested to be the most robust and consistent method by most of the authors.

## 2.6 Summary

In this chapter, a large portion of the published literature works in regards to the entire strategy of full vehicle and component AD testing has been discussed elaborately. These days, durability testing of individual component has gained more popularity on account of its capacity to alter the design and assembling procedure at early stages with minimal effort. Nevertheless, the only drawback of component testing is the necessity of accurate test rig and design of appropriate fixture to support the test structure equivalent to the real field condition. In short, the process of AD testing involves accelerated loading profile generation based on the field test, selection of a part and its critical location, instrumentation of sensors and actuators, experimental modal testing, application of appropriate loading, recording stress-strain data and at last calculation of the fatigue damage.

The majority of the steps are just as critical to anticipate a reliable AD test outcome. Both time and frequency domain strategies have been ended up being exact to anticipate theoretical fatigue life of any part. However, as indicated by the current practical experience and statistics of failure, recalls and complaints, current trends of durability testing have been proven to be inaccurate and unreliable in many reports. For instance, the number of recalls has been increased several times over the period of last 14 year in the US market as reported by National Highway Traffic Safety Administration (NHTSA) of American Government[153]. Toyota also reported the similar case as their recall expanded from 8.6 million to 15.2 million from the year 2008 to 2009[154]. There

are many publications where inaccurate durability testing procedure has been stated as one of the basic reasons for anticipation of product fatigue life[155],[156],[157],[158][159],[160].

In this work, test rigs with conventional fixtures have been distinguished as one of the conceivable sources of error in durability testing results. Direct mounting of an automotive component on the hydraulic actuators might alter the dynamic properties of infield condition. The effect of semi rigid boundary condition can be attained by introducing spring and damper element in the laboratory testing facility. Published literatures concerning the effect of spring, damper and tuning natural frequencies have been discussed earlier in this chapter. But direct relation of an elastic foundation to the accelerated durability testing is still unavailable. Therefore, the key feature of this thesis is to establish a platform where the differences between conventional and proposed testing schemes will be discussed using a combination of experimental and numerical analysis.

CHAPTER 3

# 3 MATERIALS AND METHODS

## 3.1 Theoretical Background

In this chapter, the overall theoretical background of the methods used in this thesis will be described briefly. As the main purpose of this work is to show the differences in fatigue damage between the current laboratory situation (Simply-supported beam) and actual field condition (spring-damper supported beam), mathematical modeling related to the mass spring damper boundary condition, SDOF modal parameter extraction techniques and fatigue life calculation methods are presented in the upcoming sections.

### 3.1.1 Transverse Vibration of Beam Type Elements

The fundamental equation of the lateral or transverse vibration of a beam is governed by the Euler-Bernoulli's formula. Figure 7 depicts a beam element OO' of length L, where the bending moment is denoted by $M(x,t)$, shear force is represented by $Q(x,t)$, $w(x,t)$ is the lateral displacement and $f(x,t)$ is the uniformly distributed external load. According to Euler-Bernoulli's theorem, deflection of the beam is assumed to be relatively small with negligible shear deformation[161]. Let us assume, I= Moment of inertia, E= Elastic modulus, A= Cross sectional area, ρ= mass density.

The moment and force equilibrium equation leads to:

$$-M - Q\delta x + M + \frac{\partial M}{\partial x} = 0 \tag{1}$$

$$or, Q = \frac{\partial M}{\partial x} = \frac{\partial}{\partial x}\left(EI\frac{\partial^2 w}{\partial x^2}\right) \tag{2}$$

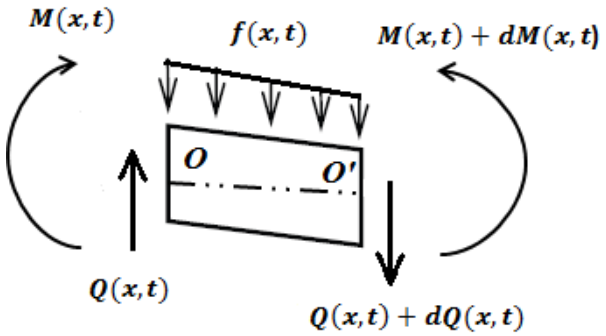


**Figure 7: A beam element in bending**

The equation of the motion can be written as,

$$-(\rho A\delta x)\frac{\partial^2 w}{\partial t^2} = -f(x,t) - Q + Q + \frac{\partial Q}{\partial x} \tag{3}$$

$$or, \qquad \rho A\frac{\partial^2 w}{\partial t^2} + \frac{\partial Q}{\partial x} = f(x,t) \tag{4}$$

Substituting equation (2) into equation (4) leads to,

$$EI\frac{\partial^4 w}{\partial x^4}(x,t) + \rho A\frac{\partial^2 w}{\partial t^2}(x,t) = f(x,t) \tag{5}$$

In case of free vibration analysis, the effect of the external force is neglected i.e. $f(x,t) = 0$. Hence, equation (5) can be rewritten as,

$$EI\frac{\partial^4 w}{\partial x^4}(x,t) + \rho A\frac{\partial^2 w}{\partial t^2}(x,t) = 0 \tag{6}$$

$$or, c^2 \frac{\partial^4 w}{\partial x^4}(x,t) + \frac{\partial^2 w}{\partial t^2}(x,t) = 0 \tag{7}$$

$$where, c = \sqrt{\frac{EI}{\rho A}} \tag{8}$$

Using the variable separation method, solution of the free vibration analysis can be found.

$$w(x,t) = W(x).T(t) \tag{9}$$

Substituting equation (9) into equation (7),

$$\frac{c^2}{W(x)} \frac{d^4 W(x)}{dx^4} = -\frac{1}{T(t)} \frac{d^2 T(t)}{dt^2} = \omega^2 \tag{10}$$

Where, $\omega^2$ can be defined as a constant. Reconstructing equation(10) gives,

$$\frac{d^4 W(x)}{dx^4} - \beta^4 W(x) = 0 \tag{11}$$

$$\frac{d^2 T(t)}{dt^2} + \omega^2 T(t) = 0 \tag{12}$$

$$\text{Where, } \beta^4 = \frac{\omega^2}{c^2} = \frac{\rho A \omega^2}{EI} \tag{13}$$

The solution of equation (11) can be expressed as-

$$W(x) = A_1 cos\beta x + A_2 sin\beta x + A_3 cosh\beta x + A_4 sinh\beta x \tag{14}$$

Where, $A_1, A_2, A_3, A_4$ in each case are different constants which can be found from the boundary conditions. So the fundamental natural frequency can be determined from equation (13) as,

$$\omega = \beta^2 \sqrt{\frac{EI}{\rho A}} = (\beta L)^2 \sqrt{\frac{EI}{\rho A L^4}} \tag{15}$$

#### 3.1.1.1 Beam with Rigid Pin Support

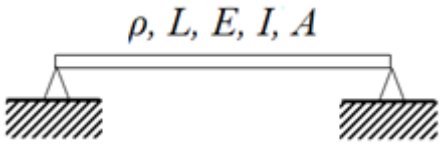


**Figure 8: Beam supported by rigid joint**

For a simply/rigidly supported beam we get the boundary conditions as,

**Table 1: Boundary condition of a simply supported beam.**

| At $x$=0 | | At $x$=$L$ | |
|---|---|---|---|
| BC-1 | $W(0) = 0$ | BC-3 | $W(L) = 0$ |
| BC-2 | $EI\frac{d^2W(0)}{dx^2} = 0$ | BC-4 | $EI\frac{d^2W(L)}{dx^2} = 0$ |

Inserting the values in equation (14) we get,

$$A_1 + A_3 = 0 \tag{16}$$

$$\beta^2(A_3 - A_1) = 0 \tag{17}$$

$$A_1 cos\beta L + A_2 sin\beta L + A_3 cosh\beta L + A_4 sinh\beta L = 0 \tag{18}$$

$$\beta^2(-A_1 cos\beta L - A_2 sin\beta L + A_3 cosh\beta L + A_4 sinh\beta L) = 0 \tag{19}$$

By putting the results in a matrix form we get,

$$\begin{bmatrix} 1 & 0 & 1 & 0 \\ -1 & 0 & 1 & 0 \\ cos\beta L & sin\beta L & cosh\beta L & sinh\beta L \\ -cos\beta L & -sin\beta L & cosh\beta L & sinh\beta L \end{bmatrix} \begin{Bmatrix} A_1 \\ A_2 \\ A_3 \\ A_4 \end{Bmatrix} = \begin{Bmatrix} 0 \\ 0 \\ 0 \\ 0 \end{Bmatrix} \tag{20}$$

Determinant of the matrix (D) equals to 0 for a non-trivial solution.

So we get, $sin\beta L = 0$

$$\beta L = n\pi \; for \; n = 1,2,3 \ldots\ldots$$

From equation (15) we get the natural frequency-

$$\omega_n = n^2\pi^2\sqrt{\frac{EI}{\rho AL^4}} \tag{21}$$

### 3.1.1.2 Beam with semi-rigid/elastic support:

Let us consider a beam connected with equal mass (m) and spring constant (k) at both ends. For the simplicity of calculation the effect of damper in the free vibration has been neglected. $F_0$ and $F_L$ is the force exerted by the mass-spring system at *x=0* and *x=L* respectively

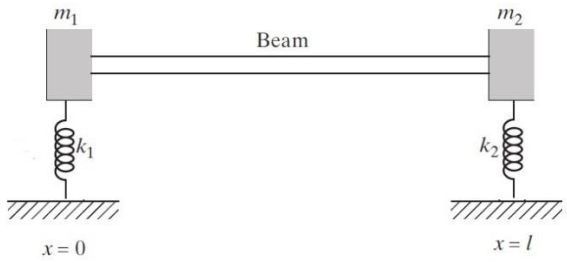


**Figure 9: Beam connected with mass and spring at both end[162]**

For a semi-rigid beam we get the boundary conditions as,

**Table 2: Boundary condition of an elastically supported beam.**

| At x=0 | | At *x=L* | |
|---|---|---|---|
| BC-1 | $EI\frac{\partial^3}{\partial x^3}[W(x).T(t)] = -F_0$ | BC-3 | $EI\frac{\partial^3}{\partial x^3}[W(x).T(t)] = F_L$ |
| BC-2 | $EI\frac{d^2W(x)}{dx^2} = 0$ | BC-4 | $EI\frac{d^2W(x)}{dx^2} = 0$ |

For boundary condition 1,

$$EI\frac{\partial^3}{\partial x^3}[W(x).T(t)] = -F_0 \tag{22}$$

$$or, EI\frac{\partial^3}{\partial x^3}[W(x).T(t)] = -k_1[W(x).T(t)] - m_1\frac{\partial^2}{\partial t^2}[W(x).T(t)] \tag{23}$$

$$or, EIT(t)\frac{\partial^3}{\partial x^3}[W(x)] = -k_1T(t)[W(x)] - m_1W(x)\frac{\partial^2}{\partial t^2}[T(t)] \tag{24}$$

$$\text{Let, } T(t) = Ae^{i\omega t} \tag{25}$$

$$\text{or, } \frac{d^2T(t)}{dt^2} = -\omega^2T(t) \tag{26}$$

Using equation (24), $$EI\frac{d^3W(0)}{dx^3} = -k_1W(0) + m_1\omega^2W(0) \tag{27}$$

Similarly for boundary condition 3,

$$EI\frac{d^3W(L)}{dx^3} = k_2W(L) - m_2\omega^2W(L) \tag{28}$$

#### 3.1.1.3 Non-dimensional analysis:

From the above mentioned equations one can simply determine the natural frequencies for a specific beam. To make it more general, the following equations have been constructed which can be used to predict the non-dimensional natural frequencies irrespective of shape and mechanical properties of the structure.

Non dimensional natural frequency, $B^2 = \sqrt{\frac{\rho AL^4\omega^2}{EI}}$ (29)

Contact/Joint stiffness, $K = \sqrt{\frac{kL^3}{EI}}$ where, k is the spring stiffness (30)

Mass ratio, $M = \frac{m}{\rho AL} = \frac{\text{point mass}}{\text{beam mass}}$ (31)

### 3.1.2 Modal Parameter Estimation

From the literature review section, we already know that modal parameters can be extracted using both frequency domain and time domain methods. In this work, modal parameters have been estimated using SDOF curve fitting technique in frequency domain and logarithmic decrement technique in time domain analysis.

#### 3.1.2.1 Frequency Domain Curve Fitting Method

In reality, structures can have infinite number of modes which are impossible to measure due to time and cost constraints. The properties of the modes can be easily defined considering a small subset of frequency response function (FRF). Sufficient points should be chosen on the structure to define the mode shapes. Usually one row or column of a FRF matrix is enough to correctly extract damping and natural frequencies as these are the global parameters. The measurement and response points should be chosen carefully so that it does not coincide into any nodal point of any mode; otherwise that mode would not be excited during the measurement. Hence, accurate measurement of FRF is the most important part to estimate reliable parameters.

FRF is defined as the ratio of Fourier transform of output signal to Fourier transform of input signal. Mathematically it can be written as,

$$H(\omega) = \frac{X(\omega)}{F(\omega)} \quad (32)$$

In this equation, $H(\omega)$= Frequency response function,

$X(\omega)$= Fourier Transform of Output signal

$F(\omega)$= Fourier Transform out Input signal

During experiment, random noise and nonlinearity can affect the quality of the FRF. In order to get accurate FRF measurements different types of estimators are used based on the Tri-Spectrum Averaging approach. In this method three spectral are estimated from two time domain signals (input and output) which include two Auto Power Spectral (APS) and one Cross Power Spectral (XPS). APS can be found by multiplying a signal with its complex conjugate and XPS is achieved by multiplying a complex conjugate of spectrum with a different spectrum.

For noise on the output measurement $H_1$ estimator is used and $H_2$ estimator is used for a measurement if the input signal is noisy.

$$H_1(\omega) = \frac{XPS(\omega)}{Input\ APS(\omega)} \tag{33}$$

$$H_2(\omega) = \frac{Output\ APS(\omega)}{XPS(\omega)} \tag{34}$$

In order to perform SDOF curve fit, it is assumed that the modes are well separated with light modal density. This method is simple to use and it is expected that resonance behavior around the frequency is almost fully dominated by that particular mode.

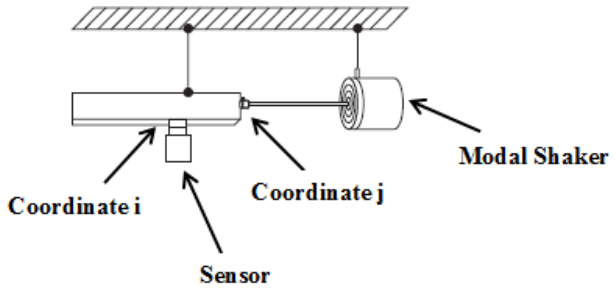


**Figure 10: Experimental FRF measurement**

**Table 3: Variables used in FRF calculation**

| | |
|---|---|
| $\omega$ | Frequency of external force (rad/sec) |
| $N$ | Degrees of freedom (=1 for SDOF system) |
| $\omega_k$ | Natural frequency for mode k (rad/sec) |
| $\omega_{dk}$ | Damped natural frequency for mode k |
| $\xi_k$ | Damping ratio for mode k |
| $\Phi_{ik}$ | Modal displacement at response DOF |
| $\Phi_{jk}$ | Modal displacement at excitation DOF |
| $A_k$ | Residue for mode k |
| $A_k *$ | Complex conjugate of residue for mode k |
| σ | Decay rate |
| $p$ | Pole location |
| $M_k$ | Modal mass |
| $a_k$ | Scaling constant |
| Q | Quality factor |

The modal parameter model for a SDOF FRF can be written as,

$$H_{ij}(\omega) = \frac{A_k}{j\omega - p} + \frac{A_k *}{j\omega - p *} \tag{35}$$

Residue of any mode can be expressed as, $A_k = a_k . \Phi_{ik} . \Phi_{jk}$ (36)

For a driving point measurement where the response and excitation correspond to the same point,

$$A_k = a_k . {\Phi_{ik}}^2 \tag{37}$$

In equation (37), the value of $A_k$ and $\Phi_{ik}$ is known, so the scaling factor $a_k$ can be determined easily. Equation (36) and (37) are necessary only for scaling the mode shapes. Modified equation of residue, pole location, damped natural frequency and decay rate are-

$$A_k = -j\frac{1}{2M_k\omega_{dk}} \tag{38}$$

$$A_k *= j\frac{1}{2M_k\omega_{dk}} \tag{39}$$

$$p = \sigma + \mathrm{j}\omega_{dk} \tag{40}$$

$$p *= \sigma - \mathrm{j}\omega_{dk} \tag{41}$$

$$\omega_{dk} = \omega_k\sqrt{1-\xi_k^2} \tag{42}$$

$$\sigma^2 = \omega_k^2 - \omega_{dk}^2 \tag{43}$$

Equation (35) can be expanded for a MDOF system using the following equation[163],

$$H_{ij}(\omega) = \sum_{k=1}^{N}\left(\frac{A_k}{j\omega - p} + \frac{A_k *}{j\omega - p *}\right) \tag{44}$$

Putting equation (38) to (42) into equation (35) will yield to a curve fitting equation to determine the modal parameters. A set of trial functions can be generated by varying the natural frequencies $\omega_k$, damping ratios $\xi_k$ and modal mass $M_k$. Then each trial function is subtracted from the experimental data. The function with the least residual error is used to obtain modal parameters.

The damping ratio can also be obtained using Half Power Bandwidth method. Once the peak of the FRF function is determined, the -3dB slope from the peak amplitude will yield to the half power point.

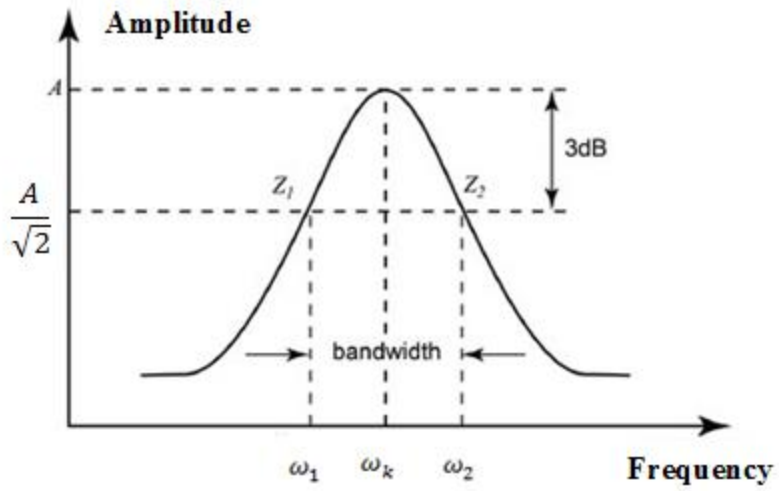


**Figure 11: Half-Power bandwidth method[164]**

The quality factor (Q) of the function is attained by,

$$Q = \frac{\omega_k}{\Delta\omega} = \frac{\omega_k}{\omega_2 - \omega_1} \tag{45}$$

$$Q = \frac{1}{2\xi_k} \tag{46}$$

### 3.1.2.2 Time Domain Curve Fitting Method:

As the dynamic response of a damped system decays over time, free vibration equation of a damped structure can be used to determine the natural frequency and damping using time domain curve fit method. The equation can be stated as-

$$y(t) = \sum_{k=1}^{n} Xe^{-\xi_k \omega_k t} \sin(\omega_{dk} t + \theta) \tag{47}$$

Here, $y(t) =$ Amplitude function

t = time

X = Amplitude constant

$\theta$ = Phase angle

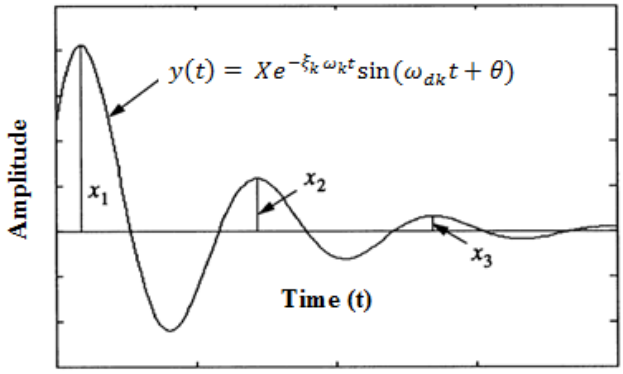


**Figure 12: Logarithmic decrement**

Free vibration equation of any structure can be assumed to be sum of a number of sinusoids. At first, random numbers are generated for each variable in equation (47). Using trial and error method the closest result with the experimental data is chosen to be appropriate function to extract the modal parameters. However, the method is accurate to estimate the natural frequency and damping of first couple of modes. Longer time history should be avoided in this technique.

### 3.1.3 SDOF Base Excitation Response

A structure can be excited in different ways e.g. direct excitation, rotating eccentric mass, base motion etc. A vehicle running on the road experiences irregular loads transferred via tire and suspension systems. For the simplification of calculation the mathematical modeling of a SDOF system experiencing harmonic base excitation will be investigated in this section.

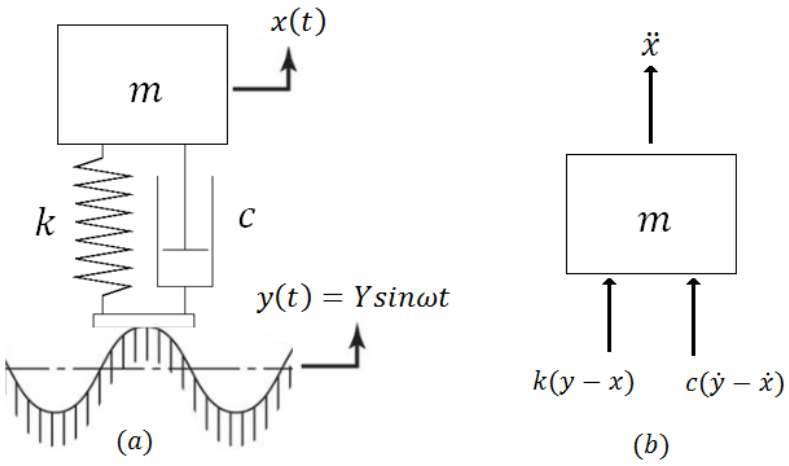


**Figure 13: Base excitation, (a) SDOF system (b) free body diagram**

Figure 13 depicts a SDOF system experiencing harmonic base excitation where mass, stiffness and damping coefficient is represented by m, k and c respectively. Let's say, x(t) is the absolute displacement of the mass and y(t) is the input base displacement. From the free body diagram we can write the force equivalent equation as-

$$\sum F = m\ddot{x} \tag{48}$$

$$m\ddot{x} = -k(x-y) - c(\dot{x}-\dot{y}) \tag{49}$$

$$m\ddot{x} + c\dot{x} + kx = c\dot{y} + ky \tag{50}$$

Let, $y(t) = Y sin\omega t$ (51)

Here, ω is the excitation frequency and Y denotes the amplitude of the forcing function. Using equation (51) equation (50) yields,

$$m\ddot{x} + c\dot{x} + kx = c\omega Y cos(\omega t) + kY sin(\omega t) \tag{52}$$

For a linear system the solution of the steady state can be found using superposition of the two individual particular solutions. Hence, the particular solution of the system will be equal to the sum of the individual particular solution of above mentioned sin and cosine forcing functions.

By convention,

$$\frac{c}{m} = 2\xi\omega_n \tag{53}$$

$$\frac{k}{m} = \omega_n^2 \tag{54}$$

Where, $\omega_n$ is the natural frequency of the system and $\xi$ is the damping ratio. From equation (52),

$$\ddot{x} + 2\xi\dot{x} + \omega_n^2 x = 2\xi\omega_n\omega Y cos(\omega t) + \omega_n^2 Y sin(\omega t) \tag{55}$$

Assume, $F_1 = 2\xi\omega_n\omega Y$ and $F_2 = \omega_n^2 Y$. So according to superposition theorem, equation (55) can be separated as-

$$\ddot{x} + 2\xi\dot{x} + \omega_n^2 x = F_1 cos(\omega t) \tag{56}$$

$$\ddot{x} + 2\xi\dot{x} + \omega_n^2 x = F_2 sin(\omega t) \tag{57}$$

Let, particular solution of equation (56) and (57) be $x_{1p}$ and $x_{2p}$. Using rectangular form,

$$x_{1p} = A_1 cos\omega t + B_1 sin\omega t \tag{58}$$

$$x_{2p} = A_2 cos\omega t + B_2 sin\omega t \tag{59}$$

According to literature[165] the value of constants $A_1, A_2, B_1, B_2$ can be found as,

$$A_1 = \frac{(\omega_n^2 - \omega^2)F_1}{(\omega_n^2 - \omega^2)^2 + (2\xi\omega_n\omega)^2} \tag{60}$$

$$B_1 = \frac{2\xi\omega_n\omega F_1}{(\omega_n^2 - \omega^2)^2 + (2\xi\omega_n\omega)^2} \tag{61}$$

$$A_2 = \frac{-2\xi\omega_n\omega F_2}{(\omega_n^2 - \omega^2)^2 + (2\xi\omega_n\omega)^2} \tag{62}$$

$$B_2 = \frac{(\omega_n^2 - \omega^2)F_2}{(\omega_n^2 - \omega^2)^2 + (2\xi\omega_n\omega)^2} \tag{63}$$

Now adding the sin and cosine terms to get the magnitude of the full particular solution,

$$X = \sqrt{\frac{F_1^2 + F_2^2}{(\omega_n^2 - \omega^2)^2 + (2\xi\omega_n\omega)^2}} = \omega_n Y \sqrt{\frac{(2\xi\omega_n)^2 + \omega_n^2}{(\omega_n^2 - \omega^2)^2 + (2\xi\omega_n\omega)^2}} \tag{64}$$

If $\gamma = \omega/\omega_n$, equation (64) becomes,

$$\frac{X}{Y} = \sqrt{\frac{1 + (2\xi\gamma)^2}{(1 - \gamma^2)^2 + (2\xi\gamma)^2}} \tag{65}$$

Using equation (65) one can find out the steady state displacement of the response. Velocity and acceleration response may be obtained by successive differentiation.

### 3.1.4 Vibration testing

The main purpose of vibration testing is to qualify the product against the standards in the laboratory condition i.e. to obtain natural frequency and damping, locate critical location and failure modes etc. Several types of vibration tests are carried out based on the usage of any product. Out of those, sine-sweep and random vibration profiles are the most common type of excitation signal used to evaluate defects, ruggedness and durability.

#### 3.1.4.1 Sine-Sweep Vibration Test

Sine-Sweep excitation is the most widely used vibration testing signal where the excitation frequency is varied periodically starting from the lower range to the upper range of interest or vice versa with constant or different amplitude. This type of excitation is basically used to

analyse whether the model has met its specification or not, specifically in the resonance zone. Again the effect of individual frequency of excitation range can be recognized by sweeping the frequency of interest. The amplitude can be increased or decreased to simulate the real world testing environment. However, the sweep rate should be slow enough to reach to the steady state condition. The sweep rate can be varied either linearly or logarithmically with time. The theoretical overview of logarithmic sine sweep excitation will be addressed in the following section.

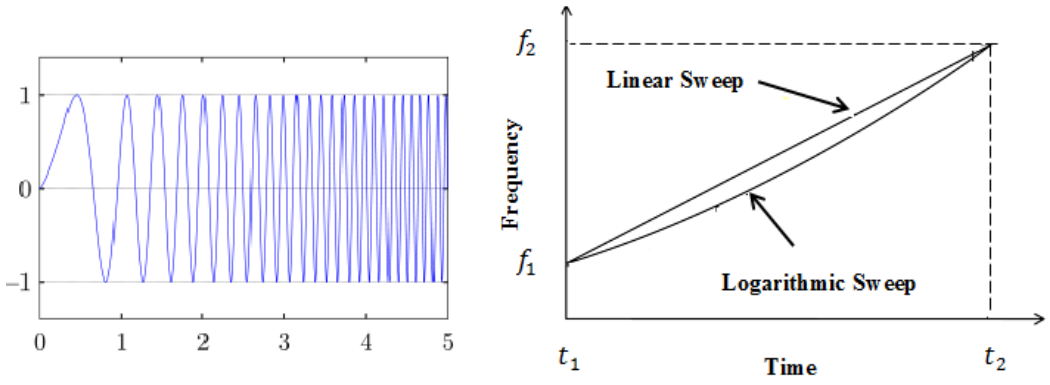


**Figure 14: Sine sweep parameters**

**Table 4: Variable description of sine sweep parameters[166]**

| | |
|---|---|
| $f_1$ | Starting Frequency (Hz) |
| $f_2$ | Final Frequency (Hz) |
| $t_1$ | Starting time (sec) |
| $t_2$ | Ending time (sec) |
| $t$ | Elapsed time (sec) |
| $F_{spec}$ | Frequency in spectral domain |

| | |
|---|---|
| $F_{time}$ | Frequency in time domain sine argument |
| $C$ | Number of accumulated cycle |
| N | Number of Octaves |
| R | Sweep Rate (oct/time) |

The fundamental representation for a unity amplitude sine wave,

$$Y(t) = sin\{2\pi[F_{time}]t\} \tag{66}$$

$$\text{Or, } Y(t) = sin\{2\pi[C(t)]\} \tag{67}$$

Number of octaves can be calculated,

$$N = \frac{ln[\frac{f_2}{f_1}]}{ln[2]} \tag{68}$$

Sweep Rate can be defined as,

$$R = \frac{N}{t_2 - t_1} \tag{69}$$

The spectral function for logarithmic sweep can be written as ,

$$F_{spec}(t) = [f_1]\left[2^{R(t-t_1)}\right] \tag{70}$$

Hence the cycle equation would be,

$$C(t) = \int_{t_1}^{t} \{[f_1]\left[2^{R(t-t_1)}\right]\} dt \tag{71}$$

Integrating from $t_1 = 0$ to $t = t$, according to reference[167] we get,

$$C(t) = \frac{\{[f_1][-1 + 2^{Rt}]\}}{R\ ln[2]} \tag{72}$$

So the time domain argument would be,

$$F_{time} = \frac{\{[f_1][-1 + 2^{Rt}]\}}{Rt\ ln[2]} \tag{73}$$

Final equation of a logarithmic sine-sweep excitation for unity amplitude would be,

$$Y(t) = sin\left\{2\pi\left\{\frac{[f_1][-1+2^{Rt}]}{R\ln[2]}\right\}\right\} \tag{74}$$

Sine-Sweep excitation is not the true loading case of automobile running on the road. Actually the input loads are the combination of random and sinusoidal vibration. Due to the simplicity and convenience of test setup this kind of loading is still used by the automotive company to meet the primary design requirements.

#### 3.1.4.2 Random Vibration Test

Random vibration is the most common type of excitation for the mechanical equipment i.e. wind turbine, earthquake, vehicle travelling on road due to surface roughness. Random Vibration by definition referred to the non-periodic and non-deterministic signal. It contains multitude of frequencies at a time. All the responses of the random vibration analysis are the standard deviation of the results and not the actual. Due to the non-deterministic properties, this kind of vibration is treated as probabilistic or statistical approach. In spite of the fact that the instantaneous amplitude of an arbitrary vibration can't be connected numerically as an exact function of time, it is conceivable to determine the probability of occurrence using statistical aspects. In frequency domain, Power Spectral Density (PSD) is used as the input for random vibration analysis.

From the time history of Figure 15, it can be noticed that although the amplitude differs from time to time, the signal is oscillating with almost zero mean value. Multiplying the signal with itself result in a function with positive value and non-zero mean value. This kind of signal is called Auto-correlation function which will be used to characterize random vibration. The mean value of the squared amplitude time history is the root mean square value (RMS).

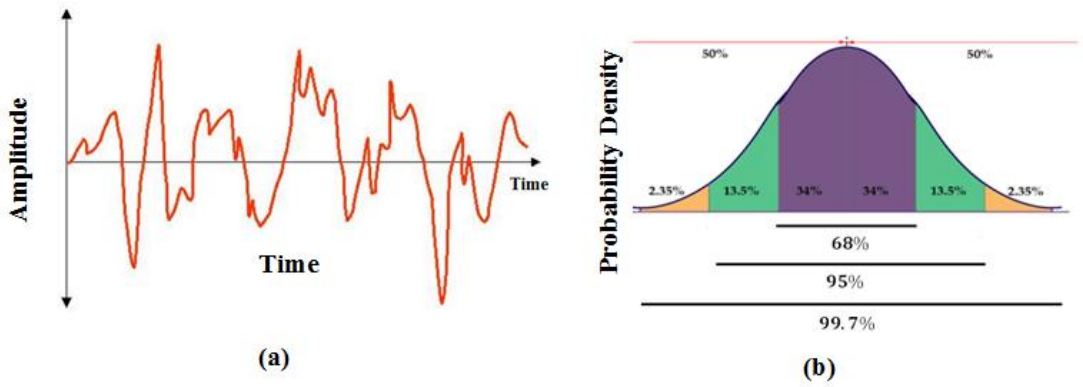


**Figure 15: Random vibration; (a) Time history (b) Probability density function**

Normal or bell shaped distribution (Gaussian) is the most common form of PDF which can be denoted as,

$$f(x|\mu,\sigma) = \frac{1}{\sigma\sqrt{2\pi}} e^{-\frac{(x-\mu)^2}{2\sigma^2}} \tag{75}$$

Here, μ is the mean of the distribution, σ is the standard deviation and $\sigma^2$ is the variance. The probability of the amplitude is given in terms of standard deviation.

**Table 5: Probability of a Normal Distribution**

| Range | Probability |
|---|---|
| 1σ | 68% |
| 2σ | 95% |
| 3σ | 99.7% |

#### 3.1.4.2.1 Power Spectral Density (PSD)

Power Spectral Density, well known by its abbreviation PSD is the spectrum plot used to illustrate the amplitude content in the frequency domain. It gives a statistical representation of a stationary random process which shows the distribution of average power of a response signal for each frequency. Looking at the PSD one can get idea about the position where most of the energy is concentrated in a frequency band. Actually large time histories are very time consuming and expensive to analysis. PSD can deal with this limitation by introducing statistical approach rather than a deterministic method. Time histories are said to be deterministic as one can easily determine the actual amplitude at any point in time. Again, the Fourier Transformation is also deterministic as all the frequency, amplitude and phase information can be found using inversion law. The main disadvantage of FT is it stores all the amplitude and phase related information in complex manner. For ergodic Gaussian random process the phase angles are solely random with a constant probability distribution between $-\pi$ to $+\pi$. As a result, storing phase information is unnecessary while the amplitude information is the most relevant with the analysis. Though PSD does not contain any phase information, it has therefore been proved that calculation process with PSD is much easier and faster.

Figure 16 represents an one sided PSD where the area under the PSD curve gives the mean square of the overall acceleration. The unit of acceleration PSD is given as $g^2/Hz$. During PSD calculation from time history the total frequency range is split into individual ranges called bins using bandpass filters. Then the response is squared to normalize it and divided by the bin bandwidth to calculate the average power. Hence, the average power will remain constant irrespective of the frequency bandwidth.

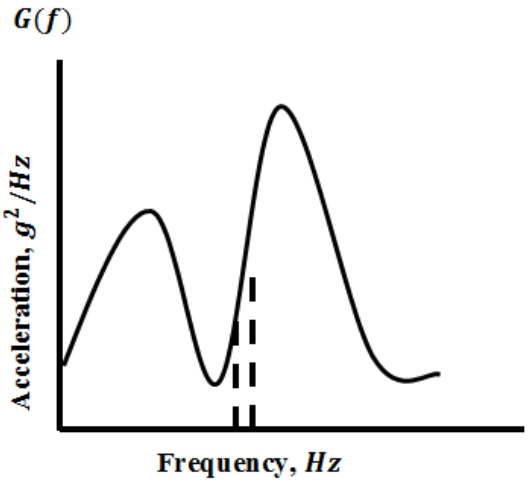


**Figure 16: PDF of a Power Spectral Density**

The Fourier Transform F of any time history can be defined as,

$$X(f) = \int_{-\infty}^{\infty} x(t)e^{-j2\pi ft}dt = F\big(x(t)\big) \tag{76}$$

The inverse of Fourier Transform can be calculated as,

$$X(t) = \int_{-\infty}^{\infty} x(f)e^{j2\pi ft}df = F^{-1}\big(x(f)\big) \tag{77}$$

The Autocorrelation function with a time lag τ,

$$R_{xx}(\tau) = \int_{-\infty}^{\infty} x(t)x(t+\tau)dt = E[x(t)x(t+\tau)] \tag{78}$$

Fourier Transformation pair is used to relate auto-spectrum function with the autocorrelation function for a two sided PSD as ,

$$S_{xx}(f) = \int_{-\infty}^{\infty} R_{xx}(\tau)e^{-j2\pi f\tau}\,d\tau \tag{79}$$

One sided PSD $G_{xx}(f)$ can be defined for $0 \leq f < \infty$,

$$G_{xx}(f) = 2S_{xx}(f) \tag{80}$$

According to the theory of random vibration, the response of the system to a single input PSD is-

$$S_{out}(\omega) = |H(\omega)|^2 S_{in}(\omega) \tag{81}$$

$$S_{out}(\omega) = \left(\frac{a_{out}}{a_{in}}\right)^2 S_{in}(\omega) \tag{82}$$

Here,

$S_{out}(\omega)$ = Response PSD

$S_{in}(\omega)$ = Excitation PSD

$H(\omega)$ = Transfer function

$a_{out}$ = Sinusoidal response

$a_{in}$ = Sinusoidal excitation

### 3.1.4.3 Fatigue Damage Estimation

Fatigue failure is the most common type of phenomena for a structure undergoing dynamic loading situation. As a result, fatigue design has become one of the most important parameters for automobile engineers. The reason of fatigue failure is the cyclic loading for a large amount of time. Even the structure experiencing much lower load than the yield or ultimate tensile strength is also susceptible for fatigue failure. Fatigue failure for a ductile material starts with the formation of nuclear crack inside any structure. The crack at first grows locally and then propagates to the points of higher tensile stress. At last fatigue failure occurs when the effective area of the applied load reduces to a certain limit.

Fatigue behavior is affected by a number of parameters e.g. stress concentration, surface roughness, environmental condition, surface conditioning, temperature etc. Any of these parameters may completely alter the fatigue life of a structure. Fatigue phenomena can be

described for a time dependent periodic signal where maximum stress is considered as $\sigma_{max}$ and $\sigma_{min}$ is the minimum stress.

The amplitude of the stress cycle can be defined as,

$$\sigma_a = \frac{\sigma_{max} - \sigma_{min}}{2}$$

And the mean stress,

$$\sigma_m = \frac{\sigma_{max} + \sigma_{min}}{2}$$

Stress ratio,

$$R = \frac{\sigma_{min}}{\sigma_{max}}$$

#### 3.1.4.3.1 Stress-Life Method

A structure can resist a number of stress cycles before it fails which can be directly combined with the stress amplitude to characterize the fatigue failure through S-N curve. In this curve, experimental stress response (S) is plotted along Y axis and the number of Cycles (N) or number of reversals (2N) is plotted along X axis. There are a few materials (e.g. ferrous alloys) which exhibits endurance limit of stress under which the material will never fail even if it undergoes unlimited amount of load cycles. Apart from that, rest of the materials will certainly fail even if the stress amplitude is quite below UTS.

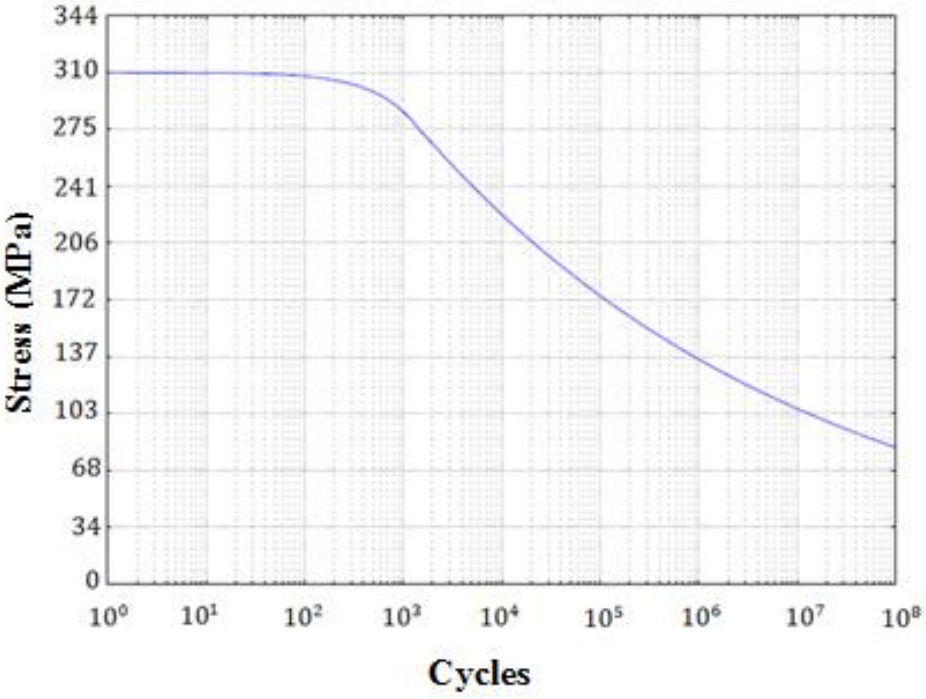


**Figure 17: S-N Curve for Aluminum 6061-T6[168]**

A characteristic S-N diagram is appeared in Figure 17 for Aluminum Alloy 6061-T6 with unity stress ratio and concentration factor which will be used as a reference for this thesis. According to stress life approach the log-log plot can be defined mathematically using power law relationship as,

$$\sigma_a = \sigma_f' N^b \tag{83}$$

Here, $\sigma_f'$is the fatigue strength coefficient and b is called fatigue strength exponent or Basquin's slope. If the stress amplitude is simply denoted by S, then we can re-write equation (83)-

$$SN^{-b} = \sigma_f' \tag{84}$$

$$NS^{-\frac{1}{b}} = {\sigma_f'}^{-\frac{1}{b}} \tag{85}$$

$$Let, m = -\frac{1}{b} = Inverse\ fatigue\ exponent \tag{86}$$

$$NS^m = {\sigma_f'}^m \tag{87}$$

Usually the value of Basquin's slope stays in the range of b= -0.12 to -0.05 or m=8 to20 for most of the metals. The value of m can be found using the following equation,

$$m = \frac{log(2N_e)}{log(\frac{\sigma_f'}{S_e'})} \tag{88}$$

Where, $S_e'$ is the endurance limit and $N_e$is the number of cycles required for failure in endurance strength. By definition, fatigue strength coefficient or $\sigma_f'$ is the stress required to fail within half cycle or one full reversal. The characteristic equation for the S-N curve plotted in Figure 17 is,

$$log10(S) \propto -0.108log10(N) \tag{89}$$

From the above relation the value of the inverse fatigue exponent can be found as, m=9.26. According to equation (87) it can be said that small change in Basquin's slope may result in a huge variation in fatigue damage as the power is raised by m.

For the above mentioned equations it is assumed that there is no mean stress effect. But in real fatigue life largely depends on the mean stress range. As indicated by the theory[169] tensile or positive mean stress lowers the fatigue live, whereas compressive or negative mean stress increases the life of the component. Many researchers have provided useful theories for mean stress correction out of which Goodman's proposal is widely recognized which is based on the UTS.

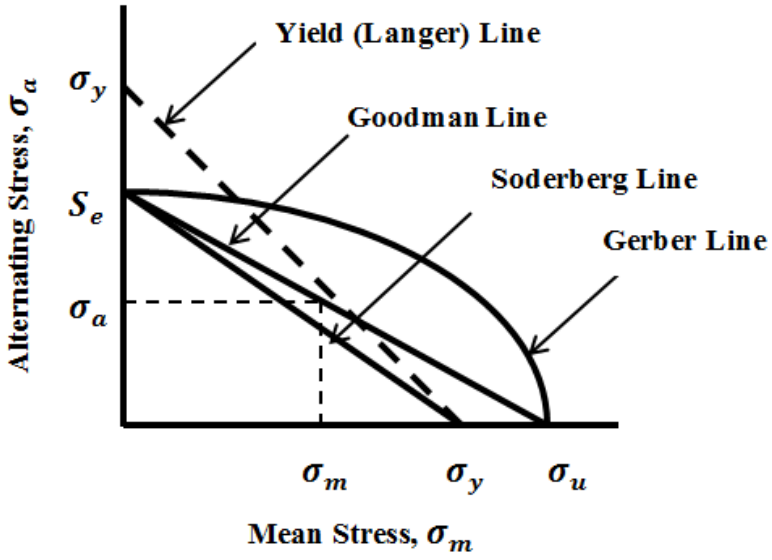


**Figure 18: Mean Stress Modification Lines**

According to Goodman's Model, $$\frac{\sigma_a}{\sigma_a'} + \frac{\sigma_m}{\sigma_u} = 1 \quad (90)$$

Where, $\sigma_a'$ is the equivalent alternating stress and $\sigma_u$is the mean stress of the metal.

#### 3.1.4.3.2 Cumulative Fatigue Damage Model

Any structure can sustain dynamic loadings up to a specific amount of cycles. There might be a number of sources or cycles which can cause fatigue damage. To simplify the effect of each cycle of variable amplitude loading, Miner[31] suggested the most straightforward model which is called 'Cumulative Damage Model'.

Let, n be the total number of cycles a component experiences for a specific stress amplitude and N be the number of cycles required to produce fatigue failure for that stress amplitude limit. According to Miner, total damage of the component will be,

$$D = \sum_{i=1}^{k} \frac{n_i}{N_i} \tag{91}$$

Where, k is the total number of cycles. Usually fatigue failure takes place when D=1, but sometimes a safety factor (Say, D=0.7) is used to make it more conservative.

#### 3.1.4.3.3 Rainflow Cycle Counting Method in Time Domain

Accurate counting of stress reversals is considered to be the most critical part of the fatigue damage estimation process. Rainflow cycle counting algorithm is a unique approach to count the number of stress cycles from a random amplitude time history that was first proposed by two Japanese professor Endo and Matsuishi[123]. They relate the stress reversals with the stream of water flowing off a Pagoda roof which was originally based on the closed loop hysteresis approach. This method allows one to use Miner's cumulative damage theory once the variable amplitude cycle counting is done. Rainflow Cycle counting algorithm can be explained as below[66]:

- At first a sequence of peaks and valleys are extracted from a reduced time history so that the cycles are easily identified.
- Then the plot is rotated 90 degrees to keep time data along Y axis and stress amplitude along X axis.
- Water flow is made from each tensile peak.
- Half cycles are counted based on the following three occurrences:
    - If the rain water merges with a flow coming from earlier tensile peak
    - If it reaches to the finishing point of the time history
    - If it faces a valley of higher magnitude.
- The above mentioned step is repeated for each compressive valley.

- Each half cycle is then assigned to a stress range equal to the difference of starting and end point.
- At last, full cycles are counted by pairing the half cycles of equal and opposite magnitude.

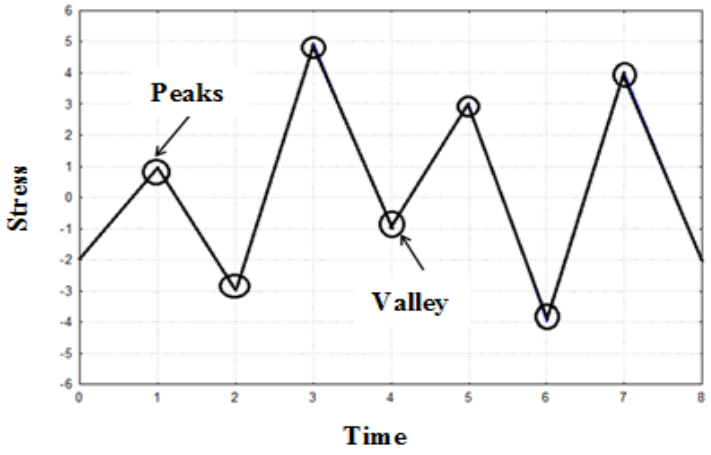


**Figure 19: Arrangement of Peak and Valleys of a Time History**

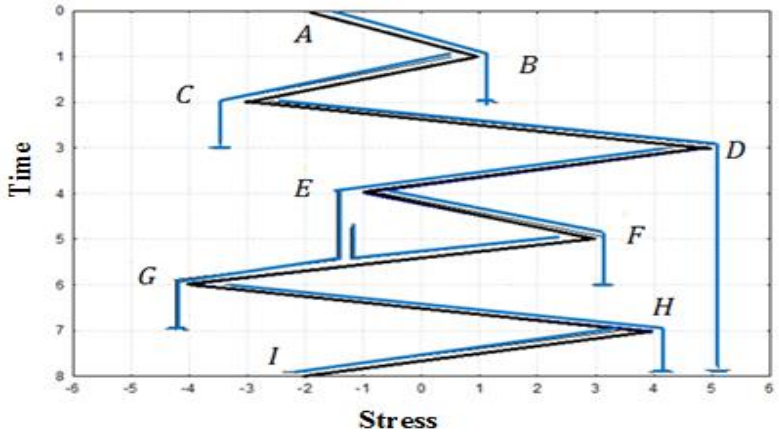


**Figure 20: Rainflow Cycle Counting Process[171]**

From Figure 20, the number of full and half cycles can be counted easily. Starting from point A to B the rain water drops to the previously started stream CD, hence it will be counted as a half

cycle. Same thing happens for BC as it falls off to another stream of water DG. But in case of EF it is counted as a full cycle as the flow is abandoned by a stream of water coming from earlier tensile peak of higher magnitude D. As a result, A-B, B-C, C-D, D-G, G-H and H-I are treated as half cycles and only E-F is treated as a full cycle.

#### 3.1.4.3.4 Frequency Domain Cycle Counting Method

The theory of Power Spectral Density (PSD) can be utilized to calculate the amplitude content of a time history in frequency domain. Spectral moments are calculated in frequency domain from the output stress PSD curve. The rate of upward peak and zero crossings are found from the PDF of output stress using the concept of spectral moments. At last, fatigue damage of the structure is obtained using the S-N curve and Miner's cumulative damage theorem. Spectral moments of a one sided PSD plot can be calculated as,

$$m_n = \int_0^\infty f^n \, G(f) df \tag{92}$$

Here, m is the spectral moment, n is the number of moment, f representing the frequency in Hz and G(f) is a one sided PSD. For fatigue damage calculation the moments are taken up to $4^{th}$ order. Putting n=0 in equation equals to the variance of a zero mean PSD which is called the $0^{th}$ moment. The square root of the $0^{th}$ moment results in the RMS of the total plot. The first moment is the mean (μ) of the random process which is equal to zero for a random shaker process. The second moment is the derivative of the variance $\sigma_{\dot{x}}^2$. Third and fourth moments are signal's skewness and kurtosis respectively. Skewness measures the positive or negative biasness of a signal and kurtosis measures the shape or peakedness of the random variable PDF.

So the RMS or the standard deviation (Mean, μ=0) of the signal is,

$$\sigma_x = \sqrt{m_0} \tag{93}$$

Irregularity factor or spread of the random process signal,

$$\alpha_i = \frac{m_i}{\sqrt{m_0 m_{2i}}} \tag{94}$$

Vanmarcke's parameter[172],

$$\delta = \sqrt{1 - {\alpha_1}^2} \tag{95}$$

Spectral width is defined as,

$$\kappa = \sqrt{1 - {\alpha_2}^2} \tag{96}$$

Expected rate of peak occurrence,

$$v_p = \sqrt{\frac{m_4}{m_2}} \tag{97}$$

Rate of zero crossings,

$$v_0 = \sqrt{\frac{m_2}{m_0}} \tag{98}$$

Expected rate of peak occurrence,

$$v_p = \sqrt{\frac{m_4}{m_2}} \tag{99}$$

According to Dirlik[144] stress ranges are weighted from the extensive Monte Carlo Simulation as sum of e thexponential and Rayleigh distribution. Number of cycles would be,

$$N(S) = v_p . T . p(S) \tag{100}$$

Here, T is time period and $p(S)$ is the PDF of the random process.

Final equation for the PDF is,

$$p(S) = \frac{\frac{D_1}{Q} e^{-\frac{Z}{Q}} + \frac{D_2 Z}{R^2} e^{-\frac{Z^2}{2R^2}} + D_3 . Z . e^{-\frac{Z^2}{2}}}{2\sqrt{m_0}} \tag{101}$$

Here,

$$Z = \frac{S}{2\sqrt{m_0}}, \qquad \gamma = \frac{m_2}{\sqrt{m_0 m_4}},$$

$$x_m = \frac{m_1}{m_0} . \sqrt{\frac{m_2}{m_4}},$$

$$D_1 = \frac{2(x_m - \gamma^2)}{1+\gamma^2},$$

$$D_2 = \frac{1 - \gamma - D_1 + D_1^2}{1 - R}$$

$$D_3 = 1 - D_1 - D_2,$$

$$Q = \frac{1.25(\gamma - D_3 - D_2 . R)}{D_1},$$

$$R = \frac{\gamma - x_m - D_1^2}{1 - \gamma - D_1 + D_1^2}$$

## 3.2 Experimental Setup

Prior to the numerical analysis, experimental modal analysis was conducted to extract the dynamic properties i.e. natural frequencies, damping and mode shapes of both of the experimental setups using a modal shaker assembly which was later utilized to tune those properties in FEM to solve base excitation problem. Sine-Sweep and random vibration response tests were also experimentally validated with the FEM model. As the main theme of this work is to compare the fatigue damage between two different boundary conditions (rigid and elastic), the experimental fixtures were designed such a way so that both of the tests can be performed using a single setup.

### 3.2.1 Design of Fixtures

Reliability of an accelerated durability test mostly depends on the testing environment and boundary conditions. That's why design of accurate jigs and fixtures is one of the most critical benchmarks that must be fulfilled while performing an accelerated laboratory test. The general trend of current lab test includes a rigid fixture to mount the test piece directly with the shaker table. In this work, both rigid and an elastic fixtures were designed to compare their dynamic properties. The following criteria were considered while designing the fixture:

(a) First natural frequency of the beam with elastic or semi-rigid fixture must fall within the range of 7-12 Hz as this is the common range of natural frequency of suspension system components for most of the ground vehicles[173]. As the natural frequency of the beam increases with higher stiffness support/boundary conditions, the natural frequency of the beam with rigid foundation is higher than the beam with elastic foundation.

(b) Damping ratio of the elastic support system should be at least 2% to take its effect into consideration[173].

(c) Both Sine-Sweep and random vibration input signals were limited to 5-80 Hz bandwidth for the simplicity of the test. The effect of all the 'out of band modes' will be negligible in this excitation range.

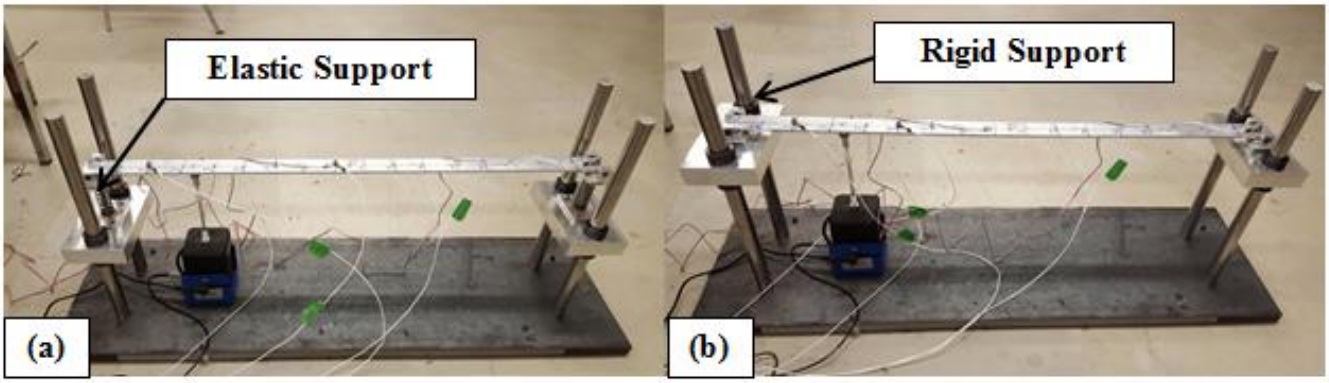


**Figure 21: Experimental Configurations: (a) Elastic Support, (b) Rigid Support**

**Table 6: Physical constants of the test piece**

| | |
|---|---|
| Material | Aluminum 6061-T6 |
| Length | 85 cm |
| Cross-section | $3.81 \times 0.48\ cm^2$ |
| Modulus of Elasticity | 68.9 GPa |
| Density | $2700\ kg/m^3$ |
| Poisson Ratio | 0.33 |

The base of the installation was produced using high quality steel ASTM A108 with a length of 107 cm, width of 30.40 cm and thickness of 2.54 cm. Total mass of the base was 64 kg which

was more than 150 times heavier than the mass of the beam so that it behaves as a rigid body while coupled with the modal shaker. Four unbending shafts were connected to the base utilizing liquid nitrogen to fit firmly inside the openings. Two primary base plates made of Aluminum were used so that the stature can be balanced inside the poles by sliding through the length of the pole. The Aluminum plates were tightened along the shaft using steel made collars. These plates were used to hold the rigid or elastically supported beam. A modal shaker with a stinger was placed firmly on the base with the help of double sided scotch tape adhesive as in Figure 21. The rigid support was attained by simply connecting the beam with the secondary base with pin joint. In case of, elastic support the pin joint was placed over a uniaxial spring and linear bearing-shaft housing which is presented in Figure 22.

**Figure 22: Bearing and Shaft Housing**

The stiffness of the uniaxial spring made of steel alloy was measured using MTS tensile test machine as shown in Figure 23. Spring with 3000-5000 N/m stiffness is preferred to keep the first natural frequency of the beam within 7-12 Hz range. Measured spring constant was found to be 3857 N/m which lies into the desired range.

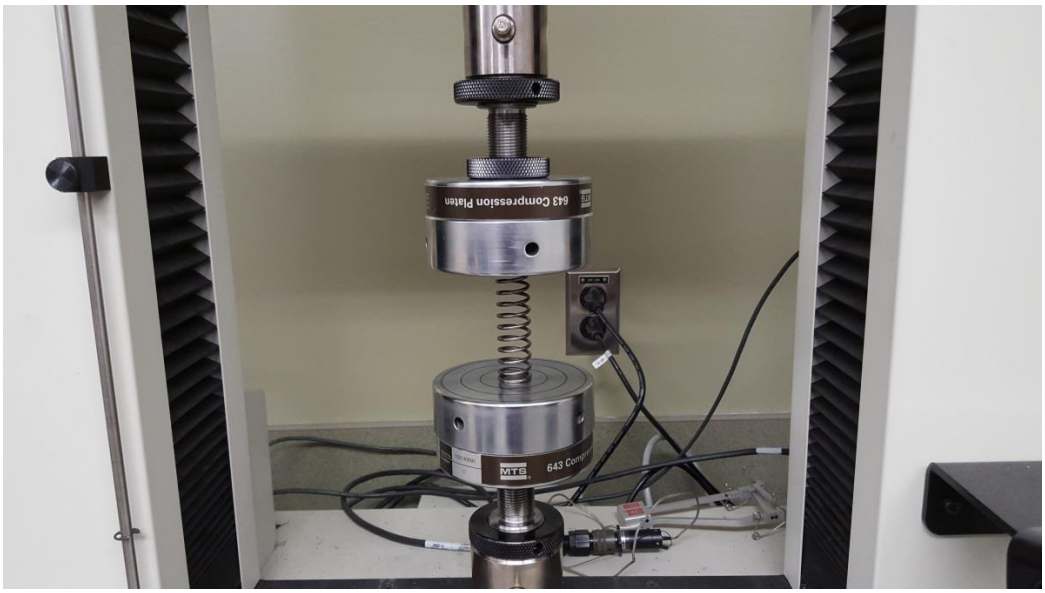


**Figure 23: Measurement of Spring Constant**

### 3.2.2 Modal Shaker

A portable modal shaker was used in the experiment instead of a shaker table. Modal shaker is relatively small and can be used to excite one point at a time; it does not have any controller to control the exact input parameters. In this experiment a mini smart shaker (Model no: K2007 E01) manufactured by TMS was used with integrated power amplifier. The capacity of the shaker is 31.14 N peak to peak forces for sine excitation and 22.24 N RMS for random excitation signals with a stroke length of 13 mm. This modal shaker consists of a rugged suspension system made of carbon fibre composite lead armature flexures. The modal shaker is directly connected with a stinger to measure uniaxial force responses. This stinger connects the test piece with the modal shaker and reduces transferring side loads from shaker to the test object. A force sensor was placed in between the stinger and test piece to divorce the stinger effect from the structure. Figure 24 offers a typical representation of instruments and connections used during a modal test event.

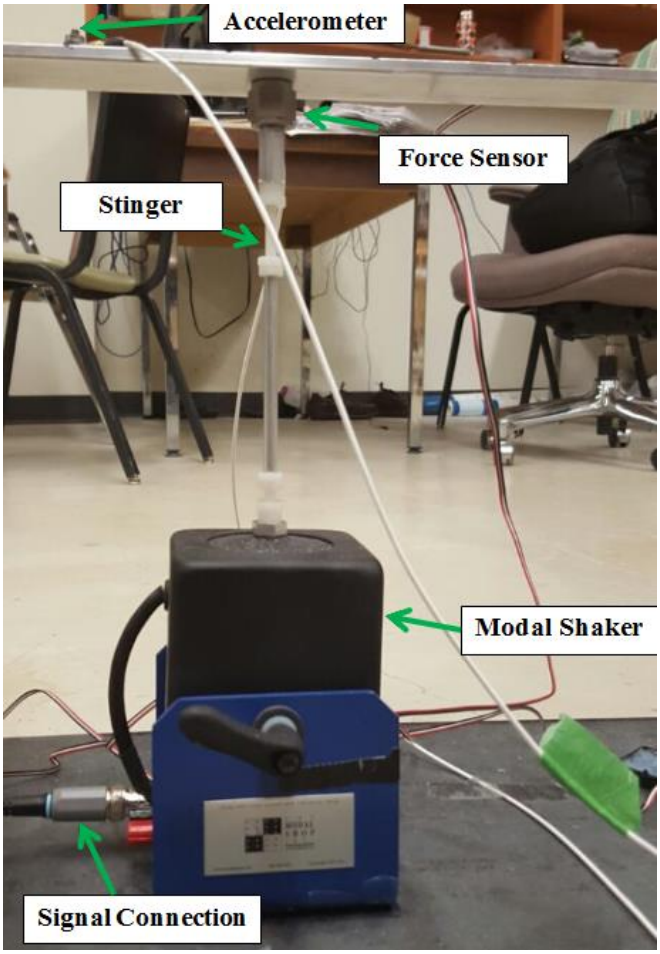


**Figure 24: Modal Test Setup**

### 3.2.3 Sensors

In this work a dynamic piezoelectric force sensor of ICP type (Model no: 208C01) was used to collect the input load data. The input loading data is important for accurate measurement of FRF. As there was no controller used to regulate the input level, trial and error method was used to achieve a particular input value. Sensitivity of the sensor was 112410 mV/kN with a mass of 22.7 gm and excitation voltage range of 18 to 30 VDC. The sensor had a 10-32 female mounting thread to connect with the stinger. As indicated in Figure 25, the top surface was used to directly connect with the test structure.


**Figure 25: Dynamic Force Sensor**

Two types of output measurement sensors were used in this experiment. First one was piezoelectric accelerometer (Model no: 352C65) from Dalimar Instruments to measure the acceleration in the direction of vibration. This accelerometer was selected because of its low weight (2 gm) and high shock resistance limit (±5000 g peak). Quick bonding silica gel was used as an adhesive to bond it with the structure. And other type of sensor was a Vishay Micro Measurements uniaxial strain gauge (Model no: C2A-13-062LW-350) to measure bending strain of the beam as shown in Figure 26.

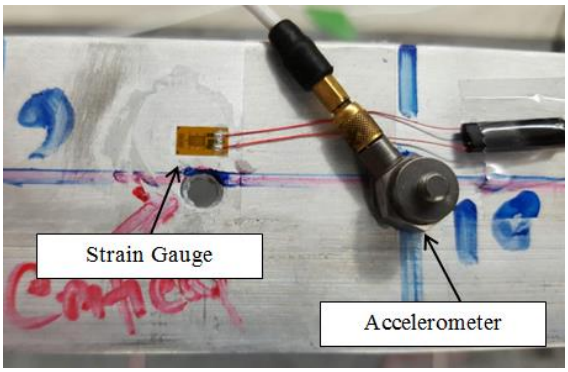


**Figure 26: Strain Gauge and Accelerometer Attachment**

### 3.2.4 Data Acquisition Systems

As the name implies, data acquisition system or DAQs are used to capture the data automatically from a physical system and converts it to a machine readable format for analysing. Sometimes sensors convert the physical property to electrical signal e.g. voltage or current (force transducers, accelerometers) and sometimes correspond to electrical characteristic like resistance, capacitance (strain gauge) which can be converted to electrical signal afterwards. In this work, three types of DAQs were used to collect and send data. Quanser QPIDe data acquisition system was used to generate sinusoidal and random loading and transfer it to the modal shaker. Accuracy and consistency were the main reasons to choose this DAQ over the signal generators. MATLAB Simulink was utilized to generate signal and pass it to the modal shaker.


**Figure 27: Signal Generation, (a) Quanser DAQ, (b) Simulink Diagram**

Force and acceleration responses were measured by a four channel sound and vibration measurement DAQ system (DT 9837) from Data Translation. A versatile FFT analyzer named QuickDAQ was used to read data from the DAQ board and produce time history and frequency

responses to acquire test measurements. Before starting any measurement there is an interface to calibrate the sensors in that particular software.

| Channel | Enable | Channel Name | Ref/Resp | Range | Coupling | Current Source | Engineering Unit (EU) | mV/EU | EU Offset | Point # | Comment | Dir |
|---|---|---|---|---|---|---|---|---|---|---|---|---|
| DT9837(00)-0 | ☑ | Ain 0 | Referen... | -1V to 1V | AC | ☑ | N | 115.09... | 0 | 1 | | X+ |
| DT9837(00)-1 | ☑ | Ain 1 | Response | -1V to 1V | AC | ☑ | g | 100.5 | 0 | 2 | | X+ |
| DT9837(00)-2 | ☑ | Ain 2 | Response | -1V to 1V | AC | ☑ | g | 97.099... | 0 | 3 | | X+ |
| DT9837(00)-3 | ☑ | Ain 3 | Response | -1V to 1V | AC | ☑ | g | 97.599... | 0 | 4 | | X+ |

Tach Channels

| Channel | Enable | Channel Name | Engineering Unit (EU) | Ticks/Rev | Max RPM | RPM Multiplier | Max mSec/Hz | Tach Edge | Comment |
|---|---|---|---|---|---|---|---|---|---|
| DT9837(00)-4 | ☐ | Tach 0 | RPM | 100 | 1000 | 1 | | Rising | |

**Figure 28: Calibration of Sensors**

Strain gauge data were collected using a 32 channel Strain-Smart data acquisition system (Model no: 7000-32-SM). To obtain the data at the same time sampling frequency was set to 3000 Hz and all the three DAQs were triggered using rising edge voltage method.

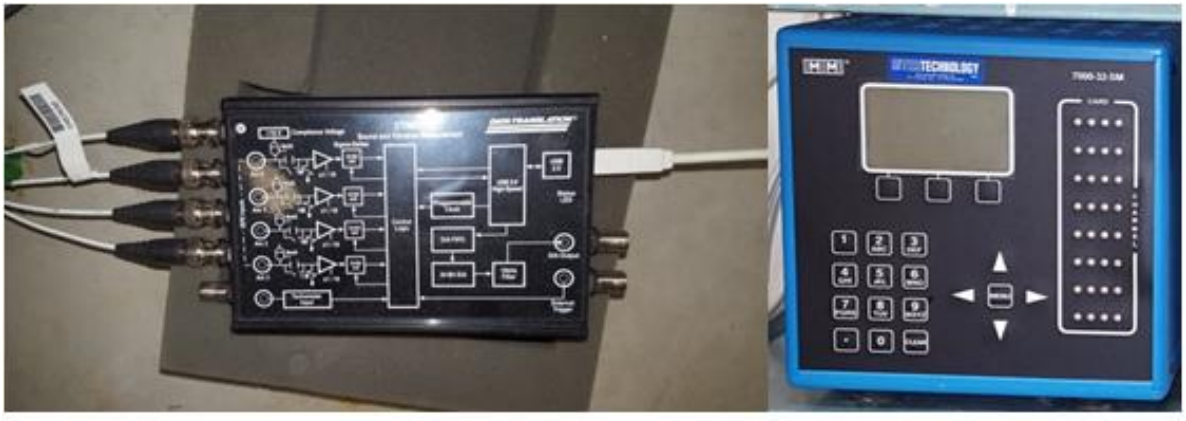


**Figure 29: Data Acquisition System, (a) Acceleration and Force Measurement, (b) Strain Measurement**

### 3.2.5 Experimental Methodology

The experimental setup was designed such a way so that the boundary condition at each end can be changed using nut bolt mechanism. At first, the position and alignment of the modal shaker was set properly to minimize the effect of side force and twisting. During modal testing the excitation point was kept constant and response locations were varied.

The beam was divided into 18 points each were 5 cm apart from each other to properly obtain the mode shape. The location of driving point was set in between point 14 and 15 to avoid exciting any of the nodal points as shown in Figure 30. This is a crucial part of modal testing because if any of the response or excitation point coincides within a nodal point that mode would not be excited.

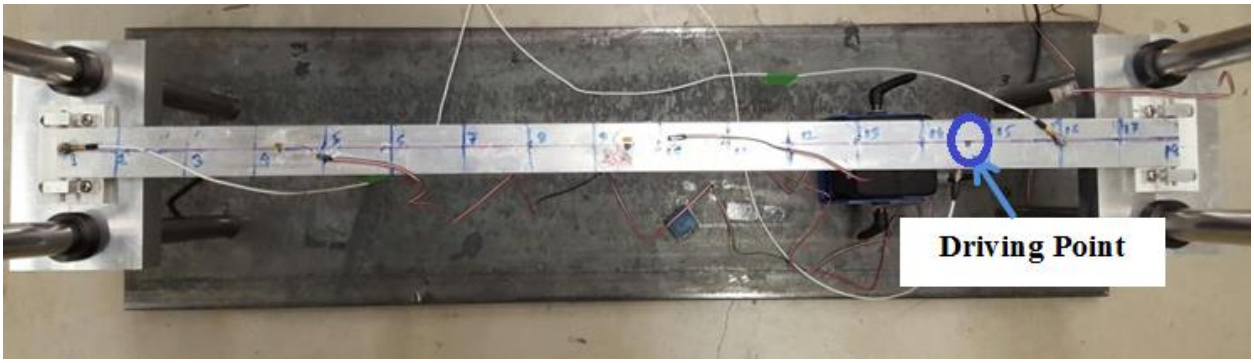


**Figure 30: Measurement Points**

At first the resonance frequencies were identified by simply sweeping the frequency from 5 Hz to 80 Hz with a rate of 0.20 octaves/minute as the input excitation of the beam. The frequencies were recorded up to 512 spectral lines with 0.095 Hz resolution. Then a closer sine sweep test was carried out in 5 Hz frequency range of each resonance zone to accurately obtain the modal

parameter for that particular mode. The sweep rate of the excitation signal was kept very low (e.g. 0.029 octaves/minute) to get the exact pole location which is very important for damping calculation. These steps were performed separately for the elastic and rigid boundary conditions to compare the differences.

## 3.3 Finite Element Modeling

The main reason of performing FEM analysis is to calibrate the dynamic properties obtained from experimental modal tests and later accomplish numerical fatigue analysis using base excitation technique in FEM. Necessary geometry changes and implementation of accurate boundary conditions were performed to make the behavior of the test piece close to real world.

### 3.3.1 Numerical Methodology

Firstly, a 3D CAD geometry was created in SolidWorks which was later transferred to ANSYS Workbench. One hole was made in the middle of the geometry for stress concentration purpose which is the highest amplitude position of first bending mode and another two were made to connect the stinger of the shaker directly with the structure. The model was made of Aluminum 6061-T6 alloy and assumed to be linear, homogeneous and isotropic elastic with insignificant humidity and temperature effect. Before analysing, fine mesh of the beam was achieved through hex dominant method.

For convergence study, the number of elements was increased near the hole by using sphere of influence method. A sphere of approximately 1 cm radius with 0.45 mm element size was used near the holes which showed a good convergence agreement that has been shown in Figure 31. Total 38,486 elements have been utilized to define a proper mesh to obtain consistency in the stress output result.

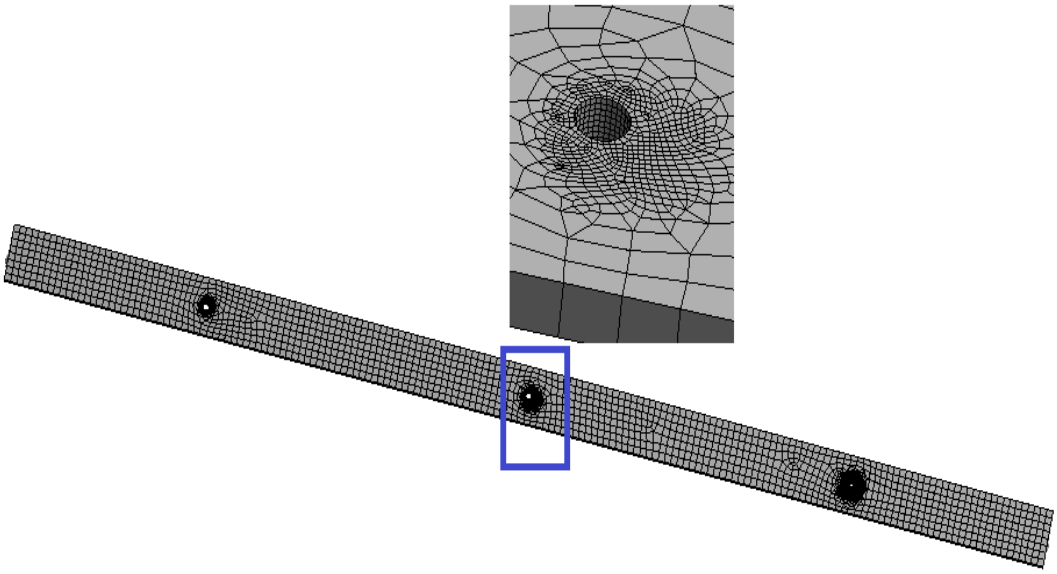

**Figure 31: Meshed Model of the Beam using Hex Dominant Method.**

The boundary condition of the elastically supported beam was tuned using point mass (A & B) and spring at both ends as shown in Figure 32. Though the damping constant has a negligible amount of effect on the natural frequency of the structure it was not considered during calibrating natural frequency. The beam was placed horizontally and both point and base excitation forces were applied vertically. Hence, all other degrees of freedom were restrained except the vertical displacement and rotation along horizontal or Z axis. Body to body connection was made during applying a spring boundary condition at the end between the beam and a rigid square piece of block. Figure 32 depicts the overall boundary condition used during modeling a semi-rigid beam.

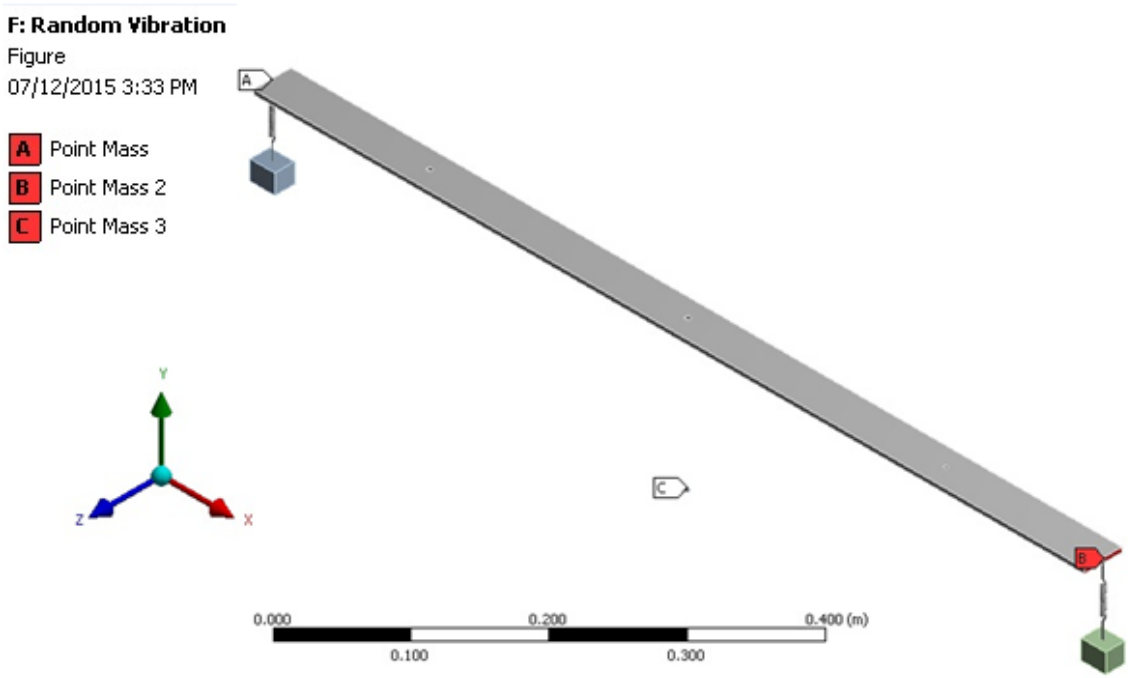


**Figure 32: Semi-Rigid Boundary condition in FEM**

Before performing any kind of response analysis in ANSYS, modal analysis is a pre-requisite for modal superposition method as shown in Figure 33. In this work, three kind of response analysis were executed e.g. harmonic analysis to achieve stress or acceleration transfer function, modal transient analysis and random vibration analysis to perform fatigue analysis. Same structures and boundary conditions were used for each method. Random vibration needs a small amount of calculation time where PSD is used as an input. Modal transient analysis is time consuming and more deterministic and will give the actual test results for a specific (60 sec in this work) time history. Hence, both methods were used to compare their results which actually showed a good agreement in the overall RMS response value.

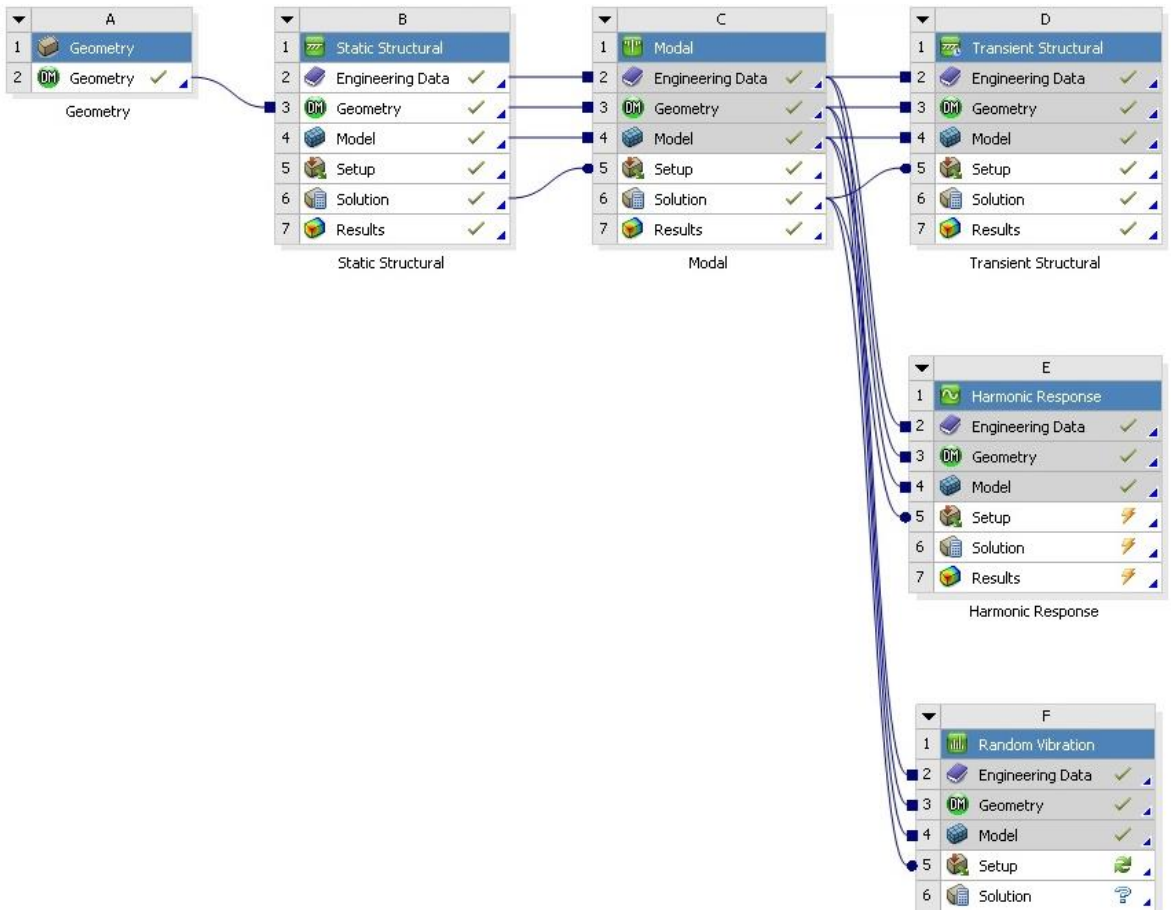


**Figure 33: ANSYS Project Schematic Diagram**

### 3.3.2 Large Mass Method (LMM)

Usually ANSYS is not capable of applying direct base acceleration to the nodal degrees of freedom of any kind of structure in harmonic and transient analysis. Hence, an alternative approach to apply base excitation has been developed which is called Large Mass Method[174]. In Figure 32, point C indicates the large mass that was utilized during this work. The main principle of this method is using a fictitious large mass (M) coupled rigidly with the base of the structure and applying a force F=Ma to the degrees of freedom along the direction of motion. The mass selected for this purpose has to be at least $10^7$ times larger than the mass of the structure. Then the base accelerations are multiplied with the mass to provide base acceleration

to the structure which is shown in Figure 34. A short ANSYS APDL code has to be written during this analysis where at first the DOF of the large mass is locked to restrain rigid body motion along Y axis and later the lock was removed once the modal analysis was done before applying the base excitation force.

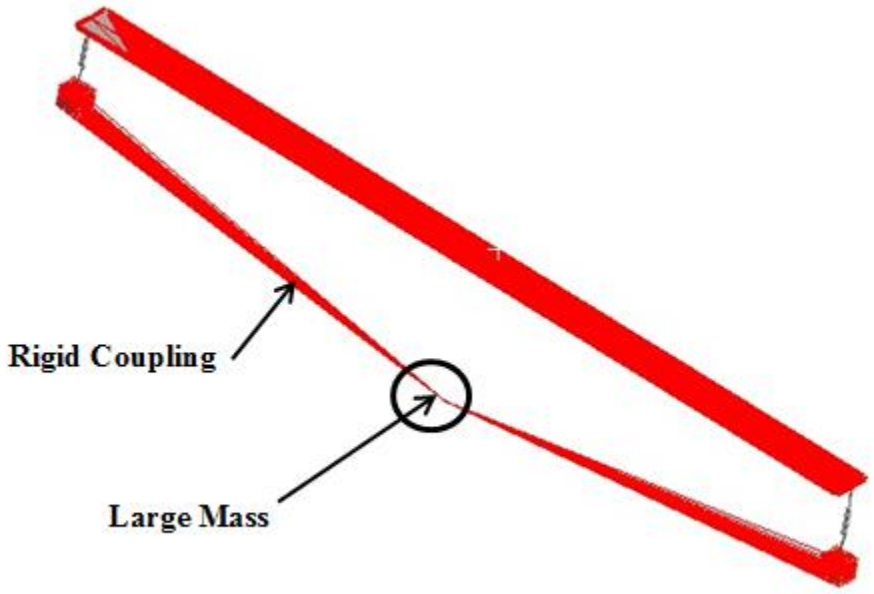


**Figure 34: Large Mass Method Utilized in ANSYS Workbench**

### 3.4 Process Flow of a Random Vibration Test

The main theme of AD testing is to increase loading intensity near the natural frequency zone so that the structure fails earlier. Loading profiles are obtained using the loads coming from different road surface and then processed in terms of SRS, ERS and FDS. Though the validation of the real world loading is not a primary concern in this work, therefore a dummy loading was used throughout the work. Here the beam with elastic foundation was assumed to be an original vehicle with suspension and tire assembly. That's why a simple road surface load was applied to

this particular structure to attain the output acceleration PSD of the test piece. Later, this response acceleration PSD was used as an input loading profile for fatigue testing of both elastic and rigid foundation. The input PSD for fatigue testing was accelerated to increase the overall RMS of the input PSD. In this thesis, overall RMS was increased by multiplying with integers but was always kept below the acceleration level that corresponds to the tensile strength of the material.

In Figure 35, the numerical process flow of fatigue analysis using FEM is described for a random test process. A full period loading profile was generated by simply applying a military standard loading specification to the original vehicle (elastically supported beam in this case). Here, the military standard loading was assumed to behave like loads coming from road surface. Once the output acceleration was found, it was multiplied with different acceleration factor before using as input for fatigue testing. Then, this full period acceleration PSD was converted to 60 sec time history using inverse Fourier transformation and low pass filtering (considered loadings only below 80 Hz). This 60 sec partial loading was fed to both elastically and rigidly supported beam structures to obtain fatigue damage using rainflow cycle counting in time domain analysis. For frequency domain random vibration analysis, the PSD was directly applied to the structures with elastic and rigid supports to obtain dynamic response in the frequency domain. Stress PSD obtained at each critical point was fed to Dirlik's cycle counting algorithm to get the fatigue damage of the test piece.

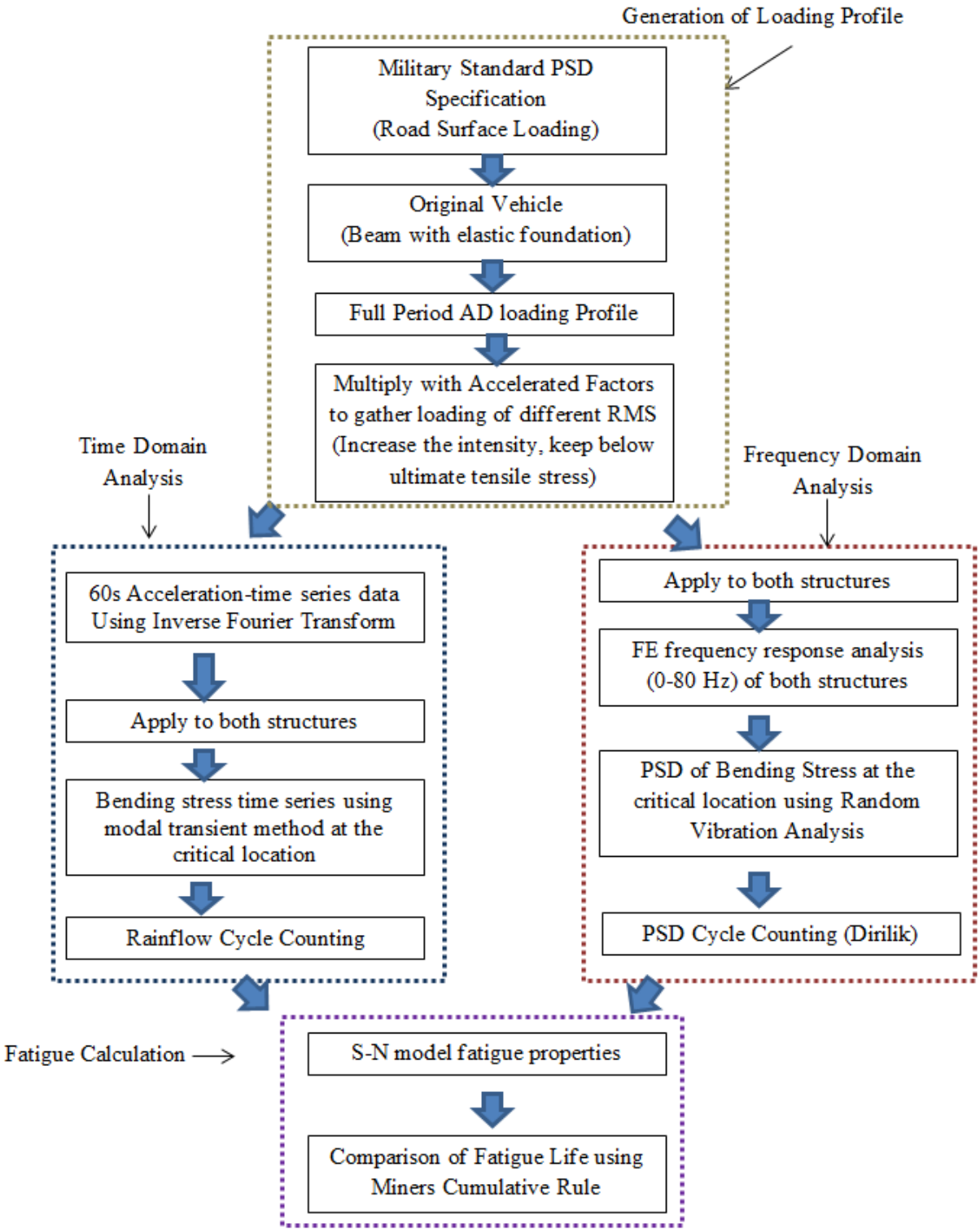


**Figure 35: Process Flow of AD Testing**

# CHAPTER 4

# 4 RESULTS AND DISCUSSIONS

This section can be categorized into three subdivisions. Firstly, the effect of elastic foundation on the dynamic properties is discussed. In the second section, results of the experimental modal analysis and the calibration of FE model based on those results are presented. At last, a comparison of fatigue life between conventional (Rigid Support) and modified (Elastic Support) test rig is discussed based on numerical vibration fatigue testing using the combination of ANSYS Workbench and MATLAB software.

## 4.1 Theoretical Results

Dynamic properties e.g. natural frequencies, damping ratios and mode shapes are hugely affected by the boundary condition of any structure. In reality, vehicles are supported by the combination of suspension systems and tires. These things can be modeled as the combination of mass, spring and damper. In this work, a beam was treated as a small subcomponent of a vehicle and support stiffness was chosen based on the joint stiffness of that particular beam. In Figure 36, the change of the dimensionless natural frequencies with respect to the joint stiffness has been demonstrated. The reason for using dimensionless term is due to the fact that different types of spring stiffness would have different effects on different sizes of beams. To avoid parameter related problems everything was brought into the same platform. Both natural frequency and joint stiffness are the

dimensionless terms. Joint stiffness is the ratio between the spring stiffness to the flexural rigidity of that beam.

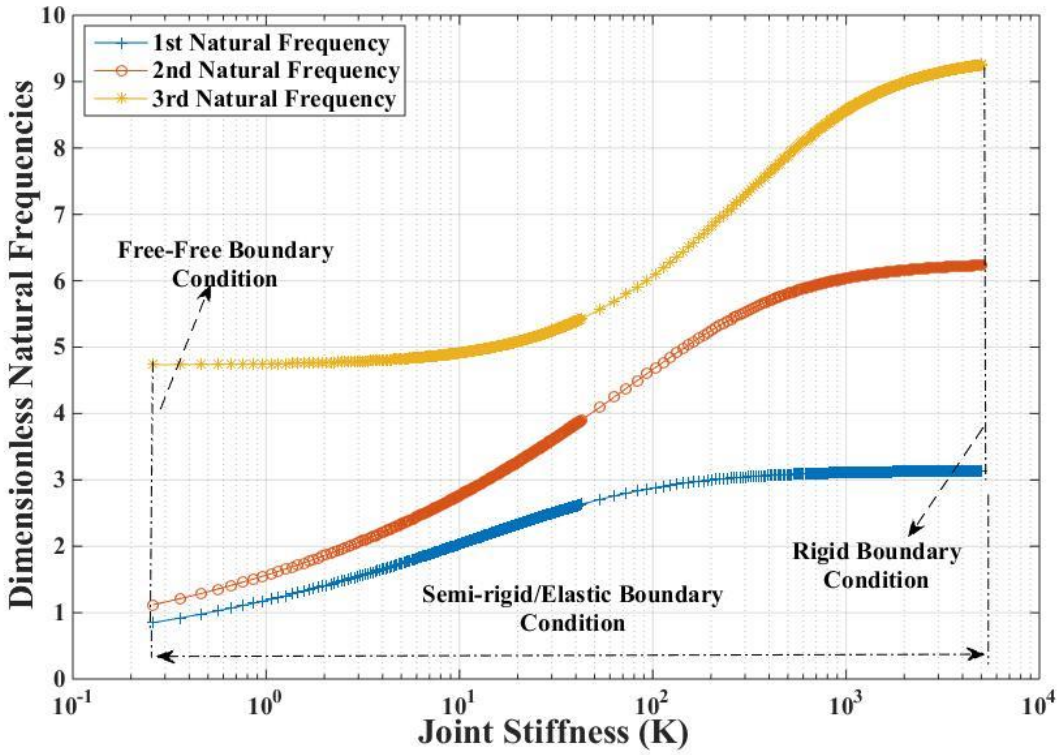


**Figure 36: Effect of Spring Constant on Natural Frequencies of the Structure**

From the plot it can be noticed that with the increase of joint stiffness, natural frequencies also increase. When the stiffness is very low, for example 0.1, the joint can be treated as a free-free boundary condition. After a certain value of joint stiffness the structure behaves like a simply supported system. Hence, further increase in stiffness does not change the frequency values. The region in-between these two boundary conditions are called semi rigid or elastic boundary condition. In reality, the boundary conditions of engineering structures like automotive vehicles fall into this region. Figure 37 depicts the percentage change of first three natural frequencies with the variation of joint stiffness. It can be seen from Figure 37 that all three natural

frequencies are very sensitive up to the joint stiffness of 1000. The first natural frequency becomes almost stable from K value of 500 onwards but other two frequencies keep changing with a faster rate.

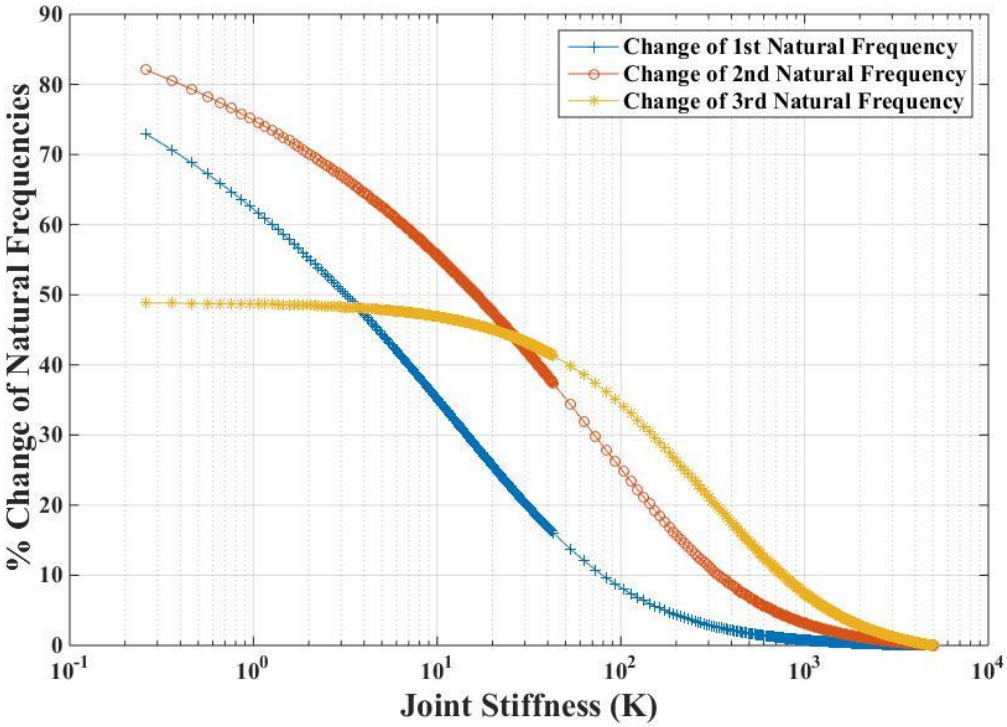


**Figure 37: Percentage Change of Natural Frequencies of a Beam by Varying Joint Stiffness**

The key purpose of this comparison is to show how the elastic boundary condition affects the natural frequencies. Usually the components of an automotive system are tested by simply mounting it in the laboratory. In an actual case the joint stiffness due to the tire and suspension system lies between the semi-rigid regions. Hence, just mounting the specimen in a testing table would not represent the actual field condition. For instance, if the joint stiffness is 100, direct mounting the beam in the laboratory will show the variation of first, second and third natural frequencies by 10%, 24% and 35% respectively with regard to the actual field condition for this

case. So, there will always be uncertainty about the reliability of the accelerated durability testing if the joint stiffness falls into this region. Hence, tuning of natural frequencies is of great importance to replicate the real field condition in the laboratory environment.

## 4.2 Experimental Modal Analysis Results with Rigid and Elastic/Semi-Rigid Supports

In this section, results obtained from the modal parameter extraction techniques are included which have been later used to calibrate the finite element model in ANSYS. Before going into the details, some pretest steps were carried out to check the reliability of the experimental results. The fidelity of the output results largely depend on the consistency of the pretest experiments[175].

### 4.2.1 Verification of the Test Setup

Trustworthiness of the complete test setup can be determined by verifying the quality of the frequency response functions. The overall experimental setup for both rigid support and semi-rigid support test fixtures were verified according to the following methods.

#### 4.2.1.1 Driving Point Measurement

Driving point measurement can be defined as the measurement where both input and output of the structure correspond to the same point. Driving point FRF should be checked to find out any kind of irregularities in the measured FRF. In this experiment a modal shaker was used as a source of excitation and an accelerometer was placed just above the beam to collect data on the same position. The conditions of a driving point measurement are:

- There must be an anti-resonance zone between two resonance points.
- The imaginary peaks will be always pointed towards the same direction.

- There should be fall of 180 degrees in the phase value during resonance and 180 degree rise during anti-resonance.

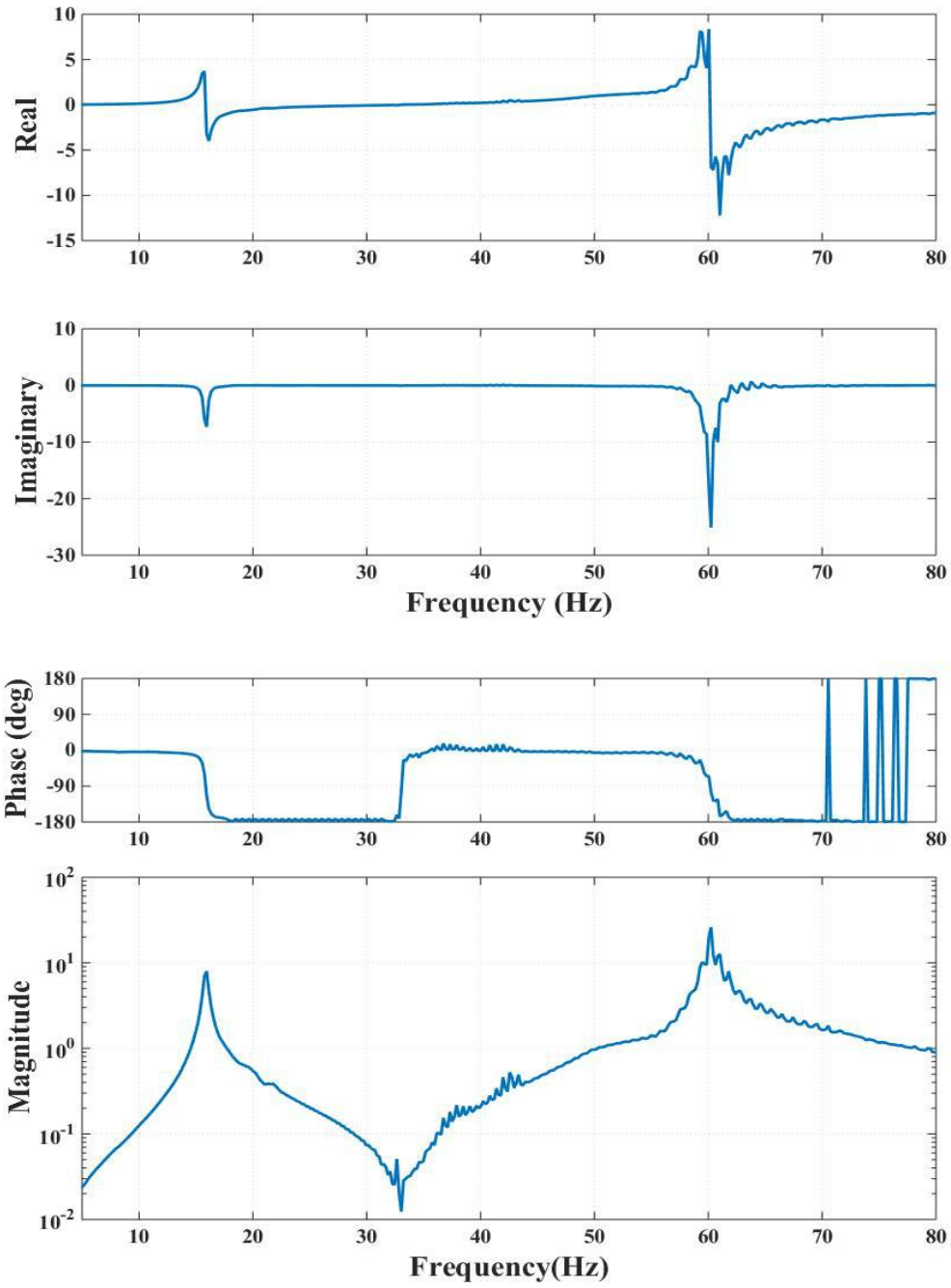


**Figure 38: Driving Point Measurement of a Beam Supported by Rigid Fixture**

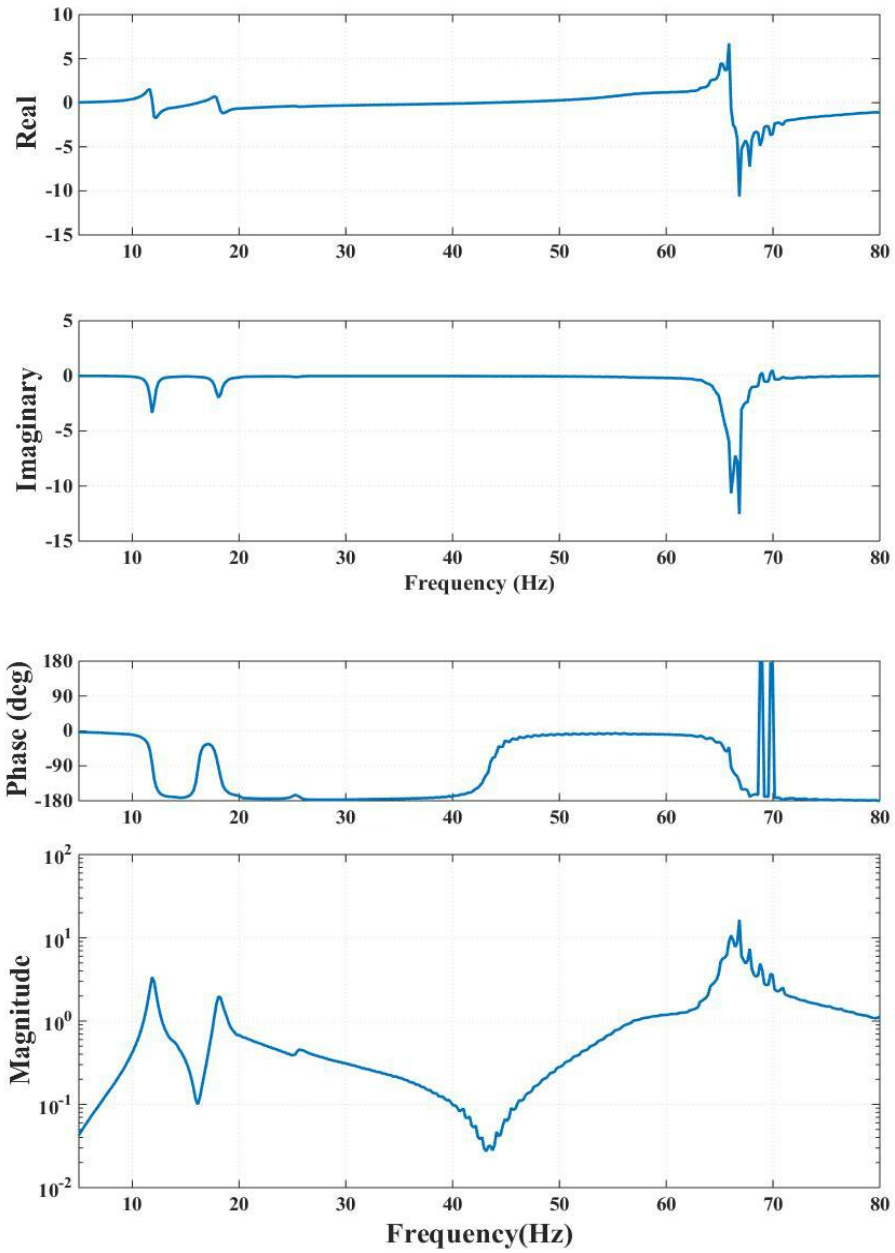


**Figure 39: Driving Point Measurement of a Beam Supported by Elastic Fixture**

The experimental FRF measurement of both rigid support and elastic support fixtures are plotted in Figure 38 and 39 respectively where all of the above mentioned conditions are fulfilled. Sometimes driving point measurement might produce poor FRF due to the improper attachment of accelerometers.

#### 4.2.1.2 Linearity Check

Another criterion to verify the FRF is to check the non-linearity of the system. For a linear structure the FRF does not depend on the excitation load. Linearity can be approximated by taking the ratio of the magnitude of two different FRFs with different excitation level along a specific frequency bandwidth which is known as Gain Ratio. Linearity estimation is demonstrated in Figure 40 and 41 for two different fixtures.

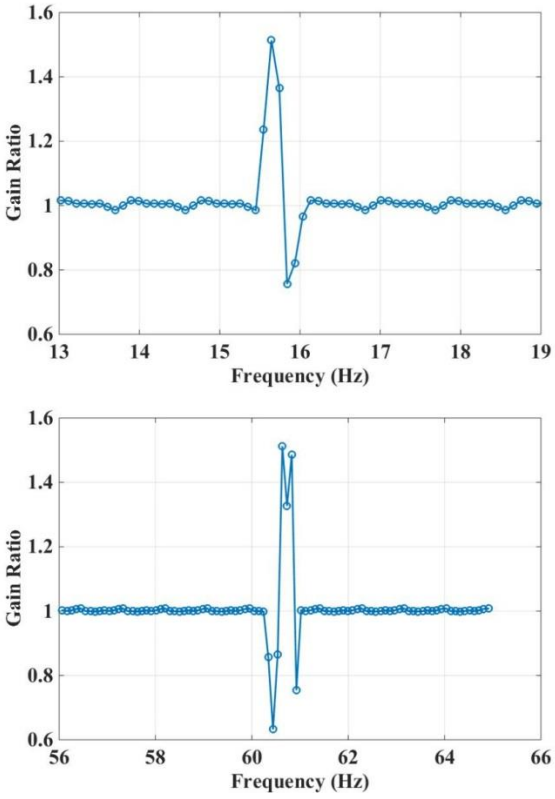


**Figure 40: Linearity Approximation of 1st and 2nd mode of a Rigidly Supported Structure**

In the case of spring supported structure, due to the position of the modal shaker, the 2nd and 3rd mode of the system were not excited properly. Hence, the effect of the 1st and 4th bending mode was considered in this case. From both of the Figures 40 and 41, it can be noticed quite easily

that the gain ratio is almost unity except near the vicinity of the resonance where non-linearity takes place.

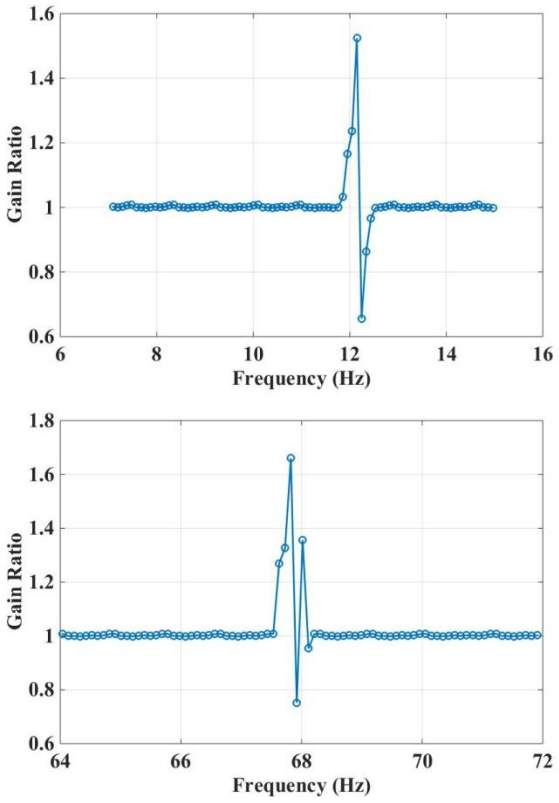


**Figure 41: Linearity Approximation of 1st and 4th Mode of an Elastically Supported Structure**

### 4.2.2 Determination of Dynamic Properties from Experiment

In this section, both frequency domain and time domain methods are introduced to determine the experimental dynamic properties e.g. natural frequencies, damping ratios and mode shapes of both rigid and spring supported structures. During the analysis, all modes within 0-80 Hz were analysed for the simplicity of the calculation. First four bending modes of a semi-rigid support fall into this region, whereas only two bending modes of rigid support fixture lies in this range.

Though the loading was applied in the vertical direction, the effects of the out of band modes were considered negligible.

Figures 42 and 43 represent the curve fit results of Accelerance function according to the equation 35. To avoid any kind of confusion, the damped natural frequency was converted to the natural frequency in the curve fit equation which considers the measured damping ratio. The basic use of curve fitting curve is to find out the accurate peak that is closer to the theoretical value and estimate the damping ratio associated with that mode.

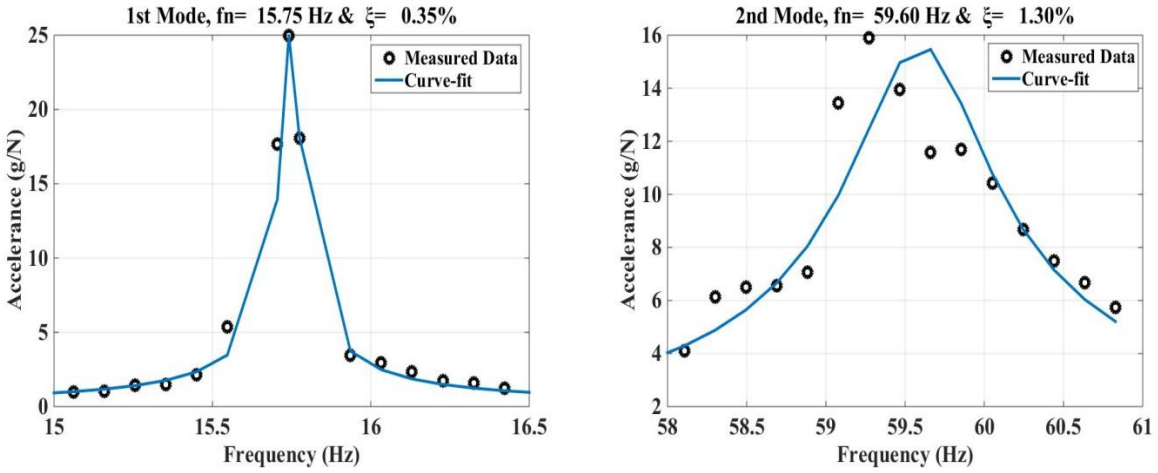


**Figure 42: Frequency Domain Modal Parameter Extraction of Rigid Support**

A SDOF curve fitting algorithm was conducted in the vicinity of the resonance zones so that the effect of other modes can be neglected in that zone. Sometimes due to the nonlinearity phenomena near the resonance it becomes very hard to find out the actual peak of the FRF. This curve fitting technique has been generated based on the least square error method where Coefficient of Determination ($R^2$) ranges from 85.22% to 99.11% and standard error lies from 0.14% to 1.59%, which is indeed a proof of very good correlation with the experimental results.

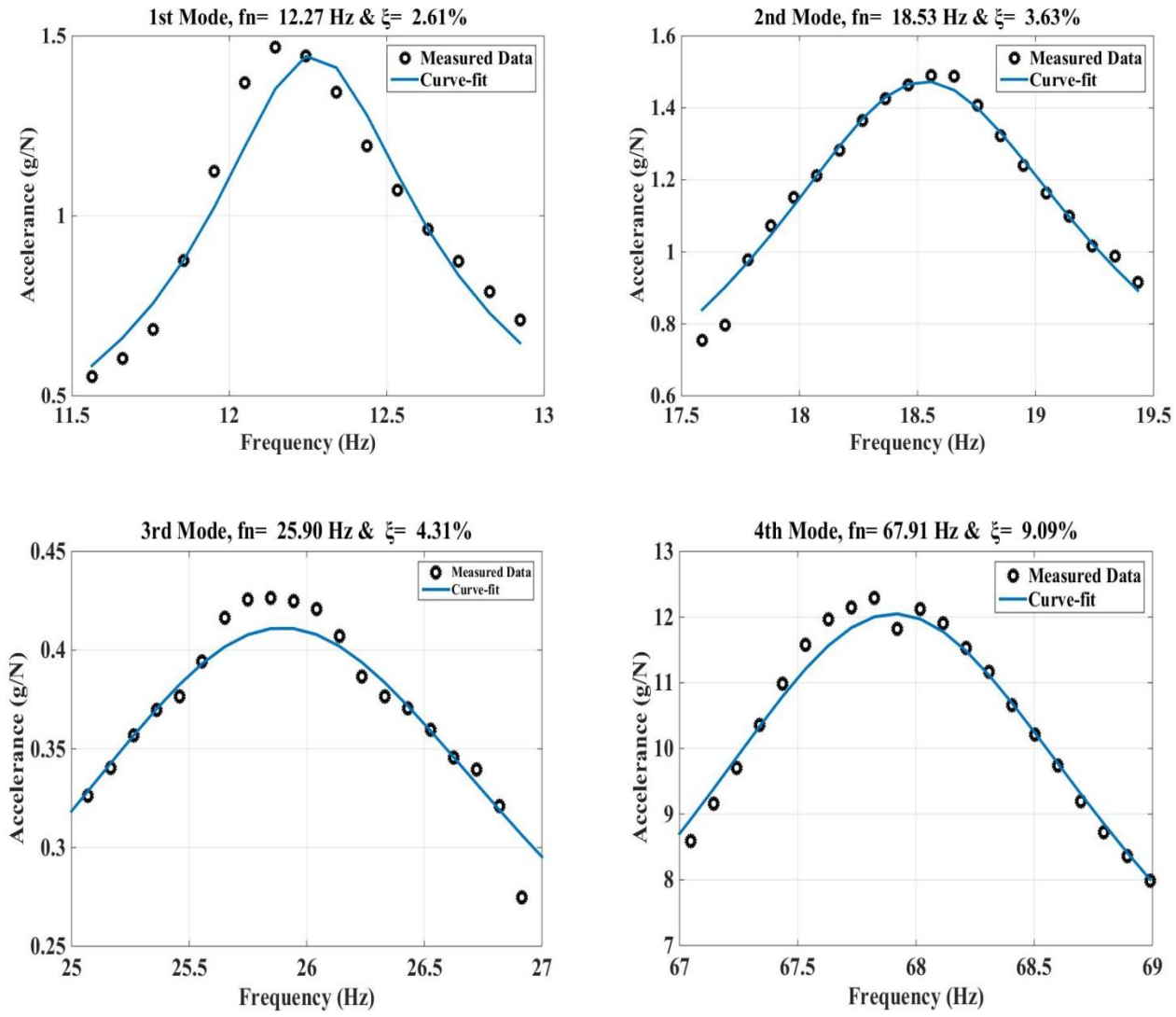


**Figure 43: Frequency Domain Modal Parameter Extraction of Elastic Support**

Natural frequency and damping ratio of lower modes can also be determined by curve fitting the free vibration time history response of both structures with a damped sine curve. Using this method, the first mode of the structure can be estimated accurately using equation 47 which gives a very close match with the results found from FRF technique. In Figure 44, the blue line represents the experimental time history data of acceleration and the black dotted line is a damped sine curve which extracts the experimental parameters from the curve.

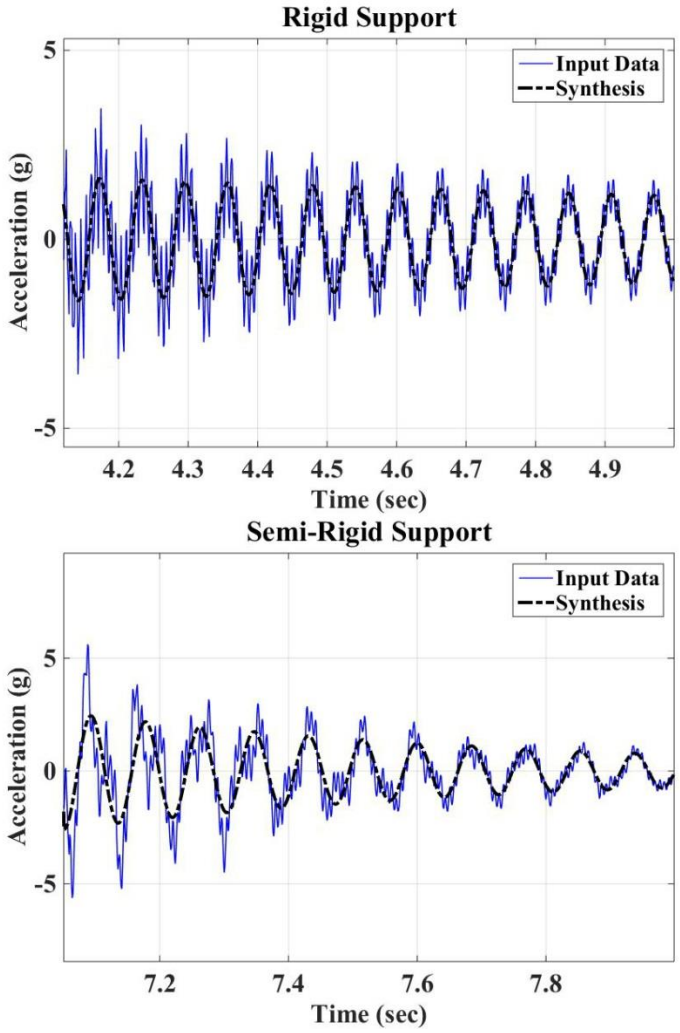


**Figure 44: Time Domain Curve Fitting Results**

Several sine sweep tests were carried out to find out the natural frequency and damping ratio of both structures. The average results of the extracted dynamic parameters from both time and frequency domain techniques are summarized in Table 7. The comparison of the dynamic properties (Natural Frequency and Damping Ratio) of first three modes between the beam with rigid and elastic foundation is shown in Figure 45. It can be noticed quite easily that the first natural frequency of the beam with rigid support is almost 21% higher than that of the elastic foundation and the difference keeps increasing for the higher modes. Again, the damping ratio of

the first mode of the beam with elastic foundation is almost 7.45 times higher than the beam with rigid foundation. This deviation shows a large amount of change of the dynamic properties in the laboratory system compared to the field condition which alters the fatigue damage significantly.

**Table 7: Experimental Dynamic Properties of Rigid and Elastic Supported Beam**

| Types of Support | Modes | Natural Frequency (Hz) | Damping Ratio (%) |
|---|---|---|---|
| Rigid Support | 1st | 15.63 | 0.34 |
| | 2nd | 59.82 | 1.21 |
| Elastic/Semi-Rigid Support | 1st | 12.25 | 2.53 |
| | 2nd | 18.34 | 3.51 |
| | 3rd | 25.81 | 4.22 |
| | 4th | 68.1 | 8.91 |

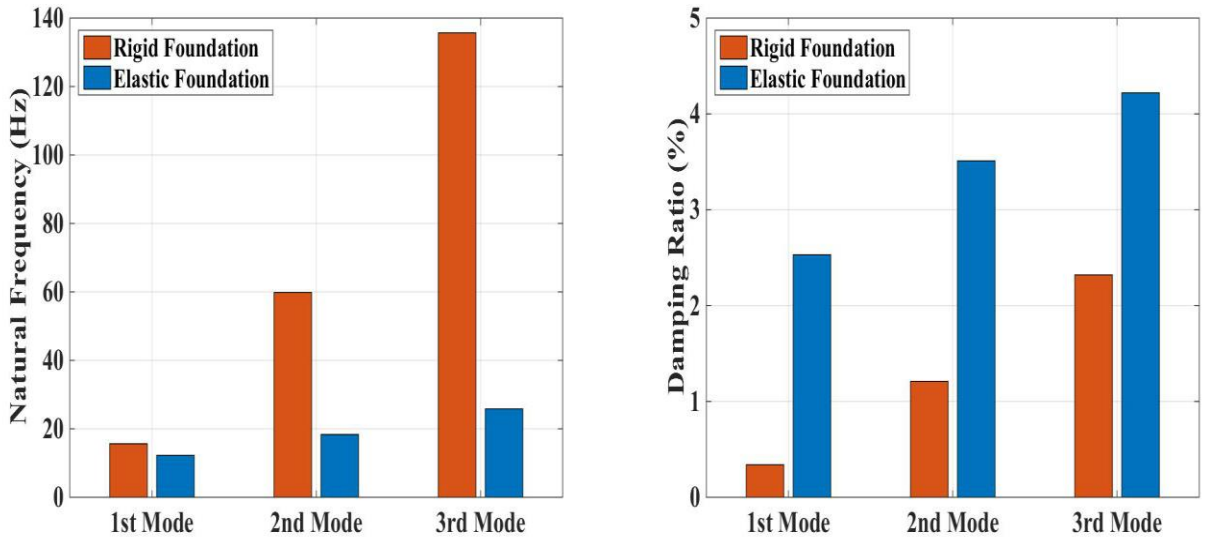


**Figure 45: Comparison of Natural Frequencies and Damping Ratio between Rigid and Elastic Foundations**

In this thesis, the spring constant was chosen from the semi rigid range of Figure 36. The value of the spring constant considered in the experiment was, k= 3857 N/m and end mass of 0.2 kg which showed a difference of 21% Hz in natural frequency of the first mode compared with the rigidly supported beam. The spring constant and joint mass was selected arbitrarily to define the real world joint stiffness of a component supported by the combination of tire and suspension system. The ratio of effective modal mass to the total mass of the first mode of both the rigid and elastic foundation was approximately 81%. Due to the higher participation factor (the amount of system mass participating in a particular mode) of the first mode, the modal damping constant of this mode was considered as the constant damping ratio for the whole structure.

The mode shapes of the structures can be obtained by connecting the peaks of the imaginary FRF along the length of the beam. Total 17 points were drawn at every 5 cm on the front side of the beam. Imaginary FRF value of each point was measured carefully using the QuickDAQ software. The most difficult part of this measurement was to find out the amplitude of the actual peak as there were some noise effect due to the DAQ and the modal shaker. This problem was overcome by using an excitation signal of lower amplitude (0.3 N) with a very small sweep rate (0.029 Octaves/minute). The response acceleration can be measured very precisely due to the higher sensitivity of the piezoelectric accelerometer.

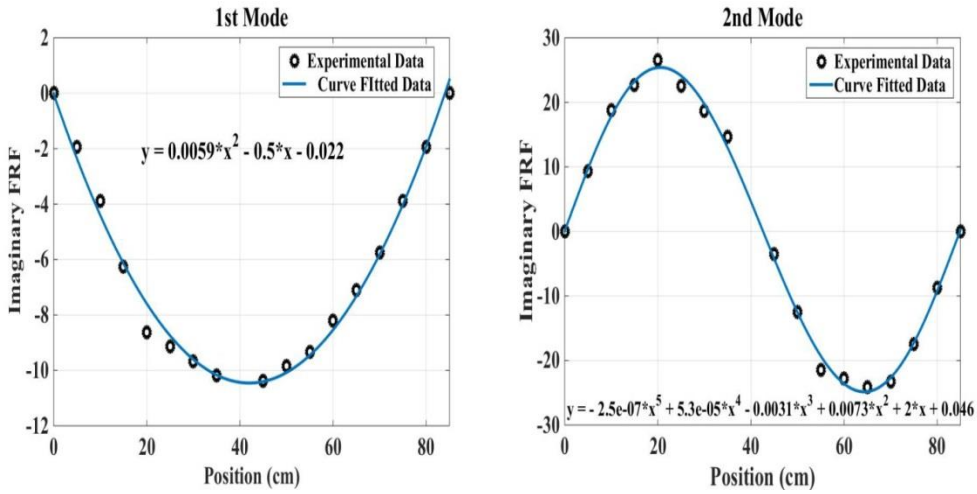


**Figure 46: Experimental Mode Shapes of Beam Supported by Rigid Foundation**

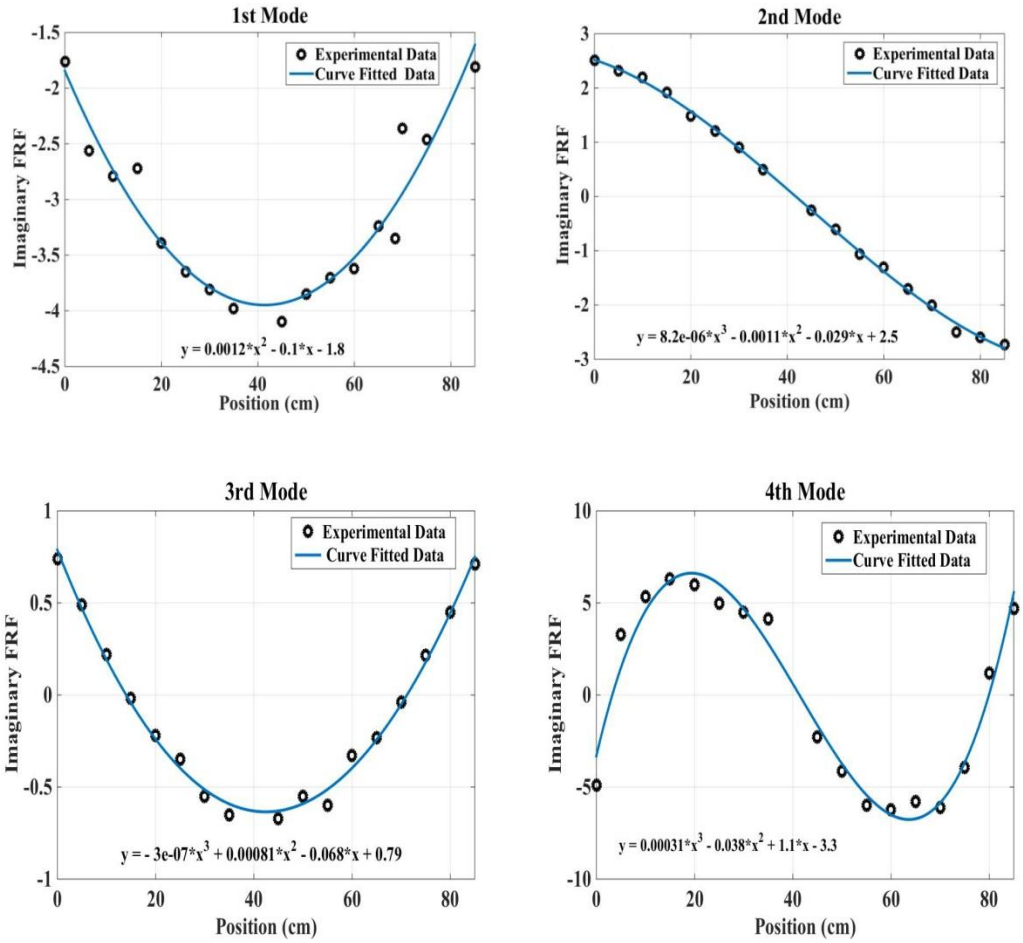


**Figure 47: Experimental Mode Shapes of Beam Supported by Elastic Foundation**

In Figure 46 and 47 the experimental data and the best fitted curve has been drawn for both rigid and elastic beam support. The coefficient of determination or the $R^2$ values ranges from 93% to 98% which demonstrates the goodness of the curve fitted results with the experimental data. Figure 48 shows the comparison between the normalized mode shapes of the beam supported by both rigid and elastic foundation. Due to the large variation in the mode shapes between this two support conditions there would be a large difference in the strain energy distribution which would alter the stress and fatigue properties significantly.

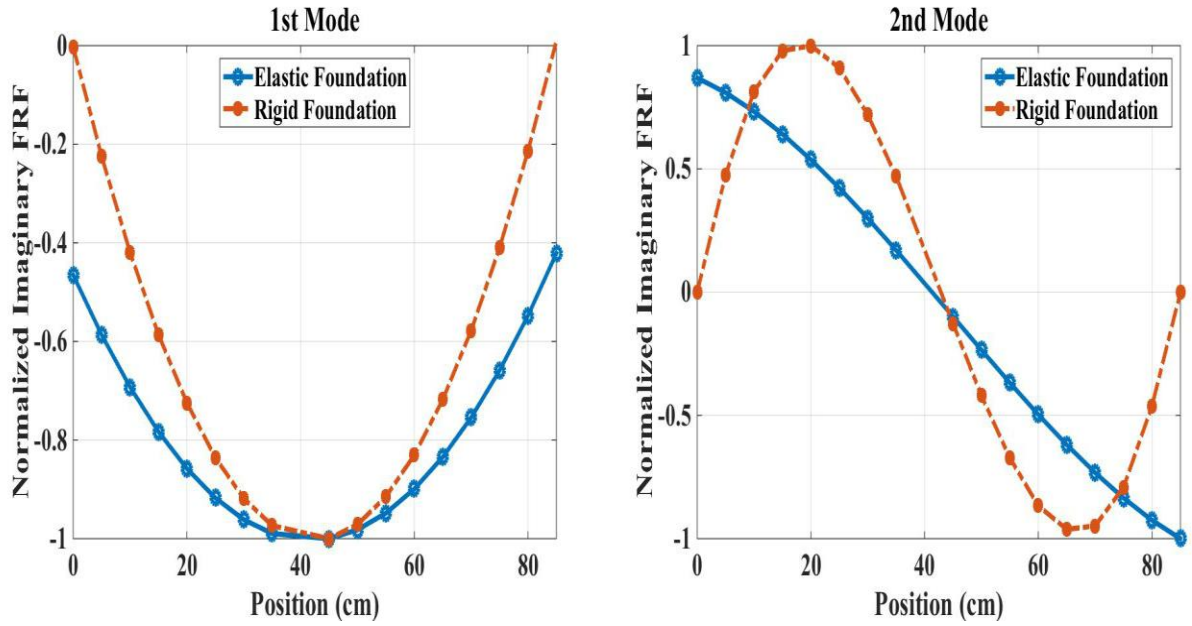


**Figure 48: Comparison of First Two Mode Shapes between Rigid and Elastic Foundations**

In Figure 49, the waterfall plot of the beam FRF function is shown where the peaks of the imaginary values were connected to obtain the mode shapes.

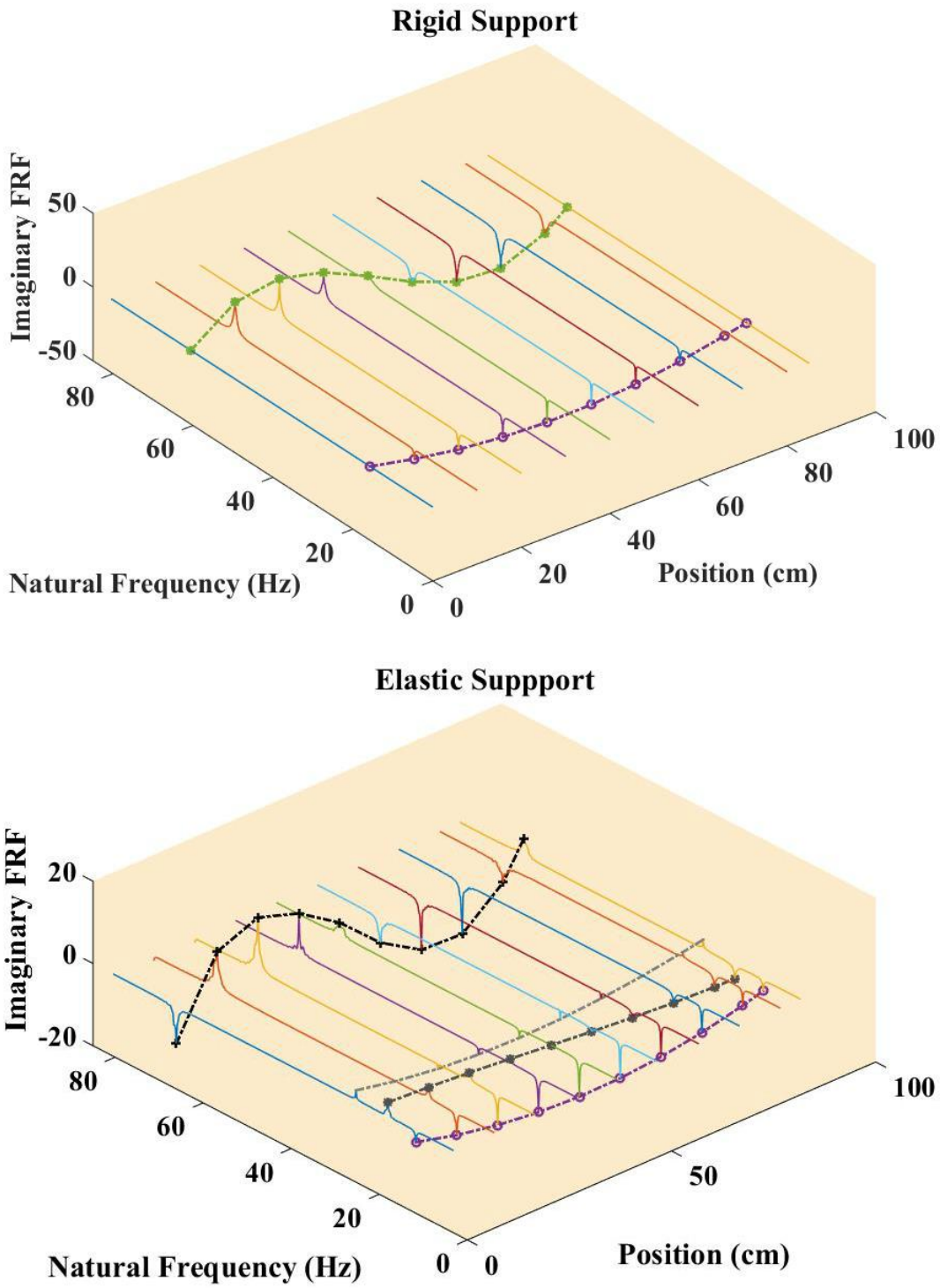


**Figure 49: Waterfall Plot of Beam Imaginary FRF**

### 4.3 Finite Element Results

To validate the numerical design and modeling of the test piece and associated boundary condition it is required to compare the results of experimental and FE analysis. Though, finding the numerical damping ratio is quite impossible, it was updated to ANSYS from the experimental results as the form of constant damping ratio (rigid support 0.34% and elastic support 2.53%). As the effective modal mass of the first mode for both types of supports was almost 81%, this mode would be excited heavily during base excitation. The critical location for this mode was most likely to fail earlier in the structure. Hence, the damping ratio of this mode was considered constant throughout the analysis.

**Table 8: Comparison of Experimental and FE Modal Analysis**

| Types of Support | Modes | Experimental Natural Frequency (Hz) | Numerical Natural Frequency (Hz) | Deviations (%) |
|---|---|---|---|---|
| Rigid Support | 1st | 15.63 | 15.13 | 3.21% |
| | 2nd | 59.82 | 60.56 | 1.82% |
| Elastic/Semi-Rigid Support | 1st | 12.25 | 11.81 | 3.59% |
| | 2nd | 18.34 | 18.87 | 2.89% |
| | 3rd | 25.81 | 25.12 | 2.67% |
| | 4th | 68.1 | 66.21 | 2.77% |

Table 8 represents the comparison of average experimental and FE modal analysis results of both supports. From this table it can be noticed that the deviation of the results are very small where

3.59% being the highest and 1.42% being the lowest deviation. This deviation may occur because of the modal shaker stinger and accelerometer effect on the structure and also the noise coming from the DAQ.

The mode shapes of experimental modal analysis and FE analysis are called an eigenvector as it gives unique shape but not necessarily unique value. To compare the mode shapes, the uncalibrated experimental and numerical mode shapes have been normalized by dividing all the eigenvalues with the highest value among them to make the highest value equal to 1. In Figure 50 and 51 the comparison of the experimental and FE results is carried out where both of the structures showed a good agreement with experimental result.

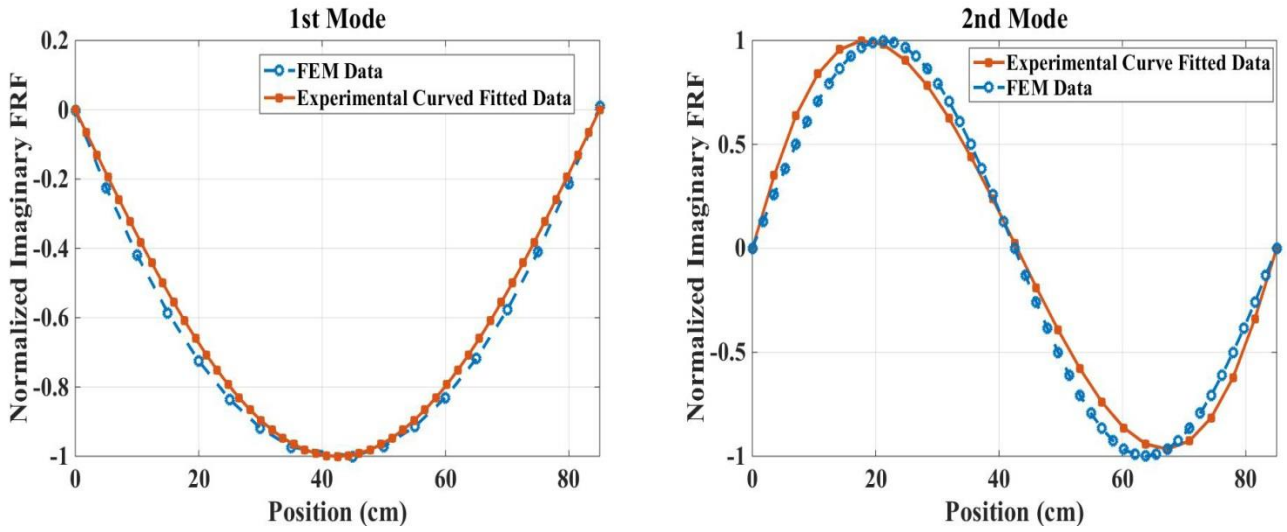


**Figure 50: Comparison of Experimental and FEM Mode Shapes of a Beam with Rigid Support**

From figures 50 and 51, the first mode of the rigid foundation and the 1st and 3rd mode of the elastic foundation are quite similar in their shape. For the 1st mode of the beam with elastic foundation, both the deflection of the springs and the beam bending lies in the same direction.

But for the 3rd mode of the elastic foundation, the deflection of the springs and beam bending takes place in the opposite direction which creates extra two nodal points along the beam axis. That is why the 3rd mode of the elastic foundation would be excited strongly after the first mode for the base excitation simulation having an effective mass to total mass ratio of 18.89%. Because of the slight deviation in the stiffness value between the two end springs and higher friction rate at high frequency content, the maximum deviation was found on the fourth mode of the beam supported by the elastic foundation.

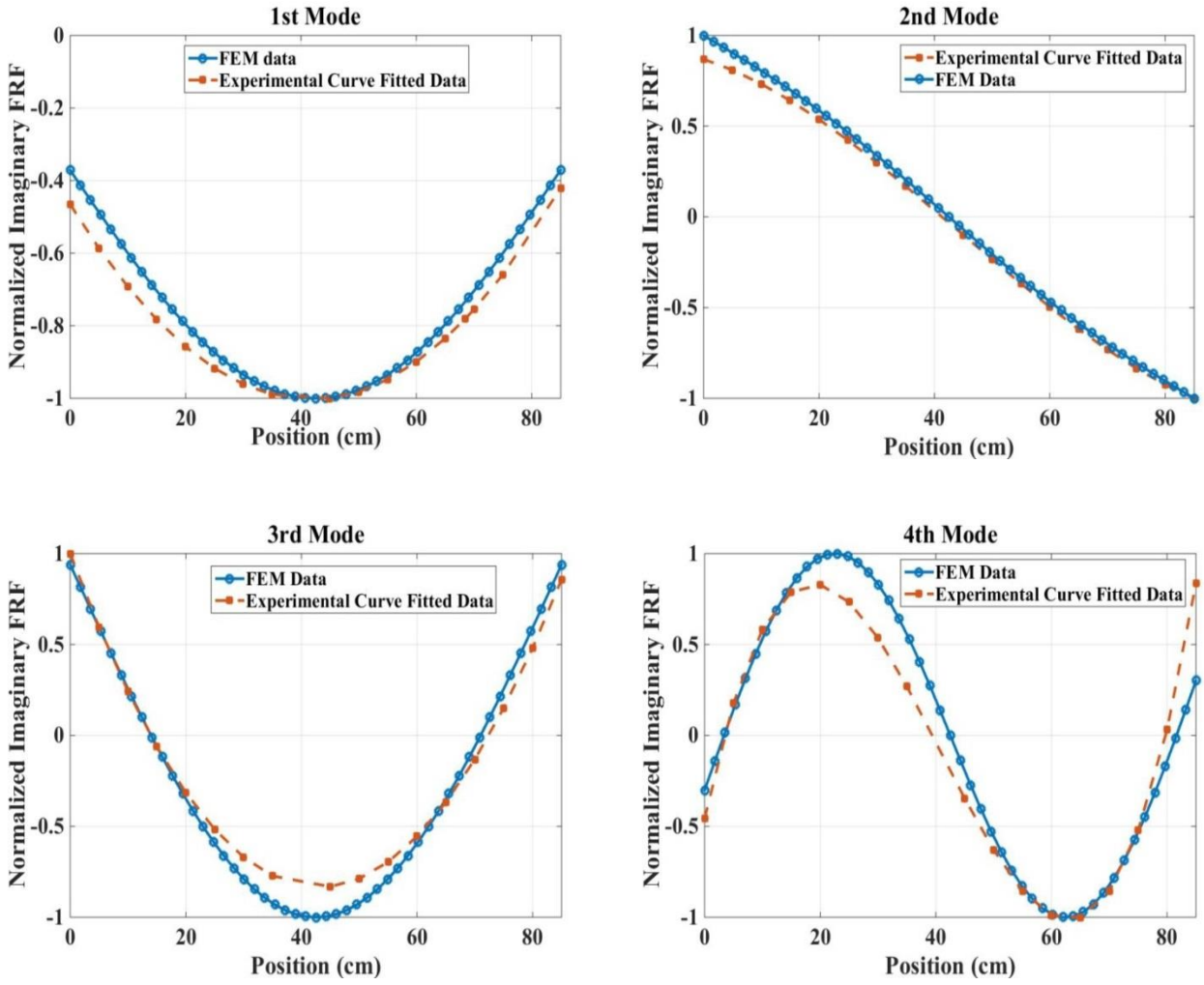


**Figure 51: Comparison of Experimental and FEM Mode Shapes of a Beam with Elastic Support**

The main reason of performing experimental modal analysis is to validate the model in FEM so that further base excitation fatigue tests can be carried out using finite element software. After the validation of experimental modal results e.g. natural frequency, damping and mode shapes, another experiment was performed to compare the overall RMS of the stress response. Though the natural frequencies were converged with a small amount of element number, the convergence study for the Modal Analysis is not shown here. But before performing the response analysis, convergence tests of the FEM was carried out to ensure the reliability of the results. To do so, a 100N static force has been applied to the stinger position and von mises stress was measured near the most critical point. Results of the convergence study is plotted in Figure 52 where number of elements is plotted in X axis and corresponding von mises stress is plotted in Y axis. As shown in Figure 50, the stress result converged upon a solution (~115 MPa) as the number of elements increased above 35,000.

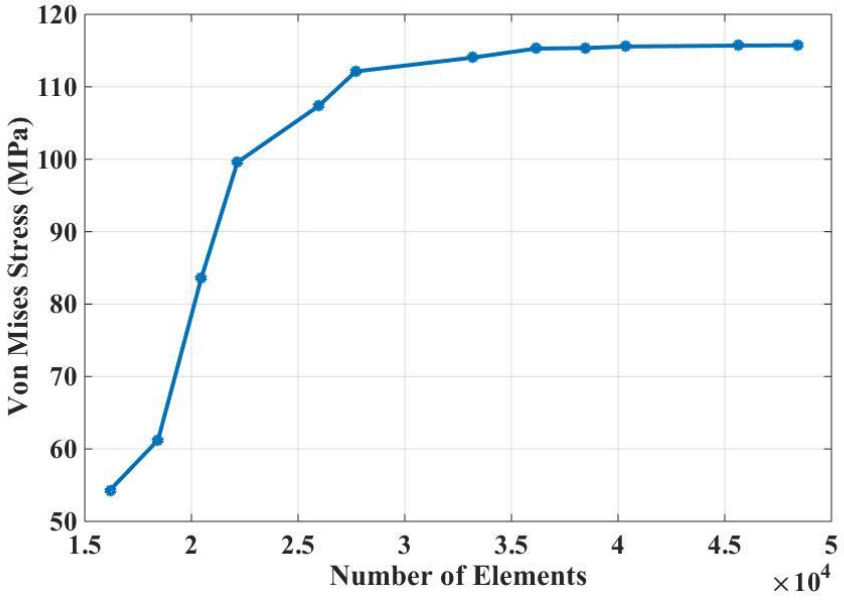


**Figure 52: Convergence Study of FEA Results**

During vibration response testing with variable frequencies, it was difficult to implement the actual loading provided by the modal shaker as there was no force controller available with the shaker. Using the signal generator function of the Simulink few random signals were passed to the modal shaker. Though the force sensor was attached directly to the beam, the same numerical input from MATLAB showed different input signals from different experiment setups due to different boundary conditions (rigid and elastic) of the beam. This problem was solved by changing the standard deviation of the input signal using trial and error method to get a closer RMS value for both rigid and elastic foundation. The axial strain gauge was mounted 5 mm above the center hole of the beam as shown in Figure 26 to measure the bending stress of that location. The same position was marked in the FE model to compare with the experimental results. Strain results obtained from the strain gauge were multiplied by the modulus of elasticity (E) to find out the corresponding stress.

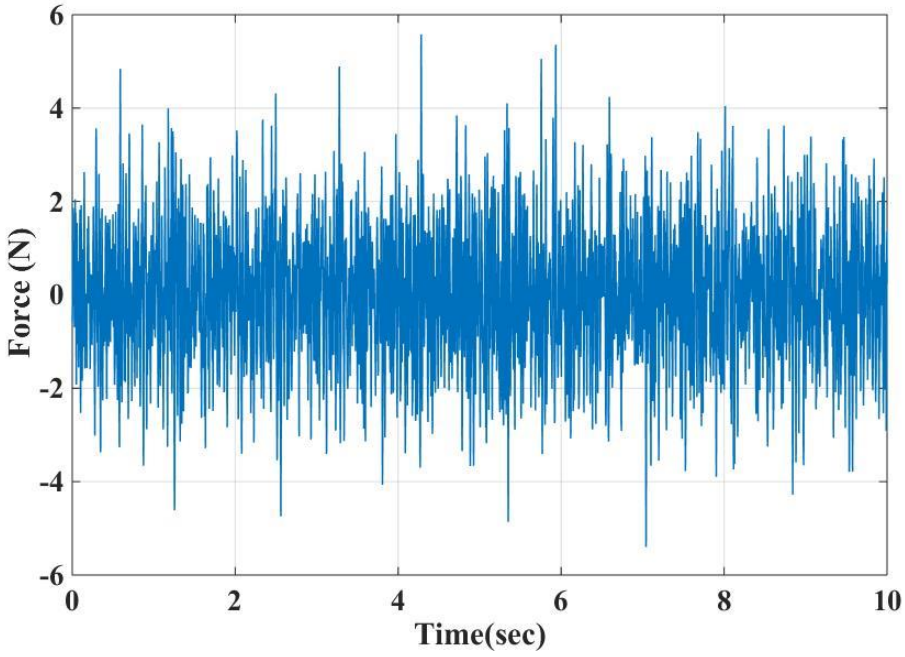


**Figure 53: Random Time History Captured by the Force Sensor**

The experimental force sensor data confirmed the oscillation of random signal about zero mean value. That is why the standard deviation was almost equal to the RMS of the signal. Figure 53 shows a sample random time history derived from the dynamic force sensor.

**Table 9: Comparison of Bending/Normal Stresses for Different Point Input Levels**

| Test Case | Boundary Condition | Input RMS (N) | Experimental Bending Stress, RMS (MPa) | FEA Bending Stress, RMS (MPa) | Percentage (%) Deviation between the experimental and FEM results |
|---|---|---|---|---|---|
| 1 | Rigid | 1.359 | 4.116 | 3.928 | 4.56% |
| | Elastic | 1.416 | 2.019 | 1.838 | 8.95% |
| 2 | Rigid | 1.898 | 14.170 | 13.334 | 5.92% |
| | Elastic | 1.922 | 5.121 | 4.821 | 5.85% |
| 3 | Rigid | 2.392 | 18.396 | 17.142 | 6.83% |
| | Elastic | 2.643 | 5.463 | 5.023 | 8.05% |

The amplitude of the input signal was kept low because of the capacity of the force sensor and the modal shaker. The force sensor could measure up to 10N compressive and tensile force. So the RMS of the input force was selected such that the maximum force remains below 10N. The response results are summarized in table 9 where the maximum deviation between the experiment and FEA is found as 8.95% and minimum deviation is found 4.56%. For each experiment at least six trials have been made and the results were selected from the average. Although the main attention of this thesis is focused on the ground vehicle base excitation

problems, the results from this point load analysis would confirm the reliability of the further numerical calculations.

### 4.4 Numerical Stress Analysis Due to Base Excitation

Once the FE model is validated with the experimental results, it can be further used to demonstrate the base excitation problems using ANSYS Workbench software. Due to the inability of ANSYS of directly applying base acceleration to the structure, Large Mass Method (LMM) was applied to model the base with a $10^7$ times larger mass than the structure. In this section, different types of stress values are determined for both types of boundary conditions using 1g, 2g and 3g RMS base excitation. Table 10 shows the comparison between different types of RMS stresses to find out the most dominating stress value.

**Table 10: Comparison of Stresses for Different Base Excitation Input Levels**

| Input RMS (g) | Boundary Condition | Output RMS | | | |
|---|---|---|---|---|---|
| | | Normal Stress (MPa) | Maximum Principal Stress (MPa) | Von-Mises Stress (MPa) | Maximum Shear Stress (X-Z Plane) (MPa) |
| 1g | Rigid | 30.95 | 30.38 | 30.32 | 9.379 |
| | Elastic | 17.49 | 17.17 | 17.45 | 5.409 |
| 2g | Rigid | 98.54 | 97.58 | 98.33 | 30.52 |
| | Elastic | 37.03 | 36.33 | 36.96 | 11.46 |
| 3g | Rigid | 122.4 | 119.6 | 122.1 | 37.88 |
| | Elastic | 57.56 | 56.89 | 57.44 | 17.80 |

According to table 10, first three stresses e.g. normal, maximum principal and von-mises stresses are almost numerically equal which depicts the dominant behavior of the bending stress.

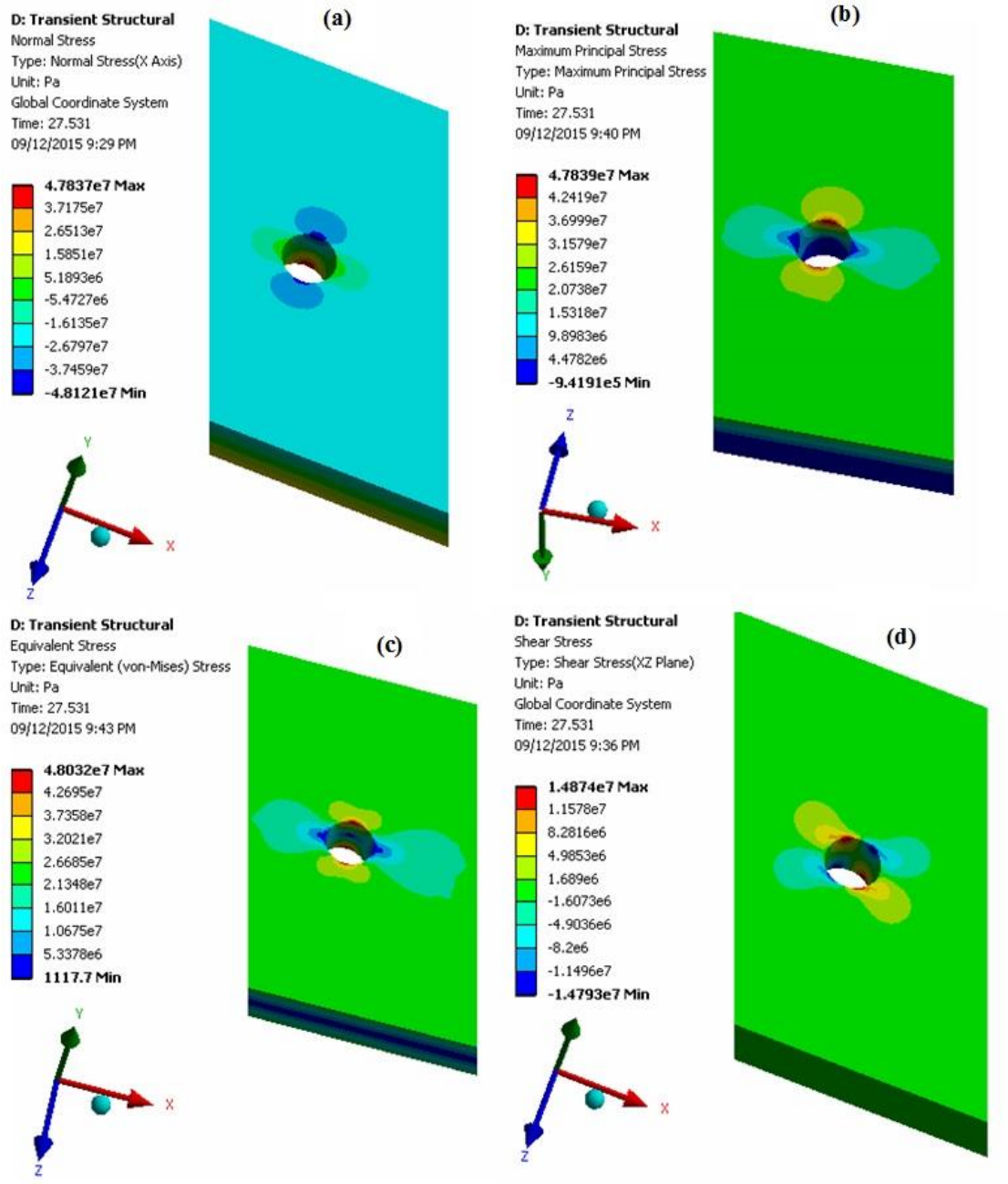


**Figure 54: Distribution of Different Types of Stresses (RMS) for 1g Base Excitation on a Beam Supported by Elastic Foundation over the Critical Point, (a) Normal, (b) Maximum Principal, (c) Von-Mises and (d) Shear Stress**

Among these four types of stresses, normal stress was the most damaging stress content for both types of boundary conditions. The shear stress along the X-Z plane was the lowest among these stresses and hence can be neglected during fatigue analysis to avoid overestimation. Hence, the normal stress was studied for the further calculations to save computational time. Due to the oscillation about the mid plane (Mean ≈ 0) the RMS value and the standard deviation (σ) can be considered to be numerically equal. For 3g base excitation input, the numerical normal stress RMS value of the rigidly supported beam was about 122.4 MPa which could introduce plasticity or direct failure as the 3σ value[143] is higher than the ultimate tensile stress (310 MPa). In Figure 54, the four types of stress distributions are shown for a beam supported by elastic foundation. Here, the maximum values of each of first three stresses are almost quantitatively equal for a 60 sec base excitation loading profile.

## 4.5 Fatigue Damage Estimation

### 4.5.1 Sine-Sweep Loading Profile

Sine-Sweep signal is one of the most commonly used loading profiles used to determine the fatigue life of ground vehicle components. Though it does not reflect the original loading scenario, still some industries are using this method to find out the initial fatigue damage during design period.

In case of a Sine-Sweep loading profile, constant peak acceleration is maintained throughout the frequency broad band. Hence, the mode with higher modal mass will have the highest response. Harmonic analysis results of the base excitation of both rigid and elastic foundation is shown in Figure 55 as a form of bending stress transfer function. As we know, base excitation is considered as a distributed loading and the resultant is always pointed towards the middle of a

beam supported by equal stiffness at both ends. The resultant loading point coincides with the nodal point of the 2nd mode for the rigid foundation and the nodal point of the 2nd and 4th mode for the elastic foundation. According to Figure 55, those modes were not excited properly during analysing the base excitation problem. In this Figure, it can be clearly seen that the response peak amplitude of the beam with rigid foundation is almost 2 times higher than the response of the beam with elastic foundation because of the lower damping ratio. The stress response of the system due to the application of the sine-sweep acceleration would follow the trend of this stress transfer function. The significance of the critical responses over the boundary condition is shown in Figure 55 for the unit base acceleration. If the excitation frequency was near 12 Hz, the amplitude of the elastic foundation would be 155 MPa/g, whereas the amplitude of the rigid foundation would be only 20 MPa/g. Again if the excitation frequency was near 15 Hz the peak stress of elastic and rigid foundation would be 18 MPa/g and 290 MPa/g respectively. Hence, it can be stated without any doubt that the change of boundary conditions in the laboratory test would surely alter the whole dynamic behavior of the structure.

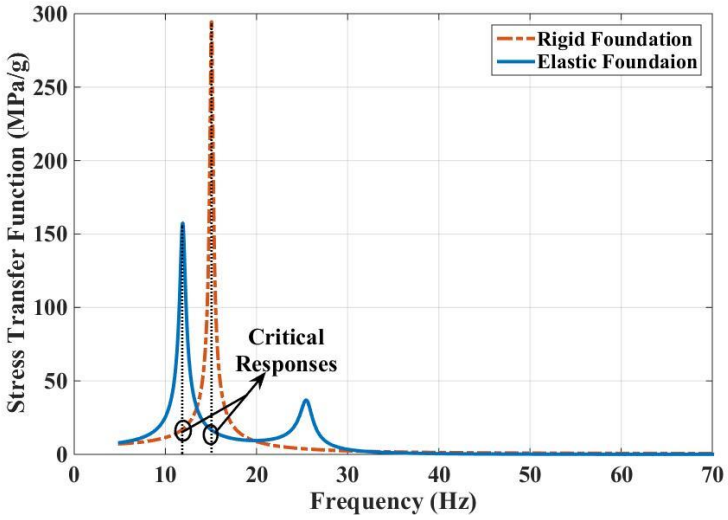


**Figure 55: Comparison of Stress Transfer Function between Rigid and Elastic Foundation**

The comparison was illustrated further by applying a 60 second transient sine-sweep loading profile as shown in Figure 56. The RMS and peak acceleration of the base excitation was 0.5g and 0.707 g respectively. The acceleration time history was generated using MATLAB code. The response time history is plotted in Figure 57.

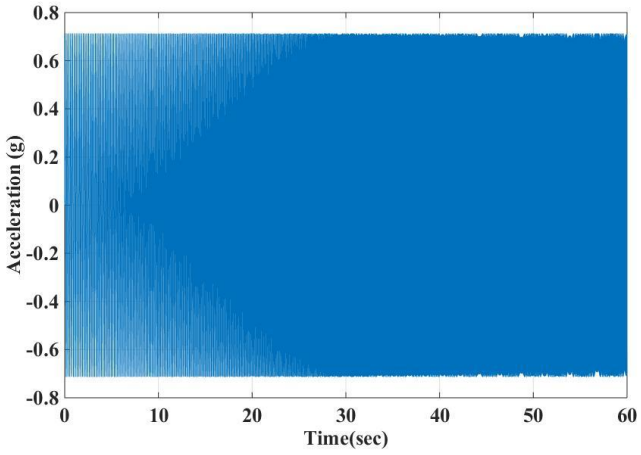


**Figure 56: Sine-Sweep Time History of 0.5g RMS**

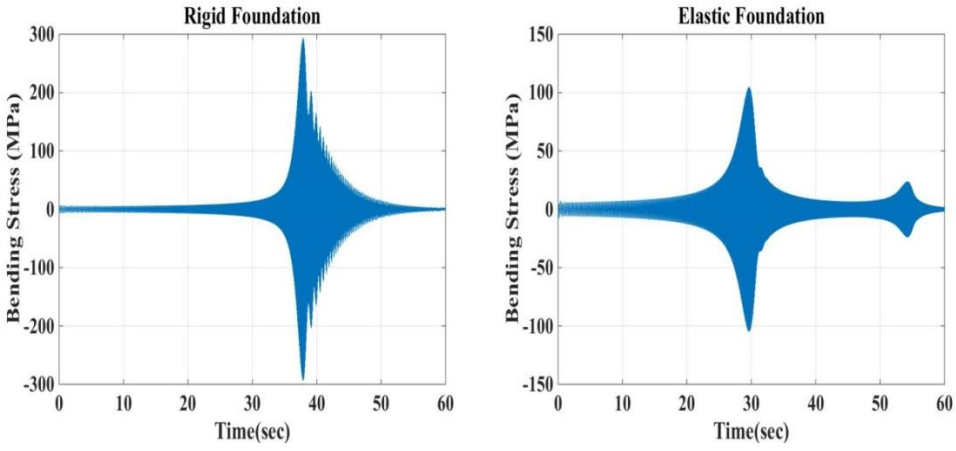


**Figure 57: Sine-Sweep Response Time History of 0.5g RMS**

Although there are two peaks in the elastic foundation response stress time history within 0-80 Hz frequency range, the overall RMS of the response stress of the rigid foundation (41.83 MPa)

is more than two times higher than the elastic foundation (17.31 MPa) which confirms higher cumulative fatigue damage in the rigid foundation. In Figure 58, the cumulative fatigue damages are plotted against different input sine-sweep acceleration level. The cumulative fatigue damage was calculated using Rainflow Cycle Counting Algorithm and Miner's cumulative fatigue damage formula. From Figure 58, it can be noticed that the increment of the fatigue damage of both of the structures is quite large compared with the increment of the input RMS acceleration. This is because of the slope characteristics of the S-N curve. From equation 87, the fatigue damage raises exponentially with the stress to the power of fatigue exponent which is a positive integer. According to Figure 58, for the same amount of input sine sweep acceleration loading the beam with rigid foundation shows several orders of higher fatigue damage than that of the beam with the elastic foundation.

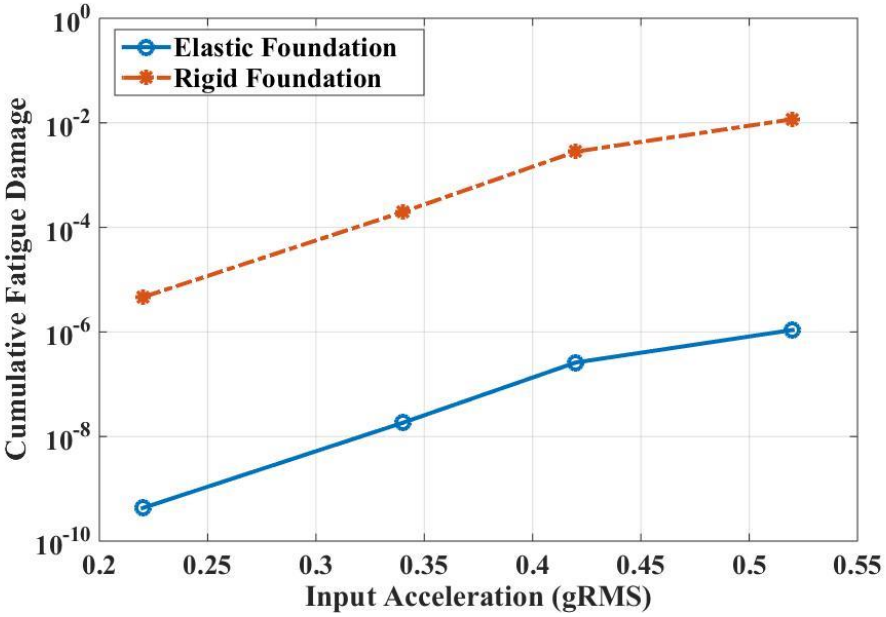


**Figure 58: Comparison of Cumulative Fatigue Damage for Sine-Sweep Loading Profile**

Hence, proper calculation of the response stress history is the fundamental foundation of fatigue damage calculation which largely depends on the joint stiffness of the structure. In short, it can be said that performing AD tests using sine-sweep loading profile might overestimate the overall fatigue damage to a very large extent if the laboratory boundary conditions are not set close to the real situation.

### 4.5.2 Random Vibration Loading Profile

Random signal is the most common and popular means of vibration testing excitation for automobile ground vehicles and aerospace components. As the automobiles especially the heavy coach and agricultural vehicles are continuously experiencing random rough road loads, this loading profile is considered to be the most effective way to determine the fatigue life of any component.

#### 4.5.2.1 Generation of Loading Profiles

Generation of appropriate loading profiles is the most important feature to calculate the reliable fatigue life of the ground vehicles. The primary aim of this work is to compare the differences in fatigue properties due to the change of the boundary conditions in the lab tests. So, a dummy loading profile was generated to compare the in-field (elastic support) and the laboratory (rigid support) boundary conditions.

Steps performed to generate a dummy loading profile:

(a) The Military Standard vehicle test PSD was applied to the base of the original field condition (Beam with Elastic Support) to simulate the dummy road surface loading.

(b) Response acceleration of the beam with elastic foundation was determined and used as the input for the accelerated durability tests.

(c) The response acceleration was multiplied with some constant acceleration factor to get different RMS input for the AD tests.

(d) The FDS and the ERS of the input acceleration profiles were compared to confirm the validity of the input loading profiles for the AD tests.

Figure 59 shows the military standard acceleration PSD specification which is assumed to be the combination of different types of random loads coming from different road surfaces. In the Random Vibration tool of the ANSYS Workbench, this loading spectrum was applied to the base of the original vehicle assembly (Beam with Semi-Rigid/ Elastic Foundation) which includes the elastic joint stiffness and damping.

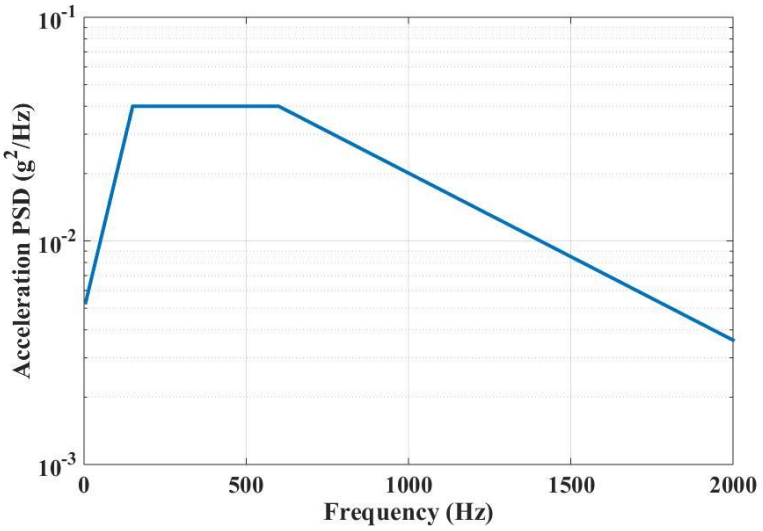


**Figure 59: Military Standard PSD Specification[176]**

The primary reason for applying this random loading is to generate a virtual proving ground environment, so that the response can be accelerated later in the laboratory tests. According to Halfpenny[45], the road load responses are modified using mission profiling and test tailoring approaches which have been skipped in this thesis to simplify the input without altering the

actual shape of the loading spectrum, e.g. the peak of the random vibration responses will be always near the vicinity of the natural frequency regions irrespective of the input load.

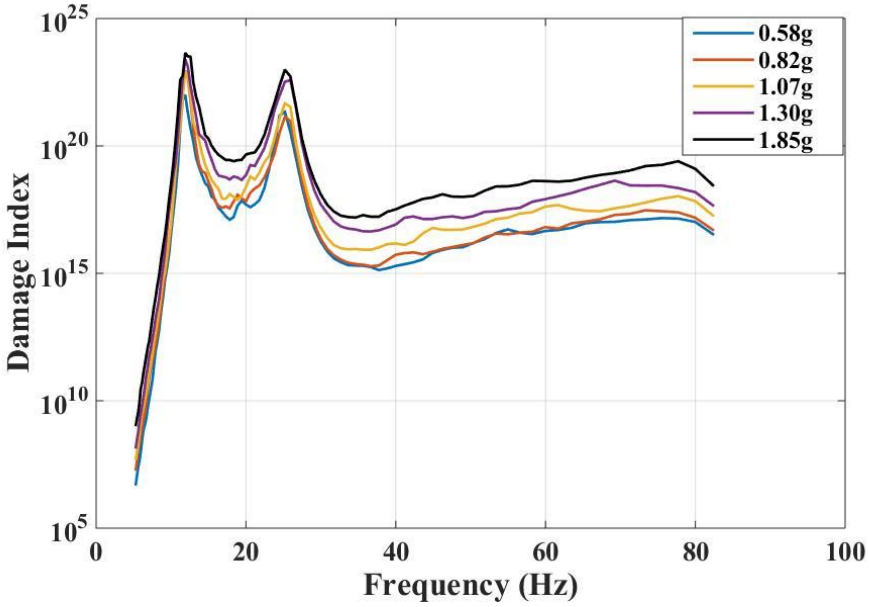


**Figure 60: Fatigue Damage Spectrum (FDS) of Input PSD**

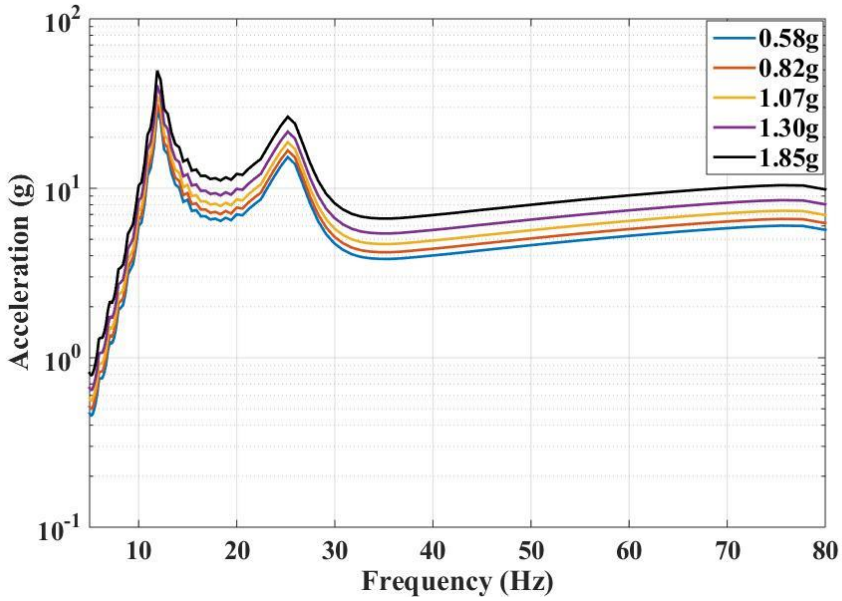


**Figure 61: Extreme Response Spectrum (ERS) of Input PSD**

In Figure 60 and 61, the FDS and the ERS are shown to check whether the generated pseudo loading profiles met the conditions of the AD test. From Figure 60, it can be noticed that the shapes of the FDS curves for all RMS input level are almost identical which confirms that the loadings will result in similar type of fatigue failure. In Figure 61, the ERS of the loadings are compared where the differences among the peak response acceleration for all five input loading level is very small which confirms the absence of any kind of unrealistic loading. Later, the validated loading profiles were passed to both kinds of boundary conditions to compare their response fatigue damage.

#### 4.5.2.2 Application of the Loading Profiles

In ANSYS Workbench, both random vibration and transient dynamic analysis was performed to find out the fatigue life in both frequency and time domain respectively. For random vibration analysis the PSD profiles were directly applied to the both rigid and elastic foundations.

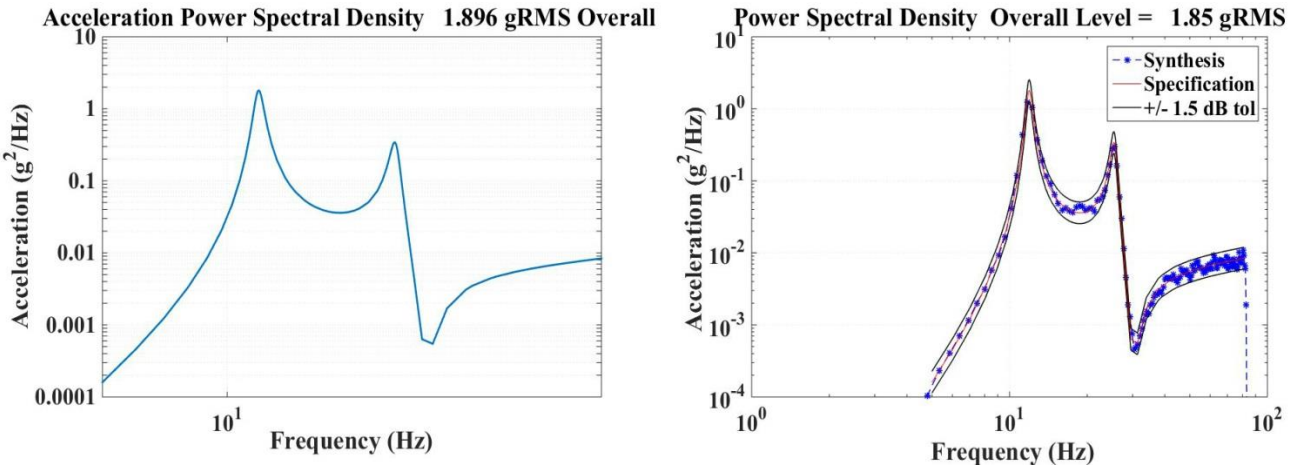


**Figure 62: Time Series Synthesis from Acceleration PSD**

For time domain analysis, the PSD was first converted to a 60 second equivalent time series loading profile as shown in Figure 62 using Inverse Fourier Transformation. The obtained time

series was within ±1.5 dB tolerance limit. According to Figure 62, for a 1.896 gRMS PSD, the synthesised time history gives an overall RMS of 1.85g which shows only 2.42% deviation with the PSD loading profile.

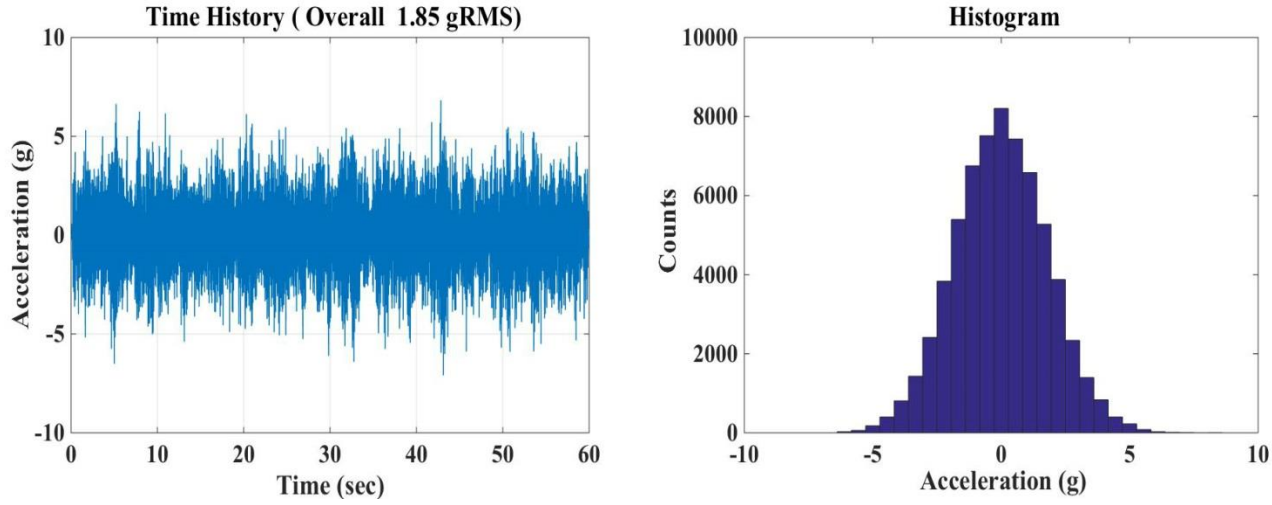


**Figure 63: Acceleration Time History & Bell-Shaped Histogram**

Figure 63 confirms the random behavior of the time history which follows the Gaussian Normal Distribution (Bell-Shaped Curve) of the histogram. Figure 64 shows the bending stress generated due to the application of transient time series to the base of the beam with rigid and the elastic boundary conditions. For both types of boundary conditions, the critical location corresponds to the same position. In Figure 65, the output stress PSD of the beam with both elastic and rigid foundations is compared for a specific input loading (1.85 gRMS). From this figure it can be noticed that the area under the elastic foundation is larger than the rigid foundation curve which confirms the higher output RMS of the elastically supported beam. As the position of the peak amplitude of the input loading spectrum and the natural frequency of the elastic foundation coincide with each other the response of the beam with elastic foundation becomes higher around that region. But the amplitude of the input loading is not high enough to excite the beam with

rigid boundary condition to a higher level as marked as dotted circle in Figure 65. As a result, the overall RMS of the beam with rigid boundary condition yields to a smaller value than the beam with the elastic foundation.

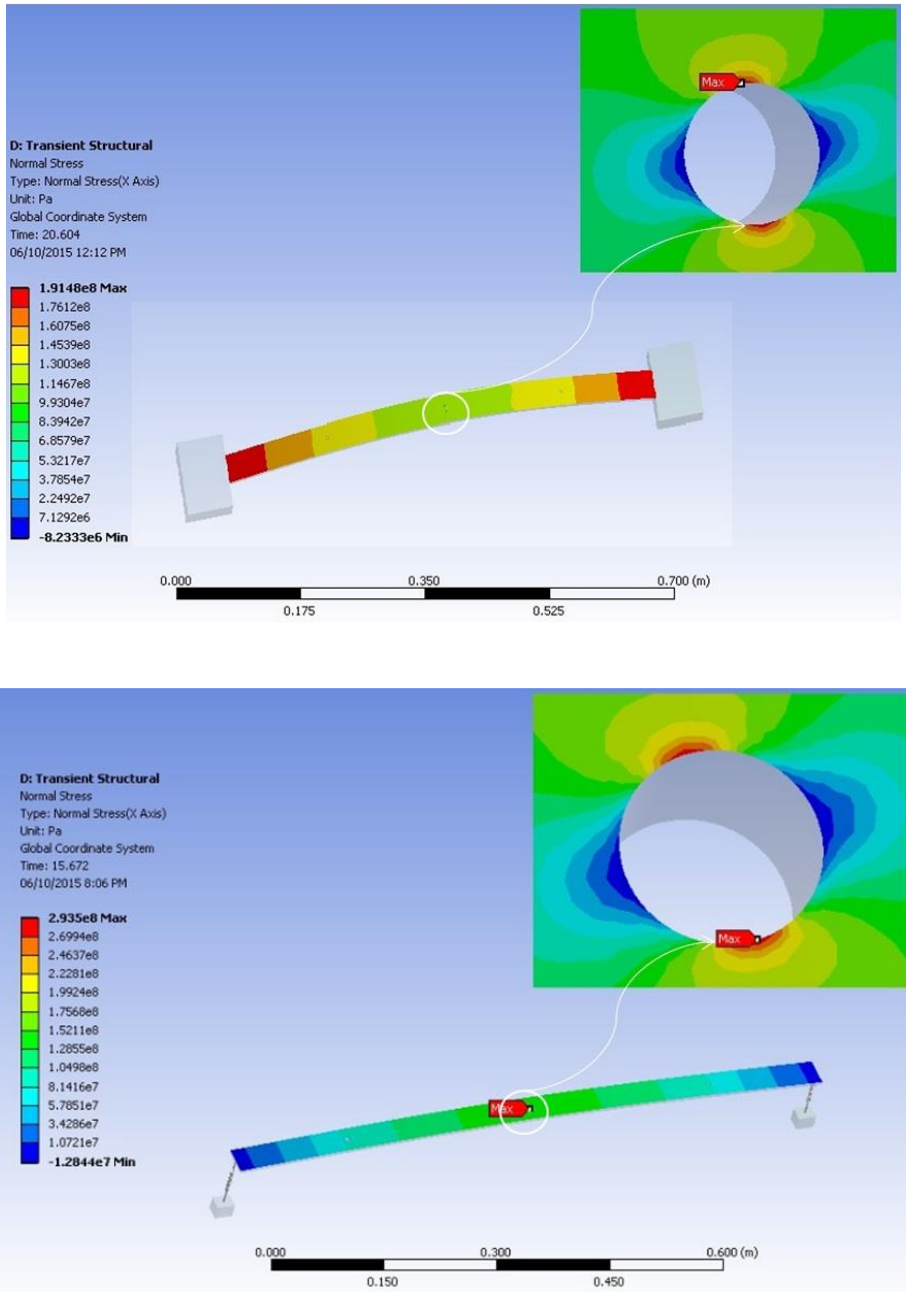


**Figure 64: Bending Stress due to the Input PSD loading, Beam with Rigid Support (Top), Beam with Elastic Support (Bottom)**

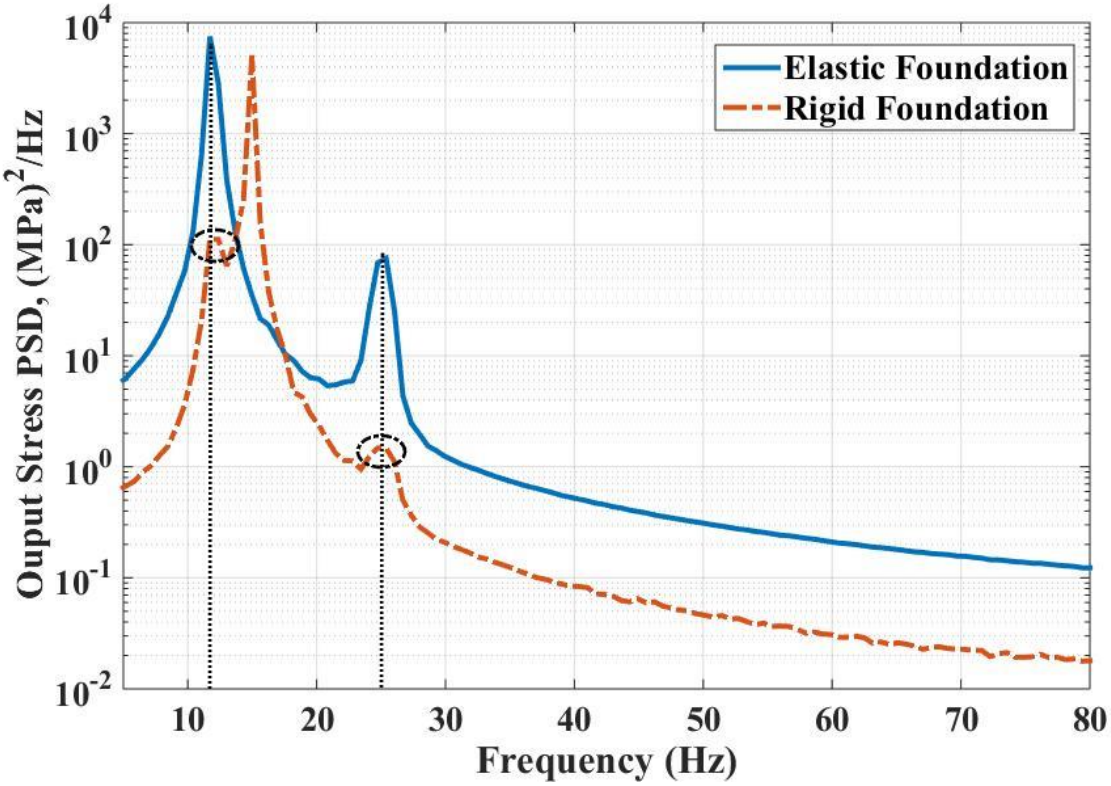


**Figure 65: Output Stress PSD Comparison**

From figure 65 it can be easily anticipated that the fatigue damage of the elastic support would be higher than the rigid support due to the higher stress RMS. In this thesis, random vibration fatigue damage is calculated using both time domain and frequency domain cycle counting algorithms. Table 11 represents the estimated fatigue damage of both elastic and rigidly supported beam using different types of cycle counting methods. Due to the complex analytical formulation of different probability distribution functions for different algorithms, the final fatigue damage was chosen by taking the average of all the methods. Figure 66 depicts the cumulative fatigue damage for typical random loading of different RMS for both types of structures. According to this figure, the cumulative damage on the beam supported by the rigid foundation is almost 100 times smaller compared to the beam supported by the elastic foundation

for a range of acceleration input level. Due to the coincidence of the position of the peak amplitude of the input loading spectrum and the natural frequency of the elastic foundation, it showed higher fatigue damage compared with the rigid support which significantly underestimates the fatigue failure of the real field. As a result, it can be predicted that the component would fail earlier in real field than the laboratory testing environment.

**Table 11: Estimated Fatigue Damage Using Different Cycle Counting Algorithms**

| Input Accl$^{n}$ RMS (g) | Boundary Conditions | Cumulative Fatigue Damage | | | | |
|---|---|---|---|---|---|---|
| | | Time Domain (Rainflow) | Frequency Domain | | | Average |
| | | | Dirlik | Narrowband | Zhao-Baker | |
| 0.58g | Rigid | 1.28E-09 | 1.32E-09 | 1.48E-09 | 1.59E-09 | 1.42E-09 |
| | Elastic | 2.46E-07 | 2.31E-07 | 2.39E-07 | 2.57E-07 | 2.44E-07 |
| 0.82g | Rigid | 1.47E-08 | 1.86E-08 | 1.91E-08 | 1.75E-08 | 1.75E-08 |
| | Elastic | 7.80E-06 | 7.51E-06 | 7.98E-06 | 7.73E-06 | 7.76E-06 |
| 1.07g | Rigid | 1.37E-07 | 1.11E-07 | 1.53E-07 | 1.47E-07 | 1.37E-07 |
| | Elastic | 6.69E-05 | 7.11E-05 | 6.89E-05 | 6.93E-05 | 6.91E-05 |
| 1.30g | Rigid | 2.09E-06 | 2.41E-06 | 2.17E-06 | 2.29E-06 | 2.24E-06 |
| | Elastic | 1.55E-03 | 1.76E-03 | 1.61E-03 | 1.88E-03 | 1.70E-03 |
| 1.85g | Rigid | 2.42E-05 | 2.72E-05 | 2.51E-05 | 2.48E-05 | 2.53E-05 |
| | Elastic | 2.33E-02 | 2.39E-02 | 2.66E-02 | 2.53E-02 | 2.48E-02 |

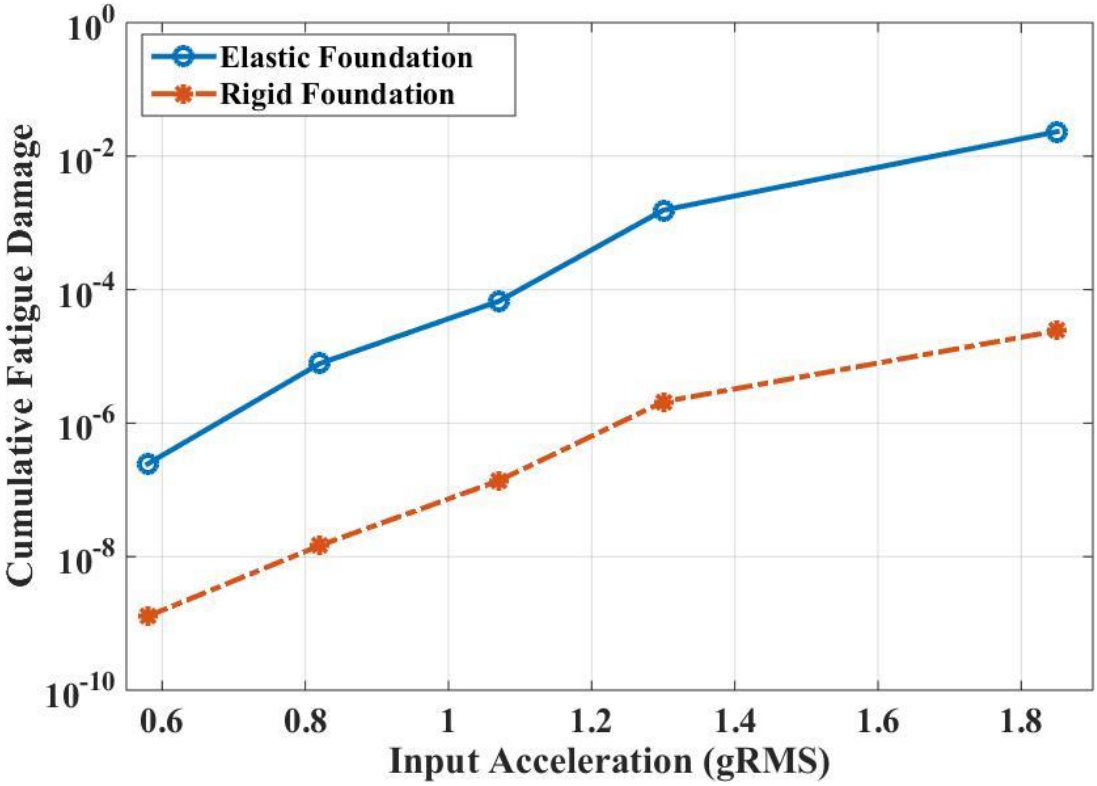


**Figure 66: Comparison of the Cumulative Fatigue Damage for Random Vibration Loading Profiles**

#### 4.5.2.3 Effect of the Joint Stiffness

For a specific random vibration loading profile, the fatigue damage is largely dominated by the joint stiffness of the structure. The AD loading profiles are generated such a way so that maximum energy concentrates near the fundamental natural frequency of the vehicle component. As a result, the fatigue damage increases at the joint stiffness which results in a natural frequency close to the high amplitude content frequency of the input loading spectrum. This behavior of the random vibration loading profiles is shown in Figure 67. In this figure for a specific damping ratio (2.53%), the fatigue damage reaches to the highest value ($\approx 10^{4}$) as the spring stiffness approaches to 3857 N/m. This spring stiffness leads the natural frequency of the system to 11.81

Hz which coincides with the peak amplitude region of the input loading frequency spectrum. Later, with the increase of spring stiffness the fatigue damage reduces and the fatigue damage becomes almost constant with the further increase of spring stiffness from 15,000 N/m. So it can be summarized that small change of the stiffness of the boundary condition in the laboratory would bring a significant amount of change in the fatigue life compared to the real field vehicles.

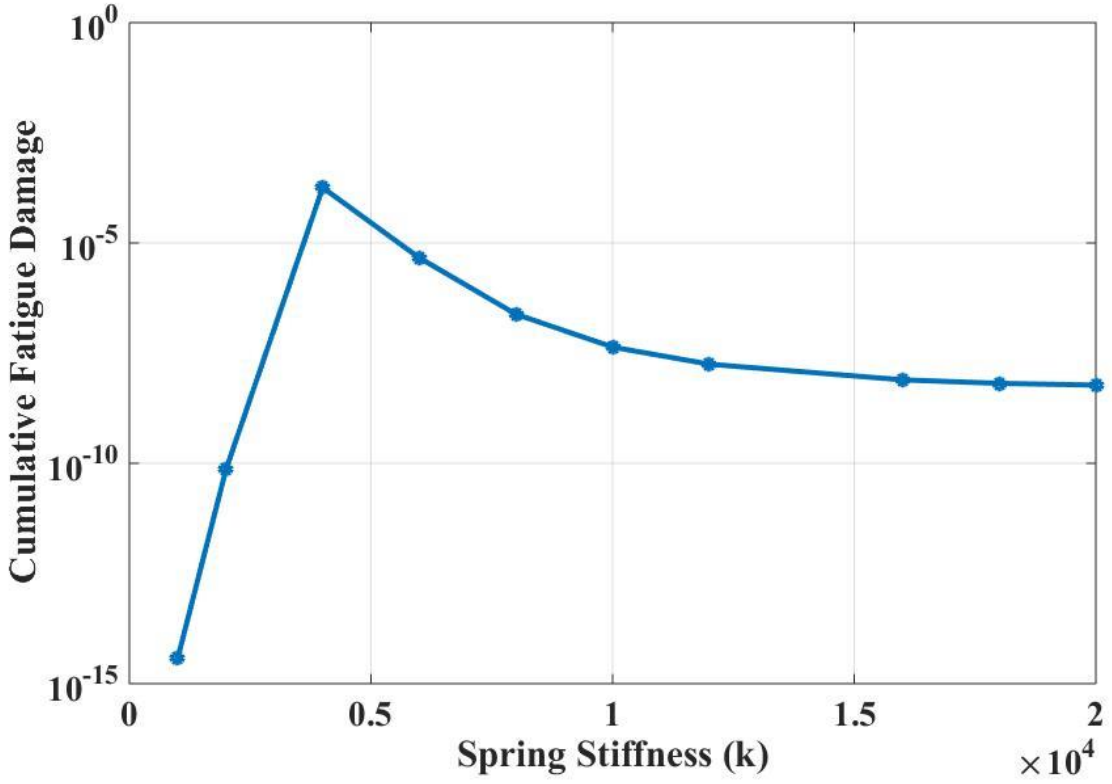


**Figure 67: Effect of Joint Stiffness on Fatigue Damage**

#### 4.5.2.4 Effect of Damping Ratio on Fatigue Damage

Damping ratio is another important factor that largely contributes to the fatigue damage of any component. For a specific spring constant (3857 N/m) and input loading (0.58 gRMS) the change of fatigue damage due to the change of damping ratio is shown in Figure 68. From this figure it can be noticed that, as the damping ratio increases fatigue reduces drastically with a stepper

slope. Damping ratio of a component attached to a vehicle usually remains in between 2 to 20% due to the addition of tire, suspension system and rubber mountings. So direct mounting of the components to the laboratory test rig would certainly alter the fatigue behavior of the original test piece as it would consider a negligible amount of damping which is not always true in the real case.

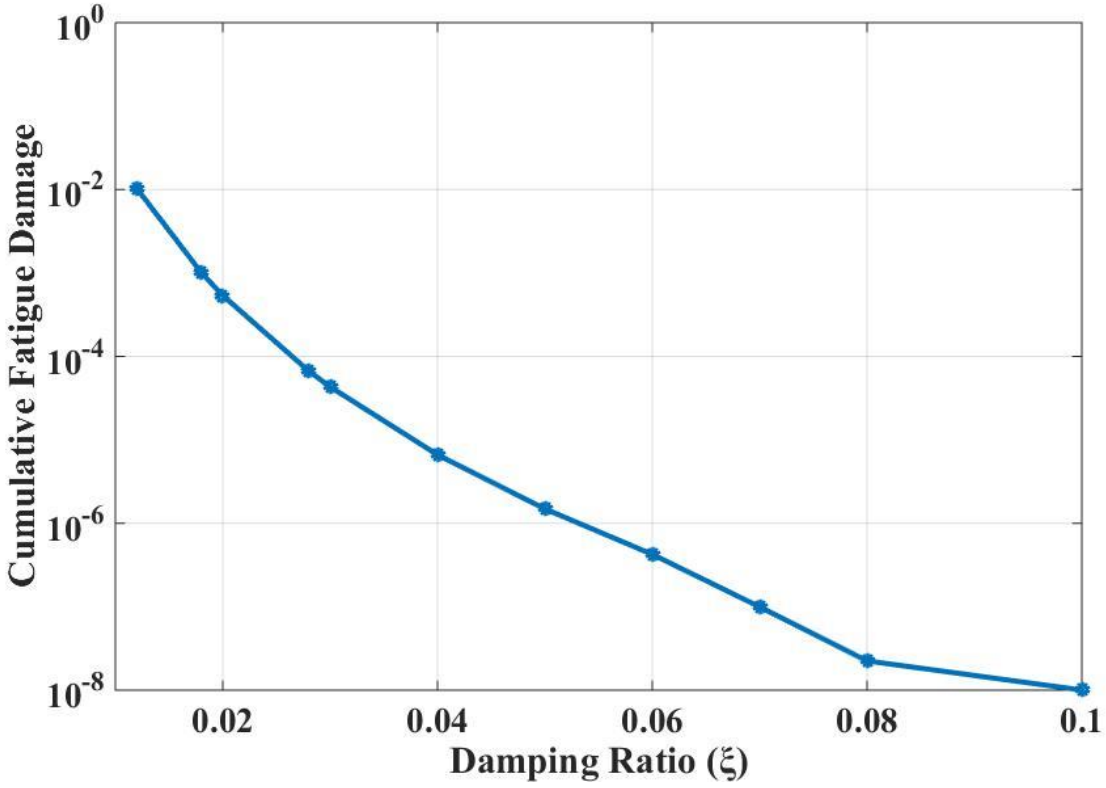


**Figure 68: Effect of Damping Ratio on Fatigue Damage**

#### 4.5.2.5 Effect of the Fatigue Exponent (m) on Fatigue Damage

Generally Fatigue exponent or inverse Basquin's slope may fall anywhere in the range of 4 to 12 depending on the material properties of the component. In S-N curve, fatigue damage is determined by specifying the linear slope of the diagram. This might significantly affect the estimation of fatigue damage as it increases exponentially with the stress level. In Figure 69,

comparison of fatigue life between the elastic and rigid foundation is shown for different fatigue exponents. It can be seen that the damage is increasing linearly in a semi-log plot with the increase in the inverse S-N curve slope (m). In this figure the beam with the elastic foundation would fail if the fatigue exponent crosses 11.5 for that specific period of loading. But the same component with same type of loading would yield to a fatigue damage of only $10^{-5}$ when the fatigue exponent is around 9. Again, the beam with the rigid foundation would not fail for that specific loading even if the fatigue exponent reaches to the highest value 12. So, proper estimation of fatigue exponent is one of most important criteria to meet the reliability of predicted fatigue life of any component in Computer Aided Modeling.

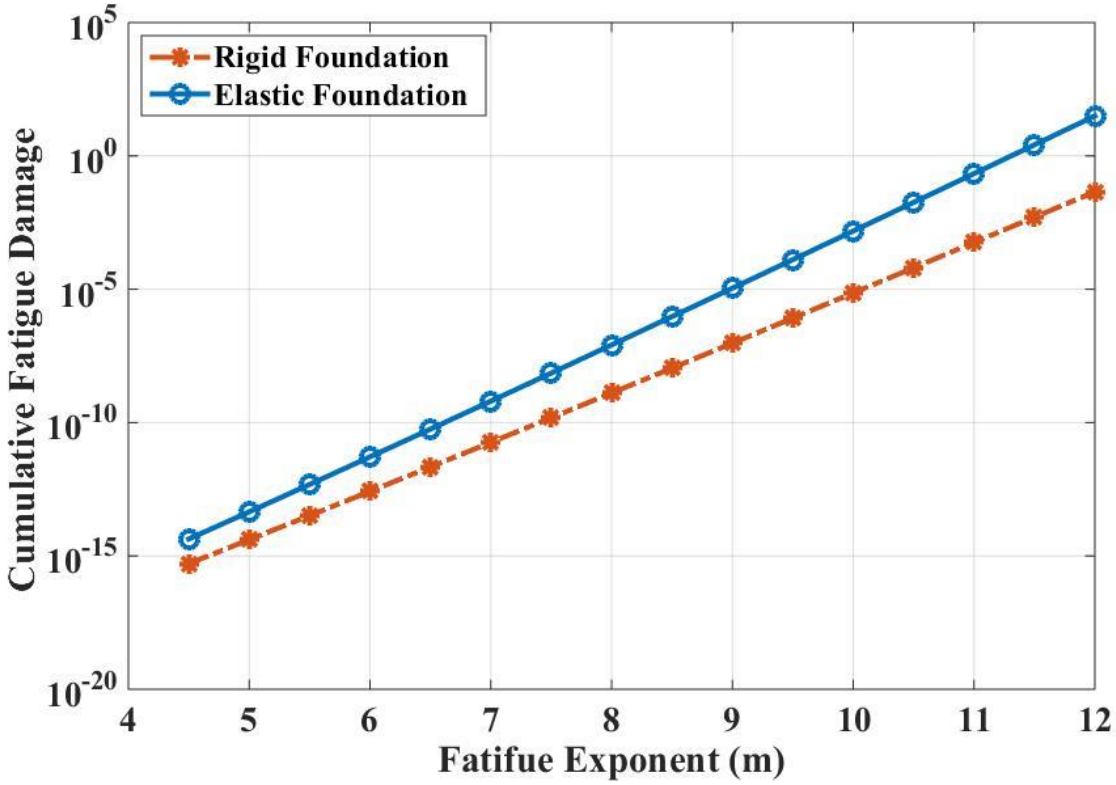


**Figure 69: Effect of Fatigue Exponent on Cumulative Fatigue Damage**

CHAPTER 5

# 5 CONCLUSIONS & FUTURE RECOMMENDTIONS

Durability testing is one of the most essential requirements that a vehicle must have to meet before it becomes available to the customer. To save both time and money, Accelerated Durability Testing in the laboratory facility has become increasingly popular among the top automobile industries. In this thesis, some of the gaps of the current testing methodologies are discussed using both experimental and theoretical explanation. Based on the knowledge of the conventional AD test rigs, significant amount of differences were noticed between the boundary conditions of an in-field vehicle component and the laboratory fixtures. In most of the cases the vehicle components are directly mounted in the test rig which somehow alters the dynamic properties of the component in service. However, dynamic modal properties of the tested structure especially the natural frequencies, damping and mode shapes change significantly with the addition of mass and elastic foundation (tire, suspension etc.) to the component so as to affect the fatigue damage analysis results. To demonstrate the changes in the dynamic modal parameters and fatigue life between the real field and the laboratory situation, a beam was designed with specific dynamic characteristics supported by the elastic foundation (spring and mass) and the rigid foundation (simply supported) respectively. Firstly, Experimental Modal Analysis (EMA) was performed to demonstrate the effect of the elastic support on the variation of modal parameters of the tested beam structure. The modal parameters obtained from the experiments were then used to tune the FE model and several dynamic response tests were carried out to validate the proper functioning and reliability of the FEM results. Then, mainly

two types of loading profiles were used to perform numerical bending stress analysis based on the literature. In FEM simulations, large mass method (LMM) was employed to simulate base loading which was compared with the enforced motion method that showed a very good agreement. Both time and frequency domain fatigue analysis results were analysed to validate the consistency of the simulation results. From the Sine Sweep Vibration test it was noticed that the rigid foundation failed earlier due to the constant amplitude loading with much lower damping ratio. Though the fatigue damage increases exponentially with the increase of the stress magnitude, slight difference in stress value brings a large amount of change in fatigue life. Simulation results showed a huge deviation in the cumulative fatigue damage plot between the two support fixtures which overestimates the overall fatigue life and proves the inability of the sine sweep profile to be used as an input loading for AD tests. In addition to the sine sweep testing, Pseudo random loads were generated to compare the fatigue damage between the elastically and the rigidly supported beam structures. According to the mission profiling and test synthesis method, the amplitude of input acceleration gets higher near the natural frequency region to insist failure in an accelerated manner. If the natural frequency is altered due to the change of the boundary conditions, the resonance zone also shifts away from the high amplitude region of the input loading profile. So it might take much more time to fail in the laboratory than it was predicted. As a result the main objective of the generation of loading profile is not fulfilled properly. The change of fatigue life due to the change of joint stiffness, damping and fatigue exponent was showed in this work. Modification of any of these parameters would bring a huge change in the total cumulative fatigue damage of the component. So it can be concluded that tuning of the dynamic properties in the laboratory tests is of great importance in order to get a reliable AD test outcome.

The above study provides comprehensive analysis between the experimental and FEM modeling, hence providing a platform to take the FEM study a step further by verifying its veracity and applicability in real life durability testing with appropriate loading. Due to the unavailability of the vertical shaker table the experimental setup could not be used for real AD test. But, in future this kind of modified test rig fixtures can be used to perform AD testing with higher accuracy. The beam model may be replaced by a real world component. The effect of proper damping effect should be considered while performing AD testing, as it will affect the amplitude of the vibration to a large extent. In future multi axial loading may be employed to get an actual overview of the real world driving condition.

## REFERENCES


[1] Wöhler, A. (1860). Versuche über die Festigkeit der Eisenbahnwagenachsen.*Zeitschrift für Bauwesen*, *10*, 160-161.

[2] Cui, W. (2002). A state-of-the-art review on fatigue life prediction methods for metal structures. *Journal of marine science and technology*, *7*(1), 43-56.

[3] Murakami, Y. (2002). *Metal fatigue: effects of small defects and nonmetallic inclusions: effects of small defects and nonmetallic inclusions*. Elsevier.

[4] Schijve, J. (2003). Fatigue of structures and materials in the 20th century and the state of the art. *International Journal of Fatigue*, *25*(8), 679-702.

[5] Ritchie, R. O. (1999). Mechanisms of fatigue-crack propagation in ductile and brittle solids. *International Journal of Fracture*, *100*(1), 55-83.

[6] Xu, K., Wu, Y., & Wu, Q. (2011, January). Development of vibration loading profiles for accelerated durability tests of ground vehicles. In *ASME 2011 Dynamic Systems and Control Conference and Bath/ASME Symposium on Fluid Power and Motion Control* (pp. 717-724). American Society of Mechanical Engineers.

[7] "Test Track Facility." [Online]. Available: http://www.pti.psu.edu/testTrack. [Accessed: 30-Oct-2015].

[8] Xu, P., Wong, D., LeBlanc, P., & Peticca, G. (2005). Road test simulation technology in light vehicle development and durability evaluation. *SAE transactions*, *114*(6), 868-879.

[9] Lin, K. Y., Hwang, J. R., Chang, J. M., Chen, C. T., Chen, C. T., Chen, C. C., & Hsieh, C. C. (2006). *Durability assessment and riding comfort evaluation of a new type scooter by road simulation technique* (No. 2006-01-0730). SAE Technical Paper.

[10] Wu, V., Andrews, G., Vermeulen, C., Wong, D., Peticca, G., & Nhan, B. (2007). *Effective solutions to decreasing load conflicts using 4DOF road test simulators* (No. 2007-01-1350). SAE Technical Paper.

[11] "Multi-Axial Simulation Table (MAST) Systems." [Online]. Available: https://www.mts.com/en/products/producttype/test-systems/simulation-systems/multiaxial-simulation-tables/index.htm. [Accessed: 02-Nov-2015].

[12] “Road Test Simulation Lab.” [Online]. Available: http://www.chryslertestservices.com/testing/road-test-simulation.html. [Accessed: 15-Nov-2015].

[13] Lin, K. Y., Chang, J. M., Wu, J. H., Chang, C. H., Chang, S. H., Hwang, J. R., & Fung, C. P. (2005). *Durability assessments of motorcycle handlebars*(No. 2005-01-0801). SAE Technical Paper.

[14] Xu. K (2011), “Development of Vibration Loading Profiles for Accelerated Durability Tests of Ground Vehicles", Copyright © 2011 by Ke Xu.

[15] Shafiullah, A. K. M., & Wu, C. Q. (2013). Generation and validation of loading profiles for highly accelerated durability tests of ground vehicle components. *Engineering Failure Analysis*, *33*, 1-16.

[16] Gillespie, T. D. (1992). *Fundamentals of vehicle dynamics* (Vol. 114). SAE Technical Paper.

[17] “SmartShakerTM w/Integrated Power Amplifier | Excitation | The Modal Shop, Inc.” [Online]. Available: http://www.modalshop.com/excitation/SmartShaker-w/Integrated-Power-Amplifier?ID=272. [Accessed: 05-Nov-2015].

[18] Klyatis, L. M. (2012). *Accelerated reliability and durability testing technology*(Vol. 70). John Wiley & Sons.

[19] “Quality from Customer Needs to Customer Satisfaction.” [Online]. Available: https://www.studentlitteratur.se/#9789144059426/Quality+from+Customer+Needs+to+Customer+Satisfaction. [Accessed: 16-Nov-2015].

[20] Bergman, B., De Maré, J., Svensson, T., & Loren, S. (Eds.). (2009). *Robust design methodology for reliability: exploring the effects of variation and uncertainty*. John Wiley & Sons.

[21] Davis, T.P. (2006). Science, engineering, and statistics. *Applied Stochastic Models in Business and Industry*, *22*(5-6), 401-430.

[22] Johannesson, P., Bergman, B., Svensson, T., Arvidsson, M., Lönnqvist, Å., Barone, S., & Maré, J. (2013). A robustness approach to reliability. *Quality and Reliability Engineering*

*International*, *29*(1), 17-32.

[23] O'Connor, P., & Kleyner, A. (2011). *Practical reliability engineering*. John Wiley & Sons.

[24] SENER, A. S. (2011). Determination of vehicle components fatigue life based on FEA method and experimental analysis. *Head of Automotive Technology Division, Vocational High Schools, Istanbul Aydin University*,*2*(1), 133-145.

[25] Grubisic, V. V., & Fischer, G. (1997). *Methodology for effective design evaluation and durability approval of car suspension components* (No. 970094). SAE Technical Paper.

[26] Bogsjö, K. (2006). Development of analysis tools and stochastic models of road profiles regarding their influence on heavy vehicle fatigue. *Vehicle System Dynamics*, *44*(sup1), 780-790.

[27] Chakhunashvili, A., Johansson, P. M., & Bergman, B. L. (2004, January). Variation mode and effect analysis. In *Reliability and Maintainability, 2004 Annual Symposium-RAMS* (pp. 364-369). IEEE.

[28] Johansson, P., Chakhunashvili, A., Barone, S., & Bergman, B. (2006). Variation mode and effect analysis: a practical tool for quality improvement.*Quality and reliability engineering international*, *22*(8), 865-876.

[29] Kouta, R., & Play, D. (1999). Correlation procedures for fatigue life determination. *Journal of Mechanical Design*, *121*(2), 289-296.

[30] Xu, P., Wong, D., LeBlanc, P., & Peticca, G. (2005). Road test simulation technology in light vehicle development and durability evaluation. *SAE transactions*, *114*(6), 868-879.

[31] Miner, M. A. (1945). Cumulative damage in fatigue. *Journal of applied mechanics*, *12*(3), 159-164.

[32] Yu, X., Chang, K. H., & Choi, K. K. (1998). Probabilistic structural durability prediction. *AIAA journal*, *36*(4), 628-637.

[33] Caruso, H., & Dasgupta, A. (1998, January). A fundamental overview of accelerated-testing analytic models. In *Reliability and Maintainability Symposium, 1998. Proceedings., Annual* (pp. 389-393). IEEE.

[34] Nelson, W. B. (2009). *Accelerated testing: statistical models, test plans, and data analysis* (Vol. 344). John Wiley & Sons.

[35] Meeker, W. Q., & Escobar, L. A. (1993). A review of recent research and current issues in accelerated testing. *International Statistical Review/Revue Internationale de Statistique*, 147-168.

[36] Colin ASHMORE, S., Piersol, A. G., & Witte, J. J. (1992). Accelerated service life testing of automotive vehicles on a test course. *Vehicle System Dynamics*, *21*(1), 89-108.

[37] Jeong, G. S., Moon, H. S., & Sung, D. U. (2003). *The development of lab-simulation test to accelerate the durability validation of engine mounting and wiring harness* (No. 2003-01-0949). SAE Technical Paper.

[38] Su, H., Ma, M., & Olson, D. (2004). *Accelerated tests of wiper motor retainers using CAE durability and reliability techniques* (No. 2004-01-1644). SAE Technical Paper.

[39] Dowling, N. E. (1988). Estimation and correlation of fatigue lives for random loading. *International Journal of Fatigue*, *10*(3), 179-185.

[40] Panse, S. M., & Gosavi, S. S. (2004). *Integrated structural durability test cycle development for a car and its components* (No. 2004-01-1654). SAE Technical Paper.

[41] Haq, S., Temkin, M., Black, L., & Bammel, P. (2005). *Vehicle road simulation testing, correlation and variability* (No. 2005-01-0856). SAE Technical Paper.

[42] Prakash, S. S. (2013). *A Method of Accelerating Durability Tests by Pseudo Damage Editing* (No. 2013-26-0138). SAE Technical Paper.

[43] Bunnori, N., Nor, N., Jiun, K., & Kudus, S. (2014). Analysis of failure mechanisms in fatigue test of reinforced concrete beam utilizing acoustic emission. *The International Journal of Multiphysics*, *8*(4), 349-358.

[44] Roberts, J. B., & Spanos, P. D. (2003). *Random vibration and statistical linearization*. Courier Corporation.

[45] Halfpenny, A. (2006, July). Methods for accelerating dynamic durability tests.

In *Proceedings of the 9th International Conference on Recent Advances in Structural Dynamic*.

[46] Norton, M. P., & Karczub, D. G. (2003). *Fundamentals of noise and vibration analysis for engineers*. Cambridge university press.

[47] Sunil, K. V., Sheepri, S., Kandula, K., & Kumar, A. (2014). *Integrated Approach for Accelerated Fatigue Testing of Resonating Structures* (No. 2014-01-0821). SAE Technical Paper.

[48] Heydinger, G. J., Bixel, R., Jebode, H., Peterman, E., & Sidhu, A. (2011). Vehicle Characteristics Measurements of Recreational Off-Highway Vehicles. *SEA, Ltd., Columbus, Ohio, USA*.

[49] Halfpenny, A., & Pompetzki, M. (2011). Proving Ground Optimization and Damage Correlation with Customer Usage. *SAE International Journal of Materials & Manufacturing*, *4*(1), 620-631.

[50] Gopalakrishnan, R., & Agrawal, H. N. (1993). *Durability analysis of full automotive body structures* (No. 930568). SAE Technical Paper.

[51] Berger, C., Eulitz, K. G., Heuler, P., Kotte, K. L., Naundorf, H., Schuetz W, Sonsino CM, Wimmer A, Zenner H. (2002). Betriebsfestigkeit in Germany—an overview.*International Journal of Fatigue*, *24*(6), 603-625.

[52] GAM EG 13, "Essais généraux en environnement des matériels.," Ministère de la Défense, Délégation Générale pour l'Armement.

[53] N. AECTP, "Validation of mechanical environmental test methods," vol. NATO AECTP, no. Final Draft, 2003.

[54] Lalanne, C. (2002). Mechanical Vibration & Shock Volume II: Mechanical Shock. *Hermes Penton Ltd., New York*.

[55] Biot, M. A. (1932). *Transient oscillations in elastic systems* (Doctoral dissertation, California Institute of Technology).

[56] Biot, M. (1933). Theory of elastic systems vibrating under transient impulse with an application to earthquake-proof buildings. *Proceedings of the National Academy of*

*Sciences*, *19*(2), 262-268.

[57] Miles, J. W. (1957). On structural fatigue under random loading. *The Journal of the Acoustical Society of America*, *29*(1), 176-176.

[58] Pompetzki, M., Dabell, B., & Lin, X. (2010). Advancements in the Automotive Durability Process. *Structural Durability & Health Monitoring*,*6*(2), 69-76.

[59] Cull, S., Yang, C., & Wu, C. (2010). *Generation and verification of accelerated durability tests. Department of Mechanical and Manufacturing Engineering, University of Manitoba*. Internal Report, 2010. Development Of Sine-On-Random Accelerated Tests Applied To Turbocharger Electronics Actuators.

[60] Zhang P. & Wu C. (2010). *Events identification of curve fitting method, Department of Mechanical and Manufacturing Engineering, University of Manitoba*, Internal Report, 2010.

[61] Halfpenny, A., & Kihm, F. Environmental Accelerated Testing. Use of Virtual test to extend physical Approach, White Paper (2008).

[62] Jung, D. H., & Gafurov, A. (2011). Reliability achievement of the driving system parts through development of vibration-fatigue evaluation method.*Procedia Engineering*, *10*, 1906-1916.

[63] Özsoy, S., Celik, M., & Kadıoğlu, F. S. (2008). An accelerated life test approach for aerospace structural components. *Engineering failure analysis*,*15*(7), 946-957.

[64] Aykan, M., & Celik, M. (2009). Vibration fatigue analysis and multi-axial effect in testing of aerospace structures. *Mechanical systems and signal processing*, *23*(3), 897-907.

[65] Wannenburg, J., & Heyns, P. S. (2010). An overview of numerical methodologies for durability assessment of vehicle and transport structures.*International Journal of Vehicle Systems Modelling and Testing*, *5*(1), 72-101.

[66] Bishop, N. W., & Sherratt, F. (2000). *Finite element based fatigue calculations*. NAFEMS.

[67] Dietz, S., Netter, H., & Sachau, D. (1998). Fatigue life prediction of a railway bogie under dynamic loads through simulation. *Vehicle system dynamics*,*29*(6), 385-402.

[68] Lee, Y. L., Barkey, M. E., & Kang, H. T. (2012). Metal fatigue analysis handbook.

[69] Kuo, E. Y., & Kelkar, S. G. (1995). *Vehicle body structure durability analysis*(No. 951096). SAE Technical Paper.

[70] Haiba, M., Barton, D. C., Brooks, P. C., & Levesley, M. C. (2002). Review of life assessment techniques applied to dynamically loaded automotive components. *Computers & structures*, *80*(5), 481-494.

[71] Liao, L. (2011, April). A study of inertia relief analysis. In *52nd Structural Dynamics and Materials Conference. Denver, Colorado: AIAA* (pp. 1-10).

[72] Bathe, K. J. (2006). *Finite element procedures*. Klaus-Jurgen Bathe.

[73] Rixen, D. (2001, April). Generalized mode acceleration methods and modal truncation augmentation. In *Structures, Structural Dynamics and Material Conference and Exhibit, 42nd AIAA/ASME/ASCE/AHS/ASC, AIAA Paper No. AIAA* (Vol. 1300).

[74] Conle, F. A., & Mousseau, C. W. (1991). Using vehicle dynamics simulations and finite-element results to generate ffatigue life contours for chassis components. *International Journal of Fatigue*, *13*(3), 195-205.

[75] Craig, R. R. (2000, April). Coupling of substructures for dynamic analyses: an overview. In *Proceedings of AIAA/ASME/ASCE/AHS/ASC structures, structural dynamics, and materials conference and exhibit* (pp. 1573-1584).

[76] Ottarsson, G. (1998). Modal flexibility method in ADAMS/FLEX. *Mechanical Dynamics, Inc*, 8-9.

[77] Tebbe, J. C., Chidambaram, V., Kline, J. T., Scime, S., Shah, M. P., Tasci, M., & Zheng, D. (2006). *Chassis Loads Prediction using Measurements as Input to an Unconstrained Multi-Body Dynamics Model* (No. 2006-01-0992). SAE Technical Paper.

[78] Liu, L., Ran, X., & Li, L. (2007). *Hybrid Vehicle Road Loads Simulation and Correlation* (No. 2007-01-1202). SAE Technical Paper.

[79] Zhang, Y., & Tang, A. (1996, September). The CAE revolution and the development of

the virtual proving ground approach. In *The 4th International LS-DYNA Conference, Minneapolis, Minnesota, Sept.*

[80] Zhang, Y., Tang, A., Palmer, T., & Hazard, C. (1999). Virtual Proving Ground-an integrated technology for full vehicle analysis and simulation. *International journal of vehicle design*, *21*(4-5), 450-470.

[81] Soderling, S., Sharp, M., & Leser, C. (1999). Servo Controller Compensation Methods Selection of the Correct Technique for Test Applications. *SAE Technical Paper Series*. doi:10.4271/1999-01-3000.

[82] De Cuyper, J. (2006). Linear feedback control for durability test rigs in the automotive industry. *Leuven: Katholieke Universiteit Leuven*.

[83] Yudong, H., Hong, Z., & Gang, X. (2012). Study on Control Algorithm of the Electro-hydraulic Servo System for Load Simulation Test. In *Future Communication, Computing, Control and Management* (pp. 533-541). Springer Berlin Heidelberg.

[84] Ledesma, R., Jenaway, L., Wang, Y., & Shih, S. (2005). *Development of accelerated durability tests for commercial vehicle suspension components*(No. 2005-01-3565). SAE Technical Paper.

[85] Wu, V., Leblanc, P., Peticca, G., Barnett, G., Brouerius, R., & Aczel, A. (2010). *Spindle Vertical Acceleration Control in Fixed-Reacted Road Test Simulations* (No. 2010-01-0283). SAE Technical Paper.

[86] Heim, R., Fischer, G., & Sonsino, C. M. (2006). *Early stage rig testing for durability approval* (No. 2006-01-0116). SAE Technical Paper.

[87] Dressler, K., Speckert, M., & Bitsch, G. (2009). Virtual durability test rigs for automotive engineering. *Vehicle System Dynamics*, *47*(4), 387-401.

[88] McGuire D. J., "FEMCI Book - Notes on Semi-Rigid Connections." [Online]. Available: https://femci.gsfc.nasa.gov/semirigid/. [Accessed: 20-Nov-2015].

[89] Cole, D. J. (2001). Fundamental issues in suspension design for heavy road vehicles. *Vehicle System Dynamics*, *35*(4-5), 319-360.

[90] Lutz, A., Rauh, J., & Reinalter, W. (2007). Developments in vehicle dynamics and the tire

model performance test. *Vehicle System Dynamics*,*45*(S1), 7-19.

[91] Bastow, D., Howard, G., & Whitehead, J. P. (2004). *Car suspension and handling* (p. 29). Warrendale: SAE international.

[92] Cheng, W. N., Cheng, C. C., & Koopmann, G. H. (2008). Dynamic beam modification using dimples. *Journal of Vibration and Acoustics*, *130*(4), 041007.

[93] Wang, K. W., Lai, J. S., & Yu, W. K. (1996). An energy-based parametric control approach for structural vibration suppression via semi-active piezoelectric networks. *Journal of vibration and acoustics*, *118*(3), 505-509.

[94] Weaver Jr, W., Timoshenko, S. P., & Young, D. H. (1990). *Vibration problems in engineering*. John Wiley & Sons.

[95] Blevins, R. D., & Plunkett, R. (1980). Formulas for natural frequency and mode shape. *Journal of Applied Mechanics*, *47*, 461.

[96] Rao, C. K. (1989). Frequency analysis of clamped-clamped uniform beams with intermediate elastic support. *Journal of Sound and Vibration*, *133*(3), 502-509.

[97] Szelag, D., & Mróz, Z. (1979). Optimal design of vibrating beams with unspecified support reactions. *Computer Methods in Applied Mechanics and Engineering*, *19*(3), 333-349.

[98] Smith, K. B., & Shust, W. C. (2004). Bounding Natural Frequencies in Structures I: Gross Geometry, Material and Boundary Conditions. In*Proceedings of the XXII International Modal Analysis Conference, Society of Experimental Mechanics*.

[99] Wu, J. S., & Chou, H. M. (1999). A new approach for determining the natural frequencies and mode shapes of a uniform beam carrying any number of sprung masses. *Journal of Sound and Vibration*, *220*(3), 451-468.

[100] Wu, J. S., & Lin, T. L. (1990). Free vibration analysis of a uniform cantilever beam with point masses by an analytical-and-numerical-combined method.*Journal of Sound and Vibration*, *136*(2), 201-213.

[101] Cha, P. D. (2005). A general approach to formulating the frequency equation for a beam carrying miscellaneous attachments. *Journal of Sound and Vibration*, *286*(4), 921-939.

[102] Naguleswaran, S. (1994). Lateral vibration of a centrifugally tensioned uniform Euler-Bernoulli beam. *Journal of sound and vibration*, *176*(5), 613-624.

[103] Wu, J. J. (2003). Use of effective stiffness matrix for the free vibration analyses of a non-uniform cantilever beam carrying multiple two degree-of-freedom spring–damper–mass systems. *Computers & structures*, *81*(24), 2319-2330.

[104] Banerjee, J. R. (2012). Free vibration of beams carrying spring-mass systems− A dynamic stiffness approach. *Computers & Structures*, *104*, 21-26.

[105] Wanxie, Z., Williams, F. W., & Bennett, P. N. (1997). Extension of the Wittrick-Williams algorithm to mixed variable systems. *Journal of vibration and acoustics*, *119*(3), 334-340.

[106] Schwarz, B. J., & Richardson, M. H. (1999). Experimental modal analysis.*CSI Reliability week*, *35*(1), 1-12.

[107] Bishop, R. E. D., & Gladwell, G. M. L. (1963). An investigation into the theory of resonance testing. *Philosophical Transactions of the Royal Society of London A: Mathematical, Physical and Engineering Sciences*, *255*(1055), 241-280.

[108] Kennedy, C. C. (2012). Use of vectors in vibration measurement and analysis. *Journal of the Aeronautical Sciences*..

[109] Pendered, J. W. (1965). Theoretical investigation into the effects of close natural frequencies in resonance testing. *Journal of Mechanical Engineering Science*, *7*(4), 372-379.

[110] Avitabile, P. (2006). PART 5: 101 WAYS TO EXTRACT MODAL PARAMETERS—WHICH ONE IS FOR ME?. *Experimental techniques*,*30*(5), 48-56.

[111] e Silva, J. M. M., & Maia, N. M. (Eds.). (2012). *Modal analysis and testing*(Vol. 363). Springer Science & Business Media.

[112] Ewins, D. J. (1984). *Modal testing: theory and practice* (Vol. 15). Letchworth: Research studies press.

[113] Richardson, M. H., & Formenti, D. L. (1982, November). Parameter estimation from

frequency response measurements using rational fraction polynomials. In *Proceedings of the 1st international modal analysis conference* (Vol. 1, pp. 167-186). Union College Schenectady, NY.

[114] Brincker, R., Zhang, L., & Andersen, P. (2001). Modal identification of output-only systems using frequency domain decomposition. *Smart materials and structures*, *10*(3), 441.

[115] Leuridan, J. M., Brown, D. L., & Allemang, R. J. (1986). Time domain parameter identification methods for linear modal analysis: a unifying approach. *Journal of vibration, acoustics, stress, and reliability in design*,*108*(1), 1-8.

[116] Ibrahim, S. R., & Mikulcik, E. C. (1977). A method for the direct identification of vibration parameters from the free response.

[117] S. Ibrahim, "Modal confidence factor in vibration testing," J. Spacecr. Rockets, 1978.

[118] Ibrahim, S. R. (1978). Modal confidence factor in vibration testing. *Journal of Spacecraft and Rockets*, *15*(5), 313-316.

[119] Juang, J. N. (1994). Applied system identification.

[120] Juang, J. N., & Pappa, R. S. (1985). An eigensystem realization algorithm for modal parameter identification and model reduction. *Journal of guidance, control, and dynamics*, *8*(5), 620-627.

[121] Moler, C. B., & Stewart, G. W. (1973). An algorithm for generalized matrix eigenvalue problems. *SIAM Journal on Numerical Analysis*, *10*(2), 241-256.

[122] Kumar, S. (2008). Analyzing random vibration fatigue. *ANSYS Advantage*,*2*(3), 39-42.

[123] Matsuishi, M., & Endo, T. (1968). Fatigue of metals subjected to varying stress. *Japan Society of Mechanical Engineers, Fukuoka, Japan*, 37-40.

[124] Zygmund, A. (2002). *Trigonometric series* (Vol. 1). Cambridge university press.

[125] Win t´ erstein, S. R. (1988). Nonlinear vibration models for extremes and fatigue. *Journal of Engineering Mechanics*, *114*(10), 1772-1790.

[126] Abdullah, S., Nizwan, C. K. E., & Nuawi, M. Z. (2009). A study of fatigue data editing using the Short-Time Fourier Transform (STFT). *American Journal of Applied Sciences*, *6*(4), 565.

[127] Dowling, N. E. (1971). *Fatigue failure predictions for complicated stress-strain histories* (Vol. 337). ILLINOIS UNIV AT URBANA DEPT OF THEORETICAL AND APPLIED MECHANICS.

[128] Canfield, R. E., & Villaire, M. A. (1992). *The Development of Accelerated Component Durabiltiy Test Cycles Using Fatigue Sensitive Editing Techniques* (No. 920660). SAE Technical Paper.

[129] Conle, A., & Topper, T. H. (1980). Overstrain effects during variable amplitude service history testing. *International Journal of Fatigue*, *2*(3), 130-136.

[130] Sharp, R., Derby, T., & Laurent, G. (2005). *Use of accumulated damage methods in the development and validation of an elastomeric isolator bench test* (No. 2005-01-2409). SAE Technical Paper.

[131] Yay, K., Ereke, I. M., Bilir, M., & Cataltepe, V. (2009). *Fatigue strength of an urban type midi bus vehicle chassis by using fem analysis and accelerated fatigue life test* (No. 2009-01-1453). SAE Technical Paper.

[132] Nelson, D. V., & Fuchs, H. O. (1975). *Predictions of cumulative fatigue damage using condensed load histories* (No. 750045). SAE Technical Paper.

[133] Stephens, R. I., Dindinger, P. M., & Gunger, J. E. (1997). Fatigue damage editing for accelerated durability testing using strain range and SWT parameter criteria. *International Journal of fatigue*, *19*(8), 599-606.

[134] Rao, J. S. (2011). Optimized Life Using Frequency and Time Domain Approaches. In *IUTAM Symposium on Emerging Trends in Rotor Dynamics*(pp. 13-26). Springer Netherlands.

[135] Petrucci, G., & Zuccarello, B. (1999). On the estimation of the fatigue cycle distribution from spectral density data. *Proceedings of the Institution of Mechanical Engineers, Part C: Journal of Mechanical Engineering Science*,*213*(8), 819-831.

[136] Halfpenny, A. (1999, June). A frequency domain approach for fatigue life estimation from finite element analysis. In *Key Engineering Materials* (Vol. 167, pp. 401-410). Trans Tech Publications.

[137] Rice, S. O. (1945). Mathematical analysis of random noise. Reprinted in: Selected Papers on Noise and Stochastic Processes, N. Wax.

[138] Bendat, J. S. (1964). Probability functions for random responses. *NASA report on contract NAS-5-4590*.

[139] Wirsching, P. H., & Shehata, A. M. (1977). Fatigue under wide band random stresses using the rain-flow method. *Journal of engineering materials and technology, 99*(3), 205-211.

[140] Chaudhury, G. K., & Dover, W. D. (1985). Fatigue analysis of offshore platforms subject to sea wave loadings. *International Journal of Fatigue,7*(1), 13-19.

[141] Kam, J. C., & Dover, W. D. (1988). Fast fatigue assessment procedure for offshore structures under random stress history.

[142] Tunna, J. M. (1986). Fatigue life prediction for Gaussian random loads at the design stage. *Fatigue & Fracture of Engineering Materials & Structures*, *9*(3), 169-184.

[143] Steinberg, D. S. (1988). Vibration analysis for electronic equipment. *New York, Wiley-Interscience, 1988, 460 p. No individual items are abstracted in this volume.*, *1*.

[144] Dirlik, T. (1985). *Application of computers in fatigue analysis* (Doctoral dissertation, University of Warwick).

[145] Liou, H. Y., Wu, W. F., & Shin, C. S. (1999). A modified model for the estimation of fatigue life derived from random vibration theory. *Probabilistic engineering mechanics, 14*(3), 281-288.

[146] PETRUCCI, G., & ZUCCARELLO, B. (2004). Fatigue life prediction under wide band random loading. *Fatigue & Fracture of Engineering Materials & Structures*, *27*(12), 1183-1195.

[147] Łagoda, T., Macha, E., & Niesłony, A. (2005). Fatigue life calculation by means of the cycle counting and spectral methods under multiaxial random loading. *Fatigue &*

*Fracture of Engineering Materials & Structures*, *28*(4), 409-420.

[148] Wirsching, P. H., & Light, M. C. (1980). Fatigue under wide band random stresses. *Journal of the Structural Division*, *106*(7), 1593-1607.

[149] Braccesi, C., Cianetti, F., Lori, G., & Pioli, D. (2005). Fatigue behaviour analysis of mechanical components subject to random bimodal stress process: frequency domain approach. *International Journal of Fatigue*, *27*(4), 335-345.

[150] Zhao, W., & Baker, M. J. (1992). On the probability density function of rainflow stress range for stationary Gaussian processes. *International Journal of Fatigue*, *14*(2), 121-135.

[151] Fu, T. T., & Cebon, D. (2000). Predicting fatigue lives for bi-modal stress spectral densities. *International Journal of Fatigue*, *22*(1), 11-21.

[152] Tovo, R. (2002). Cycle distribution and fatigue damage under broad-band random loading. *International Journal of Fatigue*, *24*(11), 1137-1147.

[153] Medford, R. (2005, April). Vehicle Safety at NHTSA. In *Presentation at the SAE G-11 meeting. Detroit, MI*.

[154] Hyde J., "2009 busy year for vehicle recalls | The Columbus Dispatch." [Online]. Available: http://www.dispatch.com/content/stories/business/2010/01/02/auto_safety_freep.ART_ART_01-02-10_A8_S7G5E5P.html. [Accessed: 16-Nov-2015].

[155] Brydon, G. M. (1994). *European Symposium on Reliability of Electron Devices, Failure Physics and Analysis (5th)*. QA REL ASSOCIATES NORTHHAMPTON (UNITED KINGDOM).

[156] Vassilious, A., & Mettas, A. (2001). Understanding accelerated life-testing analysis. In *Proc. Annnual Reliability and Maintainability Symposium, USA*.

[157] Schwab, H. L., & Dodson, B. L. (2006). Accelerated Testing: A Practitioner's Guide to Accelerated and Reliability Testing. *Warrendale, PA: Society of Automotive Engineers, 2006. 268*.

[158] Klyatis, L. M., & Klyatis, E. (2010). *Accelerated quality and reliability solutions*. Elsevier.

[159] Klyatis, L. M., & Verbitsky, D. (2010). *Accelerated Reliability/Durability Testing as a Key Factor for Accelerated Development and Improvement of Product/Process Reliability, Durability, and Maintainability* (No. 2010-01-0203). SAE Technical Paper.

[160] Lev, K. (2006). Elimination of the Basic Reasons for Inaccurate RMS Predictions. A Governmental-Industry Conference "RMS in A Systems Engineering Environment". DAU-West, San Diego. *CA. October*, 11-12.

[161] Chen, G., Krantz, S. G., Ma, D. W., Wayne, C. E., & West, H. H. (1987). The Euler-Bernoulli beam equation with boundary energy dissipation.*Operator methods for optimal control problems*, *108*, 67-96.

[162] Rao, S. S., & Yap, F. F. (1995). *Mechanical vibrations* (Vol. 4). New York: Addison-Wesley.

[163] Heylen, W., & Sas, P. (2006). *Modal analysis theory and testing*. Katholieke Universteit Leuven, Departement Werktuigkunde.

[164] Gelfuso, M. V., Thomazini, D., Souza, J. C. S. D., & Lima Junior, J. J. D. (2014). Vibrational analysis of coconut fiber-PP composites. *Materials Research*, *17*(2), 367-372.

[165] Inman, D. J., & Singh, R. C. (2001). *Engineering vibration* (Vol. 3). Upper Saddle River: Prentice Hall.

[166] Irvine T., "SINE SWEEP FREQUENCY PARAMETERS." [Online]. Available: http://www.vibrationdata.com/webinars/unit3/sweep.pdf. [Accessed: 01-Dec-2015].

[167] Tuma, J. J. (1970). Engineering mathematics handbook.

[168] Irvine, T. (2013). Miner's Cumulative Damage via Rainflow Cycle Counting.*Rn (theory)*, *1*, 26.

[169] Stephens, R. I., Fatemi, A., Stephens, R. R., & Fuchs, H. O. (2000). *Metal fatigue in engineering*. John Wiley & Sons.

[170] Shigley, J. E., Budynas, R. G., & Mischke, C. R. (2004). Mechanical engineering design.

[171] Irvine, T. (2010). Rainflow cycle counting in fatigue analysis. *Revision A, Vibrationdata*.

[172] Vanmarcke, E. H. (1972). Properties of spectral moments with applications to random vibration. *Journal of the Engineering Mechanics Division*, *98*(2), 425-446.

[173] Muluka, V. (1998). *Optimal suspension damping and axle vibration absorber for reduction of dynamic tire loads* (Doctoral dissertation, Concordia University).

[174] Grishin, A., & Sutton, M. xPSD: An External Solver To Compute Linear Responses To Random Base Excitations (PSD) In Structures Using ANSYS With The Large Mass Method.

[175] Ahlin, K., Brandt, A., & AB, S. E. (2001). Experimental modal analysis in practice. *Saven Edu Tech AB, Taby, Sweden*.

[176] Tustin, W. (2007, June). MIL-STD-810G Will Better Define Dynamic Tests. In*Presentation at Spacecraft & Launch Vehicle Dynamic Environments Workshop, El Segundo, California*.

# APPENDIX A- Tuning of Natural Frequencies

From literature, methods of tuning natural frequencies can be categorized into three sections e.g. change of geometry, application of piezoelectric material and using spring mass systems. In this section, tuning of natural frequencies has been obtained by hovering point mass on different position of the beam. Placing the mass in different position of the beam will have significant effect on the dynamic behavior of the structure. Point mass is shown in the form of mass ratio which can be defined as the ratio of point mass to the total mass of the beam.

When two point masses of equal ratio are placed on each end of the beam as indicated by Figure 38, the variation of first natural frequency almost remains constant. It can be concluded for this specific example that the second natural frequency can be changed up to 42% and third natural frequency up to 62% without altering the first natural frequency. To show the consistency of the results two different types of joint stiffness were used in this example.

From Figure 39, it can be seen that placing a mass on the middle of the beam will significantly change the first and third natural frequencies but will not affect the second natural frequency of the beam.

From Figure 40, it could be concluded that third natural frequency remains almost constant when point mass is placed about 20% of total length from both end. This information might turn into useful one when modification of third natural frequency is of great importance. Hence, optimum position and value of the point mass and joint stiffness can be obtained by studying this method.

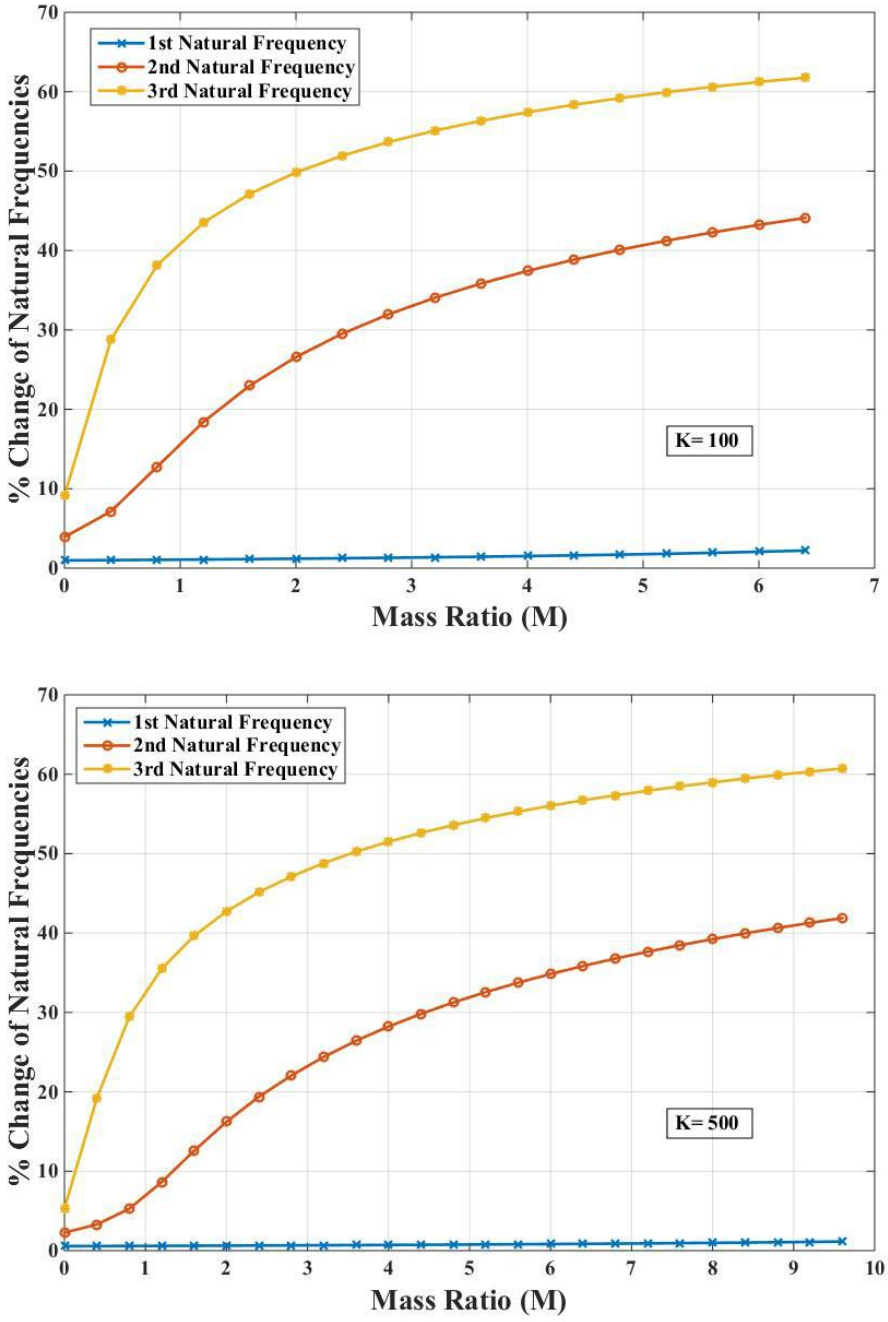


**Figure A-1: Percentage Change of Natural Frequencies of a Beam by Adding End Mass with Fixed Joint Stiffness at Both Ends**

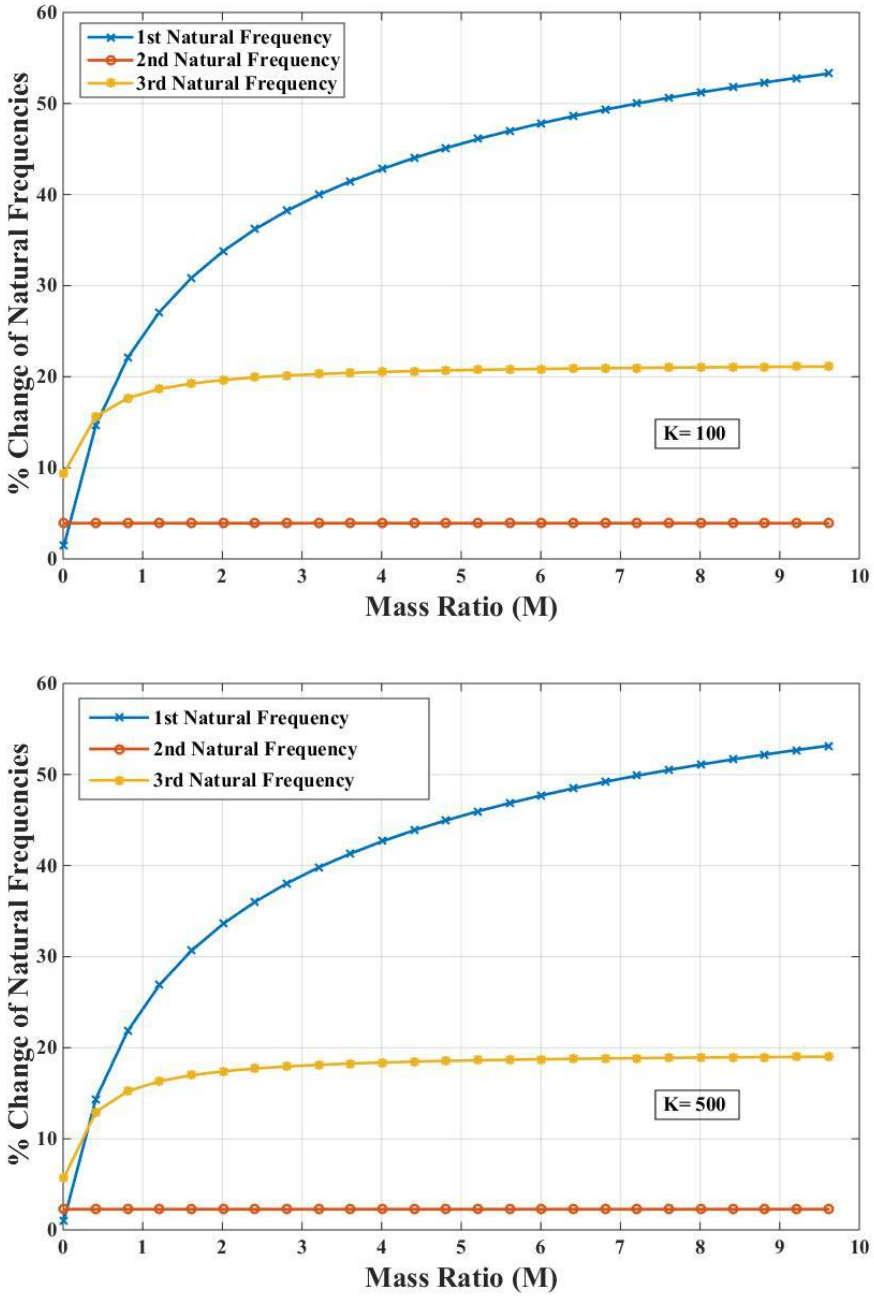


**Figure A-2: Percentage Change of Natural Frequencies of a Beam by Adding Mass in the Middle with Fixed Joint Stiffness at Both Ends**

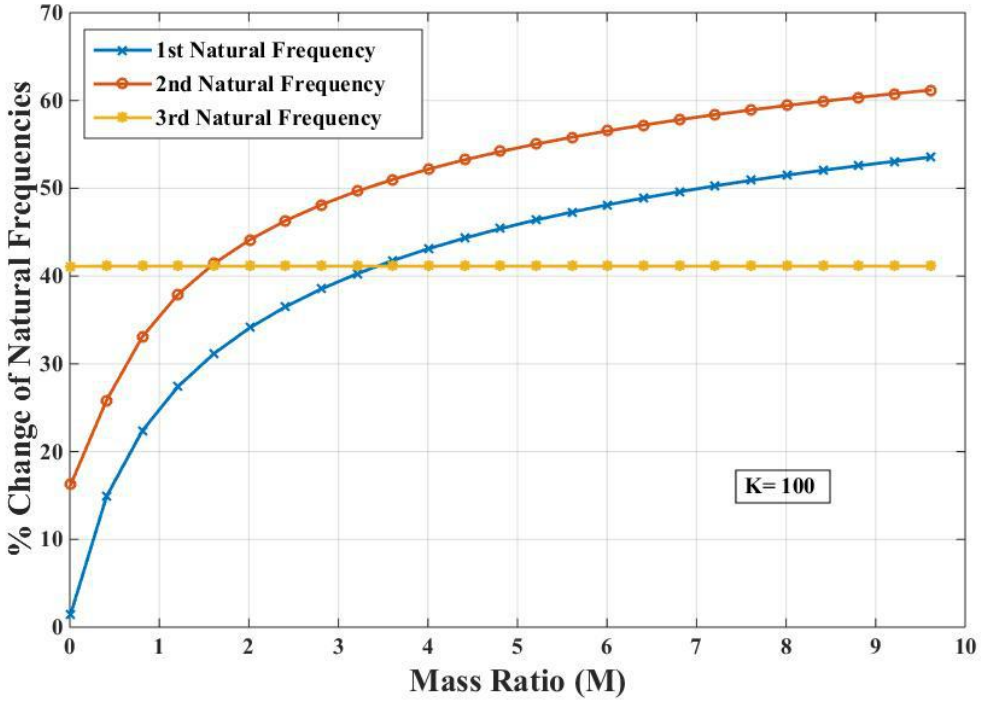


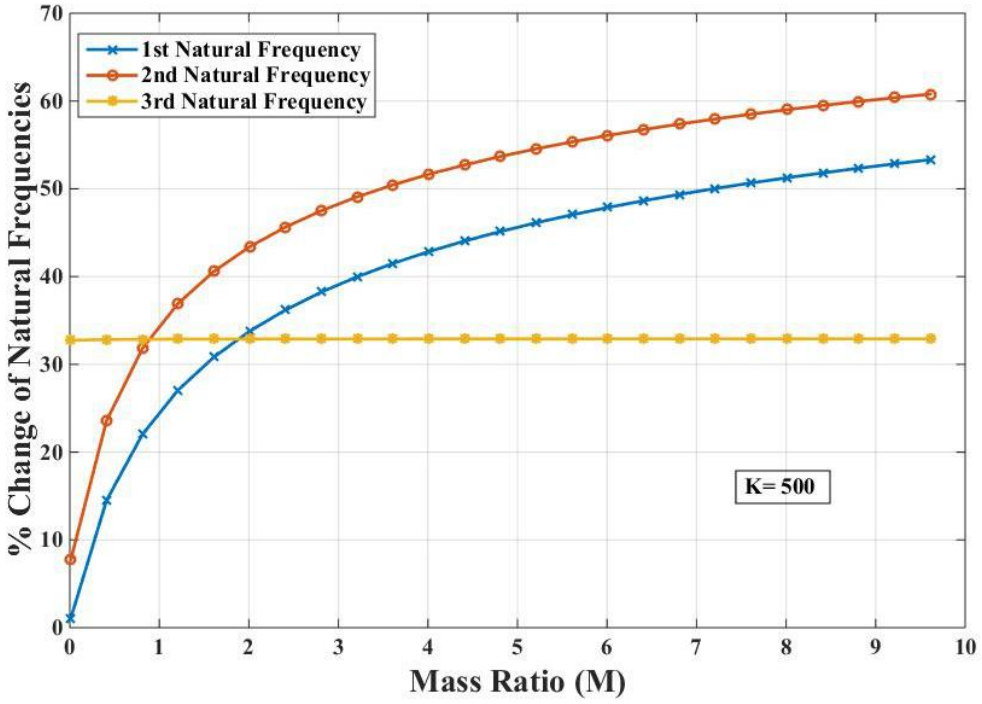


**Figure A-3: Percentage Change of Natural Frequencies of a Beam When Point Mass is Placed About 20% of the Total Length from Both Ends**

# APPENDIX B- Design of Fixtures

Appropriate design of a fixture is the most important part of this research to carry out experimental analysis. The solid model of both rigid and elastic foundation fixture is given from Figure B-1 to Figure B-4. The design of both fixtures allows withstanding both point and base motion in vertical direction. There is a space between the base and the beam to keep the modal shaker. The height could be adjusted by the mean of slide contact of the secondary base along the rigid shafts. The fixture is designed so that the first natural frequency of these fixtures remains out of the highest frequency of interest e.g. 80Hz in this case.

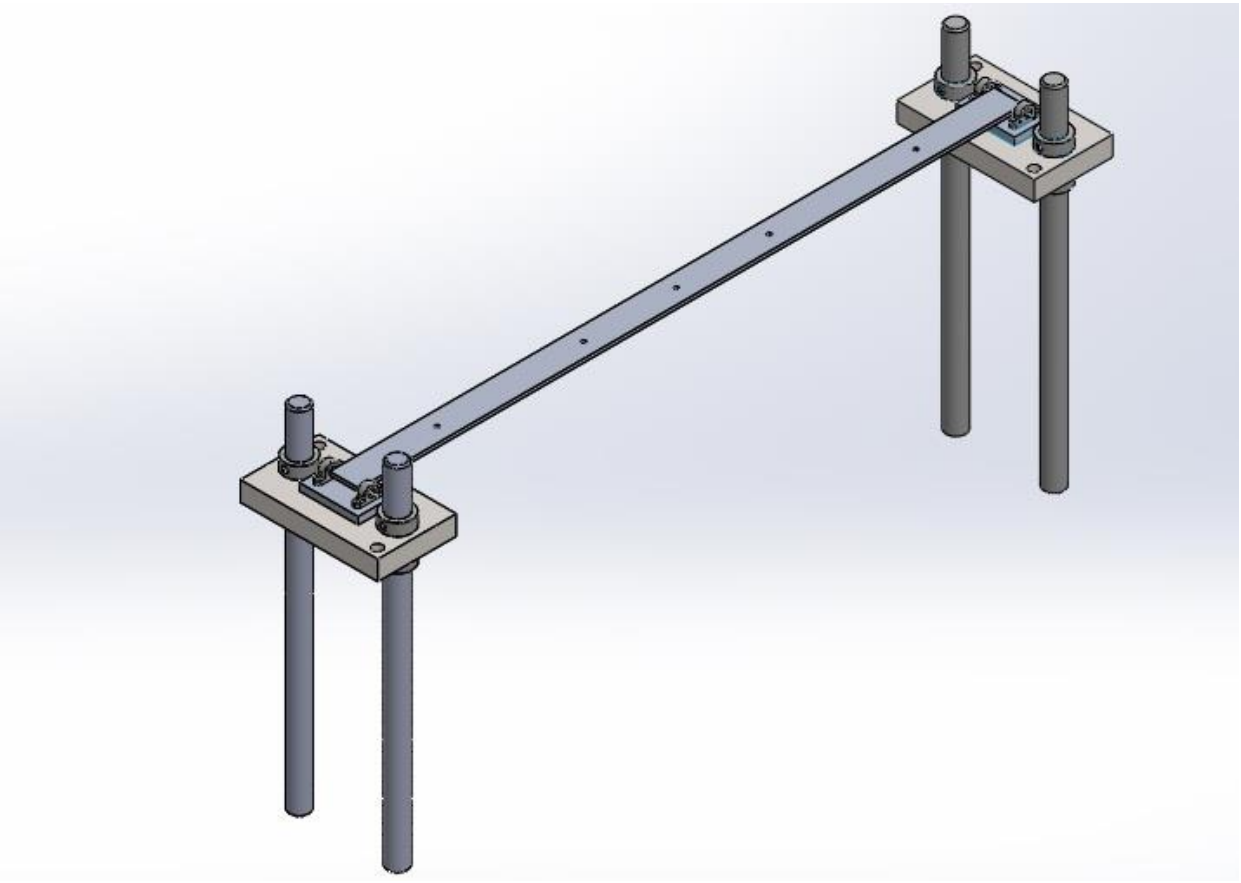

**Figure B-1: Fixture for Rigid Foundation**

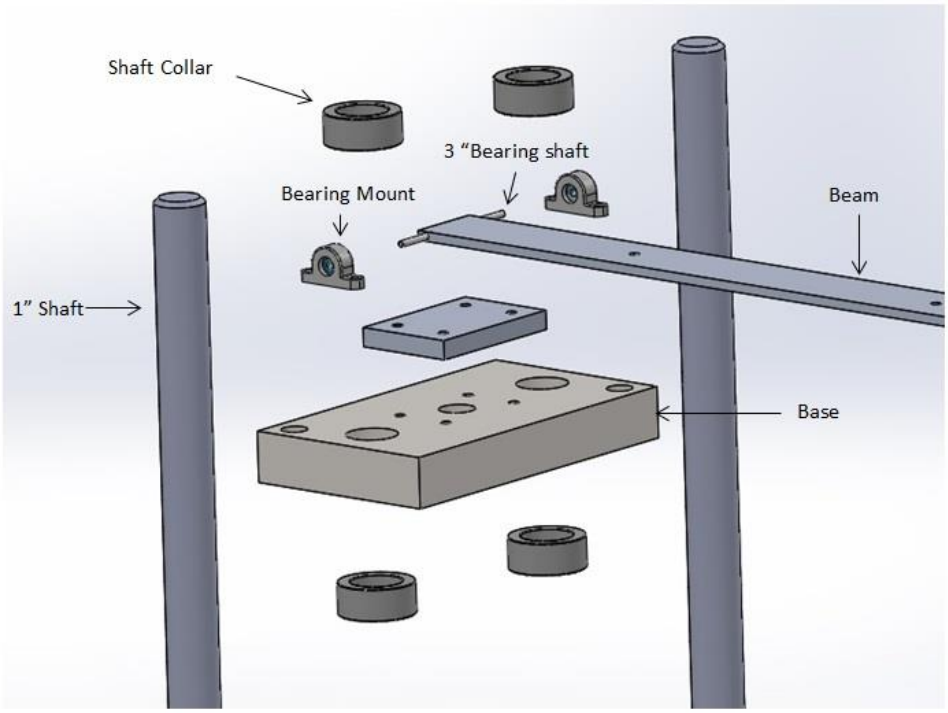


**Figure B-2: Joint Connection of a Rigid Foundation**

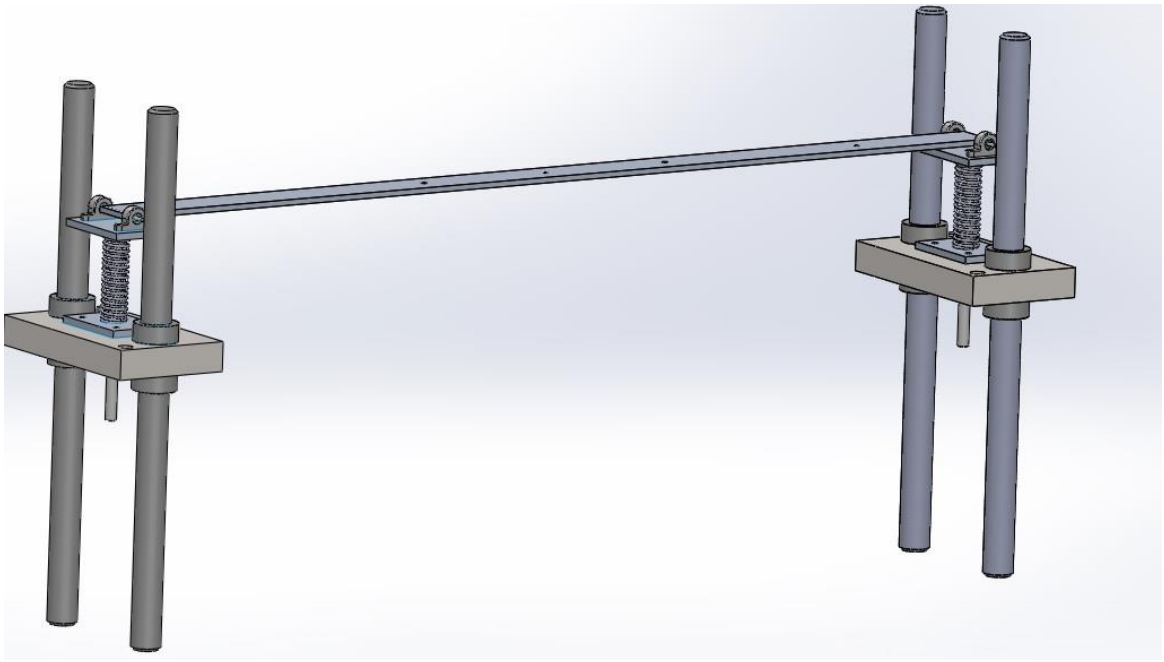

**Figure B-3: Fixture for Elastic Foundation**

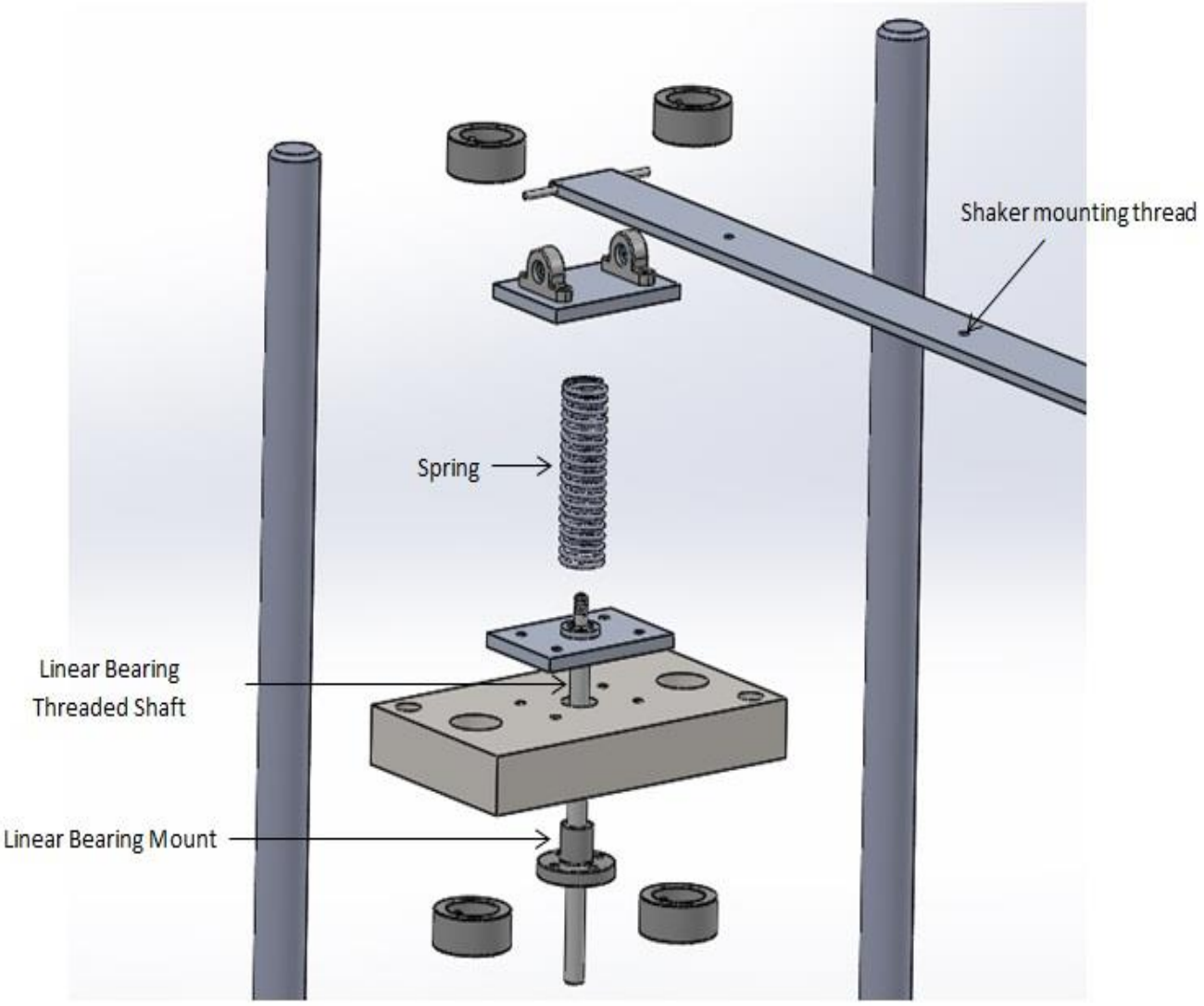


**Figure B-4: Joint Connection of an Elastic Foundation**

# APPENDIX C- Fatigue Damage Calculation

In this thesis, fatigue damage has been calculated in both time and frequency domain techniques and finally the average are taken as the final damage for both sine-sweep and random loading. In time domain fatigue analysis, firstly the Rainflow Histogram of the output bending stress is figured out. Then Miner's Cumulative Damage rule is applied for each cycle and combined to get final fatigue damage. Likewise, in frequency domain fatigue analysis the PDF is counted using different algorithm following by Miner's formula to achieve the damage.

**Sine-Sweep Loading:**

In this thesis, logarithmic sine-sweep loading has been used as shown in Figure C-1. From the spectrogram it can be seen that the time and frequency holds a logarithmic relationship and the histogram of a sine-sweep loading would be always a U-shaped curve which is called Bath-Tab diagram for its shape.

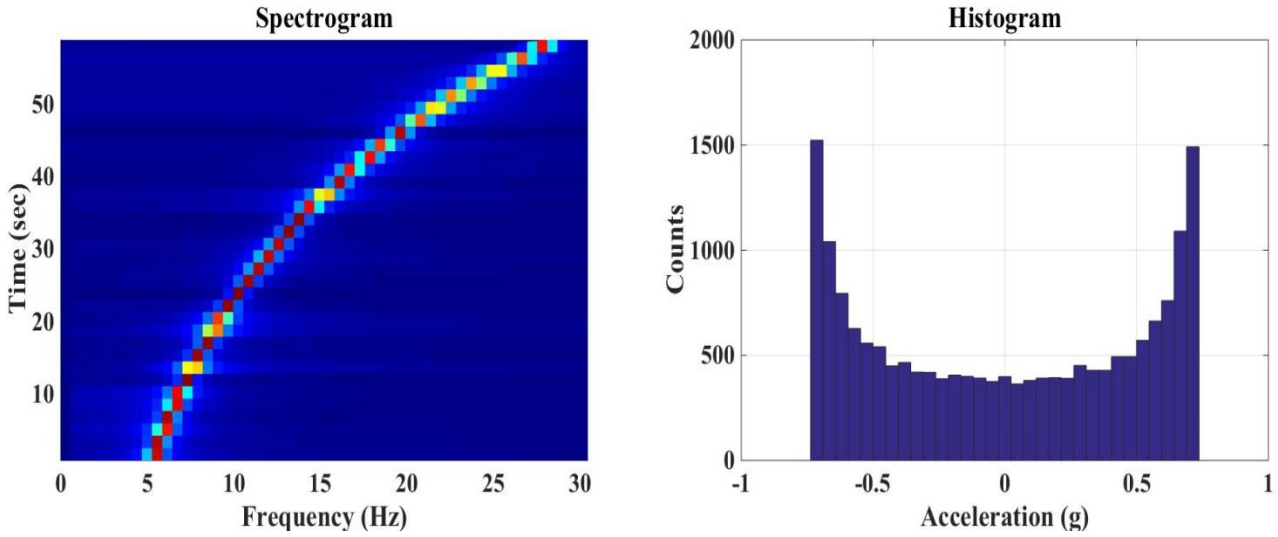


**Figure C-1: Sine-Sweep Spectrogram and Bath-Tab Histogram**

**Random Loading:**

For a random loading input the histogram is called Bell-shaped or Gaussian distribution as shown in Figure C-2. So comparing with the sine-sweep loading, random loading gives a totally different pattern of failure mechanism.

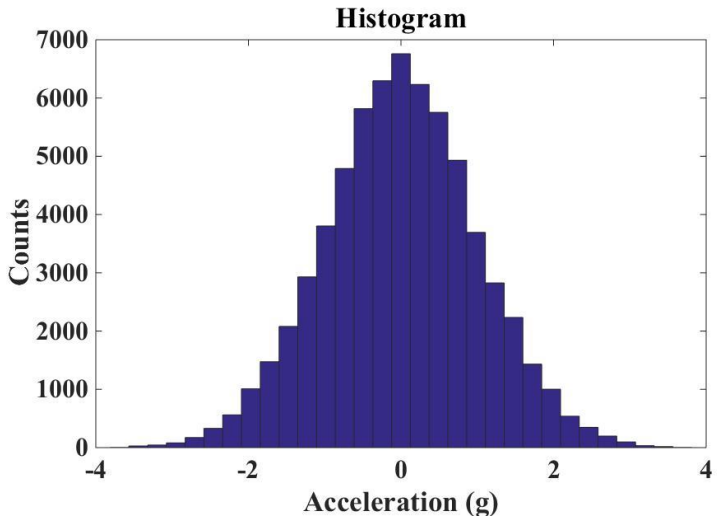


**Figure C-2: Gaussian Distribution of Random Load**

**Time Domain Fatigue Analysis:**

| Lower Range | Upper Range | Cycles | Ave Amp | Max Amp | Min Mean | Ave Mean | Max Mean | Min Valley | Max Peak |
|---|---|---|---|---|---|---|---|---|---|
| 534 | 593 | 5.0 | 281 | 297 | -8.5 | 2.7 | 11.5 | -288 | 305 |
| 474 | 534 | 20.0 | 249 | 267 | -24 | 1.09 | 20 | -273 | 271 |
| 415 | 474 | 32.0 | 223 | 237 | -27.5 | 1.33 | 13.5 | -246 | 248 |
| 356 | 415 | 49.5 | 192 | 208 | -21 | 1.51 | 35 | -218 | 230 |
| 297 | 356 | 68.0 | 163 | 178 | -16.5 | -2.99 | 27 | -191 | 192 |
| 237 | 297 | 120.0 | 134 | 148 | -29.5 | 0.0179 | 25.5 | -167 | 167 |
| 178 | 237 | 135.5 | 103 | 119 | -22.8 | 0.542 | 20.5 | -136 | 132 |
| 119 | 178 | 150.0 | 75.2 | 89 | -18 | 0.744 | 19.6 | -99.5 | 104 |
| 89 | 119 | 69.5 | 52.2 | 59.3 | -15.1 | 0.669 | 15.2 | -74.1 | 70.1 |
| 59.3 | 89 | 35.5 | 36.9 | 44 | -7.2 | 1.49 | 12.2 | -45.4 | 54.3 |
| 29.6 | 59.3 | 28.5 | 22.9 | 29.5 | -6.95 | 0.111 | 9.4 | -31 | 33.8 |
| 14.8 | 29.6 | 24.5 | 10.3 | 14.3 | -16.3 | 4.91 | 35 | -29 | 43.8 |
| 0 | 14.8 | 70.0 | 2.93 | 7.35 | -65.4 | -1.82 | 102 | -66.8 | 102 |

**Figure C-3: Rainflow Cycle Counting Table**

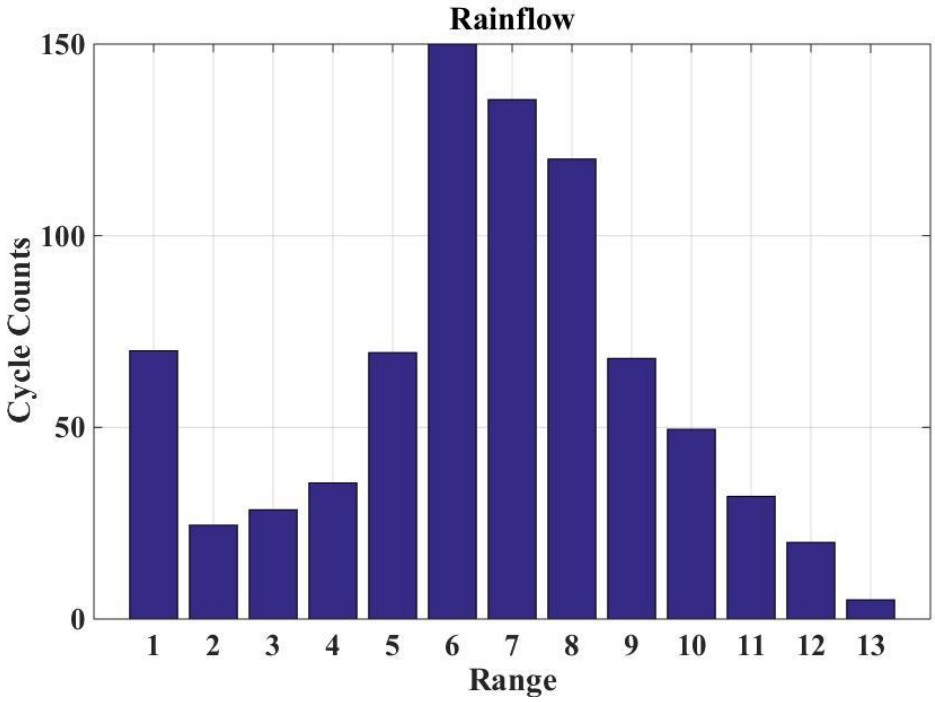


**Figure C-4: Amplitude-Range Cycle Counting**

**Frequency Domain Fatigue Analysis:**

```
Lambda Values

    Wirsching Light =   0.6208
         Ortiz Chen =    1.518
     Lutes & Larsen =   0.9884

     Cumulative Damage                Damage Rate          A*rate
                                        (1/sec)          ((MPa^9.25)/sec)

        Narrowband DNB = 0.000116,      1.9415e-06,      1.0826e+20
            Dirlik DDK = 9.54e-05,      1.5901e-06,      8.8662e+19
        Alpha 0.75 DAL = 0.000115,      1.9205e-06,      1.0709e+20
        Ortiz Chen DOC = 0.000177,      2.9481e-06,      1.6439e+20
        Zhao Baker DZB = 9.45e-05,      1.5757e-06,      8.7864e+19
      Lutes Larsen DLL = 0.000115,      1.9190e-06,      1.0700e+20
   Wirsching Light DWL = 7.23e-05,      1.2052e-06,      6.7202e+19
  Benasciutti Tovo DBT = 0.000115,      1.9103e-06,      1.0652e+20

Average of DAL,DOC,DLL,DBT,DZB,DDK

          average=0.0001186
```

**Figure C-5: Frequency Domain Fatigue Analysis Using MATLAB**